

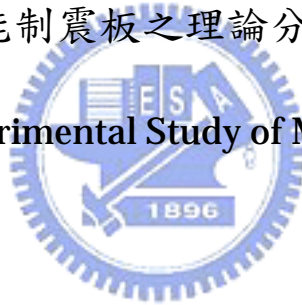
國立交通大學

土木工程學系碩士班

碩 士 論 文

金屬消能制震板之理論分析與實驗

A Theoretical and Experimental Study of Metallic Yielding Damper



研 究 生：林峻毅

指 導 教 授：王彥博 博士
李建良 博士

中華民國九十三年六月

金屬消能制震板之理論分析與實驗
A Theoretical and Experimental Study of Metallic Yielding Damper

研究生：林峻毅

Student: Chun-Yi Lin

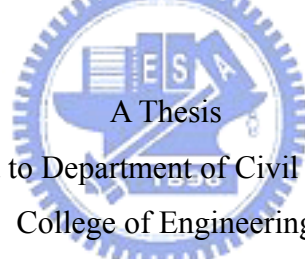
指導教授：王彥博 博士

Advisor: Dr. Yen-Po Wang

李建良 博士

Dr. Chien-Liang Lee

國立交通大學
土木工程學系
碩士論文



Submitted to Department of Civil Engineering
College of Engineering

National Chiao Tung University

in partial Fulfillment of the Requirements

for the Degree of

Master

in

Civil Engineering

June 2004

Hsinchu, Taiwan, Republic of China

中華民國九十三年六月

博碩士論文授權書

(國科會科學技術資料中心版本, 93.2.6)

本授權書所授權之論文為本人在交通大學(學院)土木工程系所

結構組九十二學年度第二學期取得碩士學位之論文。

論文名稱：金屬消能制震板之理論分析與實驗

同意 不同意

本人具有著作財產權之論文全文資料, 授予行政院國家科學委員會科學技術資料中心(或其改制後之機構)、國家圖書館及本人畢業學校圖書館, 得不限地域、時間與次數以微縮、光碟或數位化等各種方式重製後散布發行或上載網路。

本論文為本人向經濟部智慧財產局申請專利(未申請者本條款請不予理會)的附件之一, 申請文號為: _____, 註明文號者請將全文資料延後半年後再公開。

同意 不同意

本人具有著作財產權之論文全文資料, 授予教育部指定送繳之圖書館及本人畢業學校圖書館, 為學術研究之目的以各種方法重製, 或為上述目的再授權他人以各種方法重製, 不限地域與時間, 惟每人以一份為限。

上述授權內容均無須訂立讓與及授權契約書。依本授權之發行權為非專屬性發行權利。依本授權所為之收錄、重製、發行及學術研發利用均為無償。上述同意與不同意之欄位若未鈎選, 本人同意視同授權。

指導教授姓名：王彥博 教授

研究生簽名：
(親筆正楷)

學號：9116503
(務必填寫)

日期：民國 93 年 6 月 30 日

1. 本授權書(得自 <http://sticnet.stic.gov.tw/sticweb/html/theses/authorize.html> 下載或至 <http://www.stic.gov.tw> 首頁右下方下載)請以黑筆撰寫並影印裝訂於書名頁之次頁。
2. 授權第一項者, 請確認學校是否代收, 若無者, 請個別再寄論文一本至台北市(106)和平東路二段106號1702室 國科會科學技術資料中心 黃善平小姐。
(電話: 02-27377606 傳真: 02-27377689)

金屬消能制震板之理論分析與實驗

學生：林峻毅

指導教授：王彥博 博士
李建良 博士

國立交通大學土木工程研究所

摘 要

現代結構防震設計的目標在於各種強度不同的地震之下，結構物仍可保有其性能而使內部之功能正常運作。為達到此一目的，傳統一味增加結構元件尺寸的作法已被棄，取而代之的是在結構系統之中加進消能減震元件、控制系統或是隔震系統。

金屬消能制震板的基礎力學理論包含勁度、降伏位移、降伏荷載之計算，以及設計上的細節考量；實尺寸以及縮小尺寸之制震板的元件測試結果，將用於驗證這些理論的正確性。本文提出一套可行的方法，在不裝設荷重元之情況下，藉由制震板上貼附應變計量得之應變，配合 Ramberg-Osgood 遲滯模型，推估制震板所受之彎矩與剪力。為解決數值計算上之困難，並將計算流程程式化，本文推導出 Ramberg-Osgood 遲滯模型之另一種表示方程式，且提出相關之查表法。實驗結果證實藉由本文提出之方法，吾人可得合理之預測結果。

制震板之耐震性試驗藉由一系列之振動台試驗進行，制震板尺寸遵照先前參數分析結果並配合電腦模擬進行設計，目標在於同時降低一座五層樓鋼構架模型其在多種不同地震下的加速度與位移反應，實驗結果與電腦數值模擬均顯示制震板可以有效達到其設計目標。

關鍵字：消能減震、金屬制震板、遲滯迴圈、Ramberg-Osgood、應變。

A Theoretical and Experimental Study of Metallic Yielding Damper

Student: Chun-Yi Lin

Avisors: Dr. Yen-Po Wang
Dr. Chien-Liang Lee

DEPARTMENT OF CIVIL ENGINEERING
NATIONAL CHIAO TUNG UNIVERSITY

ABSTRACT

To achieve desirable seismic performance, the traditional method of increasing the dimension of structural members is discarded by introducing energy dissipation systems, control systems or seismic isolation systems into the structural design. One of the effective mechanisms available for seismic energy dissipation is through the inelastic deformation of metals.

In this thesis, the fundamentals of metallic yielding damper including determination of stiffness, yielding displacement, yielding loads and design considerations have been introduced. Component tests for both full-scale and scaled-down damper have been conducted. A novel methodology for estimating the moment and shear force from strain with the Ramberg-Osgood Hysteresis model is proposed. To overcome numerical difficulties, an alternative form of the Ramberg-Osgood equations was derived to facility programming. Experimental results show that by the proposed methodology, one may predict the inelastic behavior of the damper with satisfactory accuracy.

Seismic performance test of the damper has also been conducted via a series of shaking table tests. The dimension of the damper was determined, based on preliminary parametric studies via computer simulations by SAP2000, to meet the design goal of suppressing both the acceleration and displacement responses of the structure simultaneously. Results show that the dampers are effective in seismic response control of building structures. Both displacement and acceleration responses can be simultaneously suppressed to a large extent.

Keywords: energy dissipation, metallic yielding damper, hysteresis, strain, Ramberg-Osgood.

ACKNOWLEDGEMENT

首先最要感謝吾師 王彥博教授提供學生一個良好的研究環境，並給予學生最豐富的指導，使學生具備從事研究工作的基本功夫。此外，吾師對於學術研究所保有的熱忱與致力於解決工程實務問題的用心，亦為學生師法的典範。吾師亦常常提供許多新穎的觀念，以增加學生思考的空間，並且在學生的生涯規劃上提供許多寶貴的建議，在此特向吾師致上最誠摯的謝意。

論文口試承蒙 翁正強教授、黃武龍博士、胡宗和博士、李建良博士親臨指導，並提供諸多珍貴的意見，使得論文的組織及疏漏之處得以獲得改進，在此學生亦要表示感激之意。

感謝研究室諸學長鄧敏政博士、廖偉信博士、李建良博士（口試委員之一），嘉賞學長，同學雅婷、啟晉、逸軒及明坤等於研究上的討論與實驗上的鼎力協助，使得諸多試驗得以如期完成。此外，感謝同窗學長黃經理銘峰、鈺文、連杰等於學習過程中的相互勉勵與日常生活中的互動。

最後，謹以本文獻給我最親愛的雙親與弟弟。

謹誌於交大工程二館

2004年7月

Table of Contents

ABSTRACT (Chinese)	II
ABSTRACT (English)	III
ACKNOWLEDGEMENT	IV
TABLE OF CONTENTS	V
LIST OF FIGURES	VII
LIST OF TABLES	XI
1 INTRODUCTION	1
1.1 BACKGROUND	2
1.2 STRUCTURAL PROTECTIVE SYSTEMS	5
1.2.1 <i>Passive Energy Dissipation</i>	6
1.2.2 <i>Seismic Isolation</i>	13
1.2.3 <i>Active / Semi-Active Control System</i>	15
1.3 THE ORGANIZATION.....	16
2 FUNDAMENTALS OF METALLIC YIELDING DAMPER	17
2.1 INTRODUCTION	18
2.2 THEORETICAL DERIVATIONS	19
2.3 DESIGN CONSIDERATIONS.....	23
2.4 PARAMETRIC ANALYSIS	24
3 DEVELOPMENT OF MEASURING METHODOLOGY FOR MOMENT AND SHEAR VIA STRAIN MEASUREMENT	29
3.1 RAMBERG-OSGOOD HYSTERESIS MODEL	31
3.1.1 <i>Single-loop Model</i>	31
3.1.2 <i>Multiple-loop Model</i>	36
3.1.3 <i>Determining the Turning Points</i>	37
3.2 DERIVATION OF MOMENT AND SHEAR FROM INELASTIC STRESS-STRAIN HYSTERESIS	38
3.3 PROCEDURE FOR THE MEASURING METHODOLOGY.....	40
4 COMPONENT TESTS	43
4.1 COMPONENT TEST OF SCALED-DOWN DAMPER.....	45
4.1.1 <i>Design of the Model Damper</i>	45
4.1.2 <i>Testing Facilities</i>	47

4.1.3	<i>Test Programs</i>	53
4.1.4	<i>Testing Results</i>	54
4.1.5	<i>Discussion</i>	59
4.2	COMPONENT TEST OF FULL-SCALE DAMPER	61
4.2.1	<i>Design of the Model Damper</i>	61
4.2.2	<i>Testing Facilities</i>	63
4.2.3	<i>Test Programs</i>	66
4.2.4	<i>Testing Results</i>	67
5	SEISMIC PERFORMANCE TESTS	69
5.1	SHAKING TABLE TESTS	70
5.1.1	<i>Description of Test Facilities</i>	70
5.1.2	<i>Description of the Dampers</i>	75
5.1.3	<i>Test Programs</i>	78
5.1.4	<i>Assessments of Seismic Performance</i>	80
5.2	NUMERICAL SIMULATION USING SAP2000	111
5.2.1	<i>An Analytical Model in SAP2000</i>	111
5.2.2	<i>Simulating Results</i>	119
6	CONCLUDING REMARKS	139
	REFERENCES	141
	APPENDIX A: SOURCE CODES OF MATLAB PROGRAMS	145
	MAIN1.M	146
	NONLINEARBENDING03	147
	STRAIN02.M	150
	GENERATETABLERO.M	150
	SEARCHTABLERO.M	151
	GENERATETURNINGPOINT.M	152
	COMPAREHYSTERESIS.M	153
	FILTERDISPLACEMENT.M	154
	PLOTH.M	155
	PLOTSH.M	155
	PLOTSTRAIN.M	155
	PLOTV.M	155
	CURRICULUM VITAE	156

List of Figures

Fig. 1.1	The earth's seismicity outlines plate margins	2
Fig. 1.2	Classification of structural protective systems.....	5
Fig. 1.3	Several metallic yielding devices	7
Fig. 1.4	ADAS	8
Fig. 1.5	A photo and detailed design of TADAS	8
Fig. 1.6	A photo of RADAS	8
Fig. 1.7	Pall Friction Device	10
Fig. 1.8	A viscoelastic damper	11
Fig. 1.9	A Fluid Damper.....	12
Fig. 1.10	Buildings installed with TMD.....	12
Fig. 2.1	X-shaped metallic yielding damper.....	19
Fig. 2.2	Error of neglecting shear deformation on stiffness	21
Fig. 2.3	Stiffness ratio (k_a/k'_a) with respect to height-to-thickness ratio (h/t) for various safety factors (SF)	25
Fig. 2.4	Stiffness ratio (k_a/k'_a) with respect to height-to-thickness ratio (h/t) for various thicknesses (t)	25
Fig. 2.5	Yielding displacement with respect to height-to-thickness ratio (h/t) for various thicknesses of the damper	27
Fig. 2.6	Height-thickness ratio (h/t) with respect to yielding displacement ratio (Δ_y/Δ'_y) for various thicknesses of the damper	27
Fig. 3.1	Common mathematical models for stress-strain relationship	30
Fig. 3.2	Typical single-loop Ramberg-Osgood Hysteresis Model	32
Fig. 3.3	Illustration of a single-loop Ramberg-Osgood Hysteresis Model.....	35
Fig. 3.4	Typical multiple-loop Ramberg-Osgood Hysteresis Model	36
Fig. 3.5	Illustration of algorithm for determining turning points.....	37
Fig. 3.6	Metallic yielding damper bonded with a piece of strain gauge.....	38
Fig. 3.7	The pseudo code for finding the corresponding stresses.....	41
Fig. 4.1	Design of scaled-down metallic yielding damper	46
Fig. 4.2	MTS 407 Controller	47
Fig. 4.3	1.5-ton actuator of MTS	47
Fig. 4.4	Loadcell	48
Fig. 4.5	Data acquisition system	48
Fig. 4.6	A strain gauge for strain measurement in the tests	49

Fig. 4.7	A full view of the testing platform for component test of the scaled-down damper .	51
Fig. 4.8	A Close-up view of the set-up.....	51
Fig. 4.9	Detailed plot of the test platform for scaled-down damper	52
Fig. 4.10	The loading history specified for the component test of scaled-down damper.....	53
Fig. 4.11	Hysteresis for directly measured force-displacement relationship of the scaled-down damper	56
Fig. 4.12	Curve fitting for determining the experimental stiffness of the scaled-down damper	56
Fig. 4.13	Measured strain data from component test of scaled-down damper	57
Fig. 4.14	Predicted stress-strain hysteresis of the scaled-down damper.....	57
Fig. 4.15	Comparison of the hystereses for force-displacement relationship between directly measured and predicted results	58
Fig. 4.16	Illustration of the movement of the actuator	60
Fig. 4.17	Design of the full-scale metallic yielding damper	62
Fig. 4.18	MTS control system in the control room.....	63
Fig. 4.19	A close-up view of the full-scale damper in testing	64
Fig. 4.20	Design sketch of the testing platform for component test of a full-scale damper (Unit: mm).....	65
Fig. 4.21	The loading history specified for component test of full-scale damper	66
Fig. 4.22	Experimental hysteresis loop of the full-scale damper	68
Fig. 4.23	Curve fitting for determining the experimental stiffness of the full-scale damper ..	68
Fig. 5.1	The model structure for shaking table test.....	71
Fig. 5.2	Earthquake simulator -- shaking table system	74
Fig. 5.3	15-ton dynamic actuator of MTS	74
Fig. 5.4	Seismic performance test of the damper on a model structure via shaking table....	77
Fig. 5.5	A close-up view of a unit of the damper on the model structure.....	77
Fig. 5.6	Time history of El Centro earthquake	79
Fig. 5.7	Time history of Hachinohe earthquake	79
Fig. 5.8	Time history of Kobe earthquake	80
Fig. 5.9	Comparison of floor acceleration responses (El Centro, PGA=0.1g)	84
Fig. 5.10	Comparison of floor acceleration responses (El Centro, PGA=0.2g)	85
Fig. 5.11	Comparison of floor acceleration responses (El Centro, PGA=0.3g)	86
Fig. 5.12	Comparison of floor acceleration responses (El Centro, PGA=0.4g)	87
Fig. 5.13	Comparison of storydrift of the 1st Floor (El Centro, PGA = 0.1g).....	88
Fig. 5.14	Comparison of storydrift of the 1st Floor (El Centro, PGA = 0.2g).....	88
Fig. 5.15	Comparison of storydrift of the 1st Floor (El Centro, PGA = 0.3g).....	89
Fig. 5.16	Comparison of storydrift of the 1st Floor (El Centro, PGA = 0.4g).....	89
Fig. 5.17	Comparison of Floor Acceleration Responses (Hachinohe, PGA = 0.1g).....	90
Fig. 5.18	Comparison of Floor Acceleration Responses (Hachinohe, PGA = 0.15g)	91
Fig. 5.19	Comparison of Floor Acceleration Responses (Hachinohe, PGA = 0.20g).....	92

Fig. 5.20	Comparison of Floor Acceleration Responses (Hachinohe, PGA = 0.25g).....	93
Fig. 5.21	Comparison of Storydrift of the 1st Floor (Hachinohe, PGA = 0.1g)	94
Fig. 5.22	Comparison of Storydrift of the 1st Floor (Hachinohe, PGA = 0.15g)	94
Fig. 5.23	Comparison of Storydrift of the 1st Floor (Hachinohe, PGA = 0.2g)	95
Fig. 5.24	Comparison of Storydrift of the 1st Floor (Hachinohe, PGA = 0.25g)	95
Fig. 5.25	Comparison of Floor Acceleration Responses (Kobe, PGA = 0.1g).....	96
Fig. 5.26	Comparison of Floor Acceleration Responses (Kobe, PGA = 0.15g).....	97
Fig. 5.27	Comparison of Floor Acceleration Responses (Kobe, PGA = 0.2g).....	98
Fig. 5.28	Comparison of Floor Acceleration Responses (Kobe, PGA = 0.25g).....	99
Fig. 5.29	Comparison of Storydrift of the 1st Floor (Kobe, PGA = 0.1g)	100
Fig. 5.30	Comparison of Storydrift of the 1st Floor (Kobe, PGA = 0.15g)	100
Fig. 5.31	Comparison of Storydrift of the 1st Floor (Kobe, PGA = 0.2g)	101
Fig. 5.32	Comparison of Storydrift of the 1st Floor (Kobe, PGA = 0.25g)	101
Fig. 5.33	The analytical model of the 5-story model structure (bare frame) established by SAP2000.....	114
Fig. 5.34	The analytical model of the 5-story model structure (damper-implemented frame) established by SAP2000	115
Fig. 5.35	The parameters for the frame/cable element specified for the beams and columns in the model structure (Unit: cm).....	116
Fig. 5.36	The parameters for the frame/cable element specified for the bracing system in the model structure (Unit: cm).....	116
Fig. 5.37	The parameters for the shell element in the model structure (Unit: cm).....	117
Fig. 5.38	The parameters for the plastic (Wen) element in the model structure (Unit: mm, Kgf)	117
Fig. 5.39	The definition of parameters for the Wen's Plasticity Property.....	118
Fig. 5.40	Comparison of acceleration responses of the bare-frame model (Case 1: El Centro, PGA=0.1g).....	121
Fig. 5.41	Comparison of acceleration responses of the bare-frame model (Case 2: Hachinohe, PGA=0.1g).....	122
Fig. 5.42	Comparison of acceleration responses of the bare-frame model (Case 3: Kobe, PGA=0.1g).....	123
Fig. 5.43	Comparison of acceleration responses of the damper-implemented frame model (Case 4: El Centro, PGA=0.1g).....	124
Fig. 5.44	Comparison of acceleration responses of the damper-implemented frame model (Case 5: El Centro, PGA=0.4g).....	125
Fig. 5.45	The hystereses of the damper (Case 5: El Centro, PGA=0.4g)	126
Fig. 5.46	Comparison of acceleration responses of the damper-implemented frame model (Case 6: Hachinohe, PGA=0.1g).....	127
Fig. 5.47	Comparison of acceleration responses of the damper-implemented frame model (Case 7: Hachinohe, PGA=0.25g).....	128
Fig. 5.48	The hystereses of the damper (Case 7: Hachinohe, PGA=0.25g).....	129
Fig. 5.49	Comparison of acceleration responses of the damper-implemented frame model	

	(Case 8: Kobe, PGA=0.1g).....	130
Fig. 5.50	Comparison of acceleration responses of the damper-implemented frame model (Case 9: Kobe, PGA=0.25g).....	131
Fig. 5.51	The hystereses of the damper (Case 9: Kobe, PGA=0.25g).....	132
Fig. 5.52	Assessments of seismic performance of the damper (Case 4: El Centro, PGA=0.1g)	133
Fig. 5.53	Assessments of seismic performance of the damper (Case 5: El Centro, PGA=0.4g)	134
Fig. 5.54	Assessments of seismic performance of the damper (Case 6: Hachinohe, PGA=0.1g)	135
Fig. 5.55	Assessments of seismic performance of the damper (Case 7: Hachinohe, PGA=0.25g).....	136
Fig. 5.56	Assessments of seismic performance of the damper (Case 8: Kobe, PGA=0.1g)..	137
Fig. 5.57	Assessments of seismic performance of the damper (Case 9: Kobe, PGA=0.25g)	138



List of Tables

Table 3.1	Parameters and turning points considered for an example of the Ramberg-Osgood Hysteresis Model	35
Table 4.1	Numerical values of parameters for the scaled-down damper	45
Table 4.2	Calculated mechanic properties of the scaled-down damper	45
Table 4.3	Comparison between the experimental and theoretical stiffness for the scale-down damper	54
Table 4.4	Parameters obtained from the component test for the analytical models of the scaled-down damper	55
Table 4.5	Numerical values of parameters in the Ramberg-Osgood Hysteresis Model for the methodology of measuring shear force	55
Table 4.6	Numerical values of parameters for the full-scale damper	61
Table 4.7	Calculated mechanic properties of the full-scale damper.....	61
Table 4.8	The reduction factor and stiffness of the full-scale damper	67
Table 4.9	Comparison between the experimental and theoretical stiffness for the full-scale damper	67
Table 5.1	Detailed properties of the model structure.....	72
Table 5.2	Natural Frequency and Damping Ratio of the Model Structure Extracted from System Identification Analysis	72
Table 5.3	Comparison of Peak Floor Acceleration Responses in the El Centro Series of Tests	102
Table 5.4	Comparison of Root-Mean-Squares Floor Acceleration In the El Centro Series of Tests.....	103
Table 5.5	Root-Mean-Squares of 1st Floor Storydrift In the El Centro Series of Tests	104
Table 5.6	Equivalent Natural Frequency and Damping Ratio of the damper-Protected Model Structure.....	104
Table 5.7	Comparison of Peak Floor Acceleration Responses in the Hachinohe Series of Tests	105
Table 5.8	Comparison of Root-Mean-Squares Floor Acceleration In the Hachinohe Series of Tests.....	106
Table 5.9	Root-Mean-Squares of 1st Floor Storydrift In the Hachinohe Series of Tests	107
Table 5.10	Equivalent Natural Frequency and Damping Ratio of the damper-Protected Model Structure.....	107
Table 5.11	Comparison of Peak Floor Acceleration Responses in the Kobe series Tests	108
Table 5.12	Comparison of Root-Mean-Squares Floor Acceleration for Kobe Series of Tests	109
Table 5.13	Root-Mean-Squares of 1st Floor Storydrift for Kobe Series of Tests.....	110
Table 5.14	Equivalent Natural Frequency and Damping Ratio of the damper-Protected Model Structure.....	110
Table 5.15	Analysis cases defined in SAP2000	113
Table 5.16	Root-mean-square reduction of acceleration responses	120



1

Introduction



1.1 Background

Before human beings understood the origins of such terrifying natural phenomena as diseases and earthquakes, many thought that these phenomena were God's punishment for sin. The germ theory of disease, which was proposed in the late 19th century, provided a physical explanation for the origin of illness. More recently, the genesis of earthquake has also been elucidated in a similar fashion. Most scientists believe that the earth's shell is made up of twelve large, rigid plates (Fig. 1.1) [1]. These plates move at a rate of only a few centimeters a year, but the effect of this movement, earthquake, is spectacular.

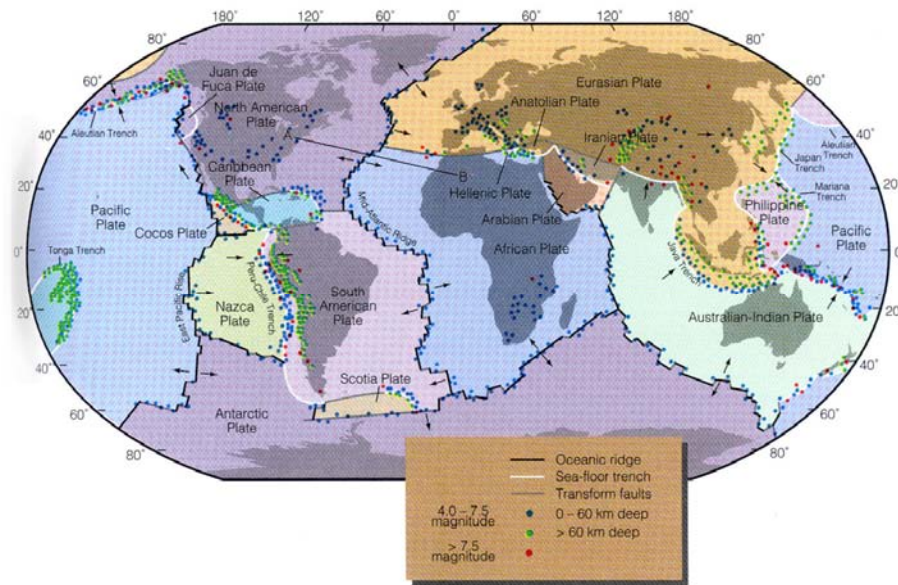


Fig. 1.1 The earth's seismicity outlines plate margins

There is a saying among geologists and engineers that earthquakes don't kill but buildings do. Shaking ground may make people fall down, and falls may break legs and arms, but they don't kill. However, shaking ground can make structures collapse, and collapsing structures can definitely kill [1]. Though this is just an old saying, how to prevent the structures from collapse is a serious and complex problem.

The worst earthquake of the twentieth century occurred on July 28, 1976. At 3:45 A.M., while 1 million inhabitants of Tang Shan, China, slept, a 7.8 magnitude quake leveled the city. Hardly a building was left standing; the few that did withstand the first quake were destroyed by the second, magnitude 7.1, which struck at 6:46 P.M. the same day. Losses were large because most of the buildings had not been constructed to withstand earthquakes [1].

The study of origin of earthquake is the field of earth science, while a branch of civil engineering, Earthquake Engineering, devotes to seeking solutions for protecting people from catastrophes rising from earthquakes. The structural design involving resistance of earthquake is called seismic design. In early years, conventional seismic design practice permits the reduction of design forces below the elastic level on the premise that inelastic action in the structures will provide significant energy dissipation potential which enables them to survive severe earthquakes without collapse [2]. The inelastic action is intended to occur in specially detailed critical regions of the structure, usually in the beams near or adjacent to the beam-column joints. While being able to dissipate earthquake input energy, the inelastic behavior (eg: forming plastic hinge) in these regions also may result in significant damage to the structural members. The structures may survive the earthquake if the inelastic behavior did happen in the way one expected. However, the actual failure pattern of most collapsed or severely damaged structures often was not in that preferable manner, as observed in the 921 Chi-Chi earthquake in Taiwan as well as other major events worldwide. Plastic hinges have never ever been found in the beams due to a substantial increase in rigidity reinforced by the slabs and walls, which in turn minimized the bending curvature of the beams and prevented them from yielding. The actual damage situation contradicts the concepts of traditional seismic design. Without plastic hinges dissipating the earthquake input energy, damages concentrate on the weakest parts of structures, leading to early collapse.

To overcome the inherent shortcomings of the conventional seismic design, a number of innovative approaches have been developed in recent years. Modern seismic structural design, if successfully applied, not only can save people's lives but also minimize the impacts on economy and society in

4 A Theoretical and Experimental Study of Metallic Yielding Damper

severe earthquake. The main idea of modern seismic design is that performances of a structure under different intensity of earthquake are accounted for. To achieve desirable seismic performance, the traditional method of increasing the dimension of structural members for earthquake-resistance is discarded by introducing energy dissipation systems, control systems or seismic isolation systems into the structural design. These systems will be briefly introduced in the next section.



1.2 Structural Protective Systems

By considering the dynamic nature of environmental disturbances, more dramatic improvements in seismic structural design can be realized. New and innovative concepts on structural protection have been advanced and at various stages of development in recent years. Modern structural protective systems can be divided into 3 major groups [3]:

1. Passive Energy Dissipation
2. Seismic Isolation
3. Active / Semi-Active Control

Each group consists of several technologies as shown in Fig. 1.2. These strategies for seismic protection of structures will be introduced briefly.

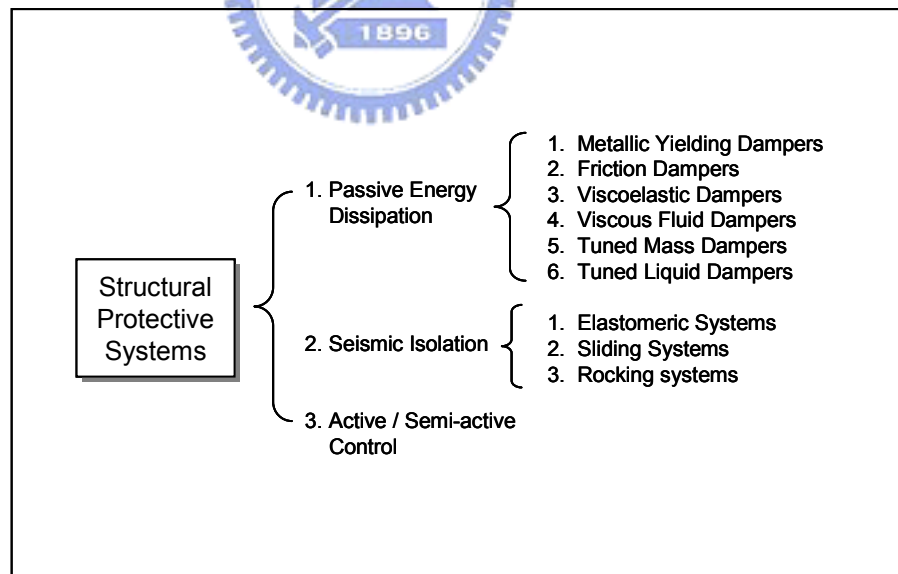


Fig. 1.2 Classification of structural protective systems

1.2.1 Passive Energy Dissipation

A passive energy dissipation system does not require an external power source. Passive energy dissipation devices impart forces that are developed in response to the motion of the structure. The energy in a passively controlled structural system, including the passive devices, cannot be increased by the passive control devices. [4] The basic energy relationship of the structures is represented in the following equation [5]:

$$E_I = E_K + E_S + E_\zeta + E_H \quad (1.1)$$

where

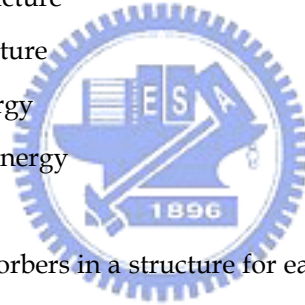
E_I = earthquake input energy

E_K = kinetic energy in structure

E_S = strain energy in structure

E_ζ = viscous damping energy

E_H = hysteretic damping energy



The aim of including energy absorbers in a structure for earthquake resistance is to concentrate hysteresis behavior in specially designed and detailed regions of the structure and to avoid inelastic behavior in primary gravity-load resisting structural members. In other words, the goal is to increase E_H so that, for a given E_I , the elastic strain energy in the structure is minimized. This means that the passively controlled structure will undergo smaller deformations for a given level of input energy than the one without energy dissipators. The major energy dissipation devices available are as follow [4]:

1. Metallic Yielding Dampers
2. Friction Dampers
3. Viscoelastic Dampers
4. Viscous Fluid Dampers
5. Tuned Mass Dampers
6. Tuned Liquid Dampers

Metallic Yielding Dampers One of the effective mechanisms available for seismic energy dissipation is through inelastic deformation of metals. The idea of utilizing added metallic energy dissipators within a structure to absorb a large portion of seismic energy began with the conceptual and experimental work of Kelly et al. (1972) and Skinner et al. (1975). The devices considered included torsional beams, flexural beams, and U-strip energy dissipators (Fig. 1.3). In recent years, a wide variety of such devices have been proposed. Many of these devices use mild steel plates with triangular or hourglass shapes so that yielding is spread almost uniformly throughout the material. A typical X-shaped added damping and stiffness (ADAS) device (Bergman and Goel, 1987 and Whittaker et al. 1991), triangular ADAS (TADAS) (Tsai et al. 1993) and reinforced ADAS (RADAS) (Tsai, 1999) are shown in Fig. 1.4, Fig. 1.5 and Fig. 1.6, respectively.

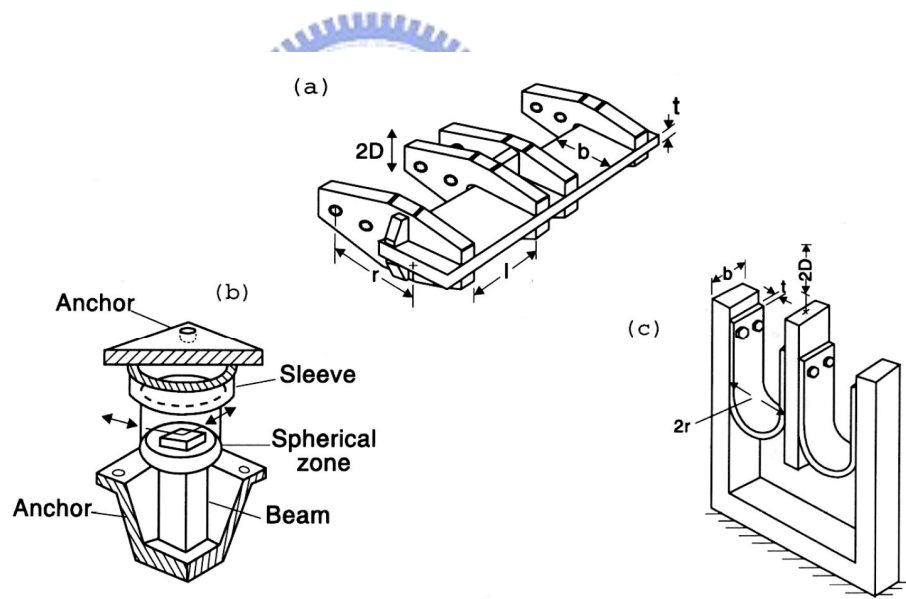


Fig. 1.3 Several metallic yielding devices
(a) Torsional Beam (b) Flexure Beam (c) U-strip

8 A Theoretical and Experimental Study of Metallic Yielding Damper

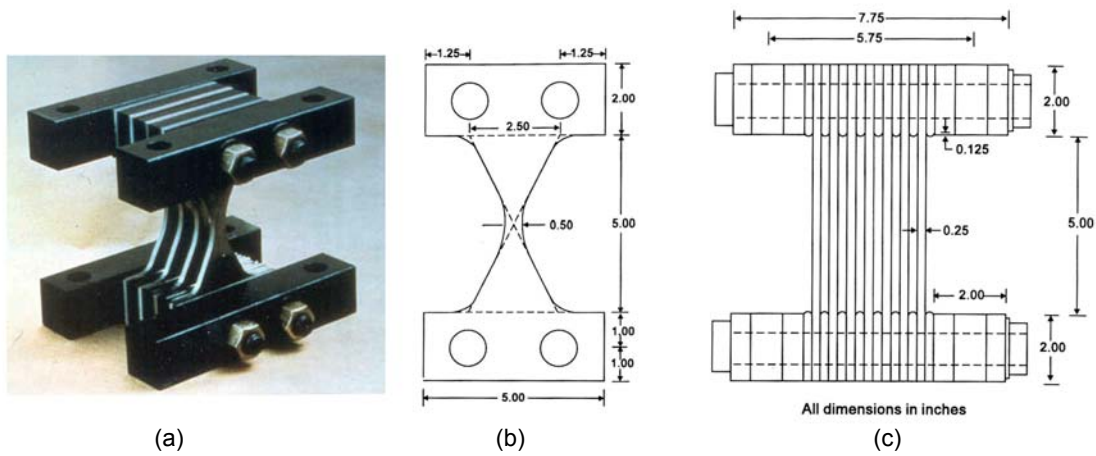


Fig. 1.4 ADAS

- (a) A photo of ADAS Unit (Bergman and Goel, 1987)
 (b) Front view of ADAS element (Whittaker et al. 1991) (c) Side view of ADAS unit

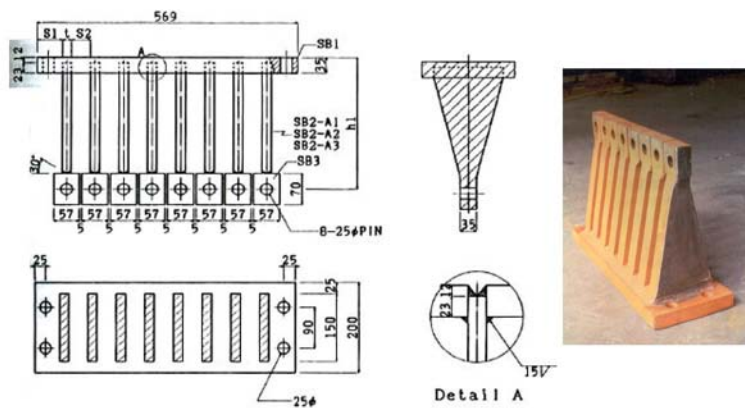


Fig. 1.5 A photo and detailed design of TADAS



Fig. 1.6 A photo of RADAS¹

¹ <http://www.radas-mfps.com.tw/index.htm>

Despite apparent differences in geometric configuration, the underlying energy dissipative mechanism for the above mentioned devices results from inelastic deformation of the metallic elements. Therefore, one must be able to characterize their hysteretic behavior under arbitrary cyclic loading. Ideally, one would hope to develop a model of any metallic device starting from micromechanical theory of dislocations [6]. However, since a direct physics approach is not yet feasible, one normally accepts a macroscopic level of description. Özdemir (1976) was the first to consider the modeling problem of material inelasticity. Shortly later, Bhatti et al. (1978) employed Özdemir's methodology to study the response of structures that used torsional bar dampers along with a seismic base isolation system. Dargush and Soong (1995) developed an inelastic constitutive model for the material of metallic yielding dampers based on a microscopic mechanistic approach and compared it with experimental data for validation. Tsai (1995) developed a finite-element formulation for ADAS and compared the simulation results with experimental data.

The hysteretical behavior of the metallic damper can be obtained via component tests of the device [4]. In case only the strains are measured, a basic form of the nonlinear stress-strain relationship is first selected, and then the related model parameters are determined via curve fitting or a macroscopic mechanical analysis of the device. By this approach, any admissible hysteretic model, such as the bilinear model, may be selected. Ou and Wu (1995) explored the hysteretical behavior of both X-shaped and triangular metallic dampers by employing a bilinear model with parameters related to size and material properties. The ultimate displacements of the devices were also determined.

The earliest applications of metallic yielding dampers to structural systems appeared in South Rangitikei viaduct in New Zealand². The dampers were installed in the pier base to control the rocking action of the bridge. Recently, ADAS devices have been installed in buildings in Italy, USA, Mexico, Japan and Taiwan for earthquake protection.

² <http://trains.wellington.net.nz/bridges.html>

Friction Dampers Friction provides another means of energy dissipation which has been utilized for years in automotive brakes to dissipate kinetic energy of motion. In structural engineering, a wide variety of devices differing in mechanical complexity and materials have been proposed and studied. Most friction damper utilizes interfaces of steel on steel, brass on steel, or graphite impregnated bronze on stainless steel. Composition of the interface is of great importance to insure longevity of the devices. A friction device developed by Pall (1982) is shown in Fig. 1.7 [4].

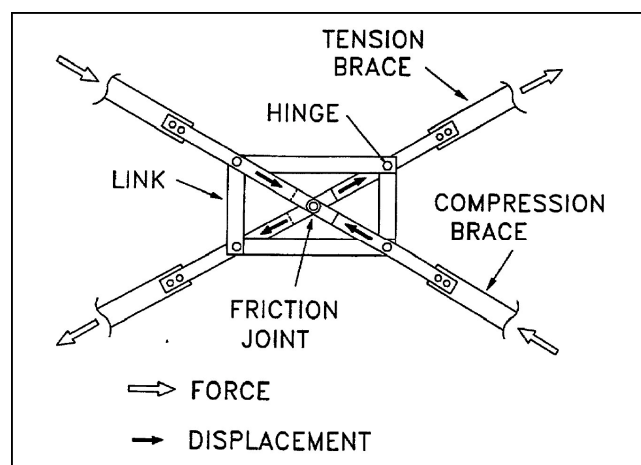


Fig. 1.7 Pall Friction Device

Viscoelastic Dampers The metallic and frictional devices are primarily intended for seismic application. Some viscoelastic solid materials, on the other hand, are used for dissipating energy at all deformation levels that allows them for both wind and seismic protection [4].

The application of viscoelastic materials to vibration control dates back to the 1950s for aircrafts as a means of controlling the vibration-induced fatigue in airframes. Their application to civil engineering structures appear in 1969 for the former World Trade Center in New York where approximately 10,000 viscoelastic dampers were installed in each of the twin towers to reduce wind-induced vibrations.

A typical viscoelastic damper, developed by the 3M Company Inc., is shown in Fig. 1.8. It consists of viscoelastic layers bonded in between steel plates. It is worthwhile pointing out that the viscoelastic material is linear over

a wide range of strain provided that the temperature is constant. At large strains, there is a considerable self-heating due to a large amount of energy dissipated. The generated heat changes the mechanical properties of the material, and the overall behavior becomes nonlinear and deteriorated.

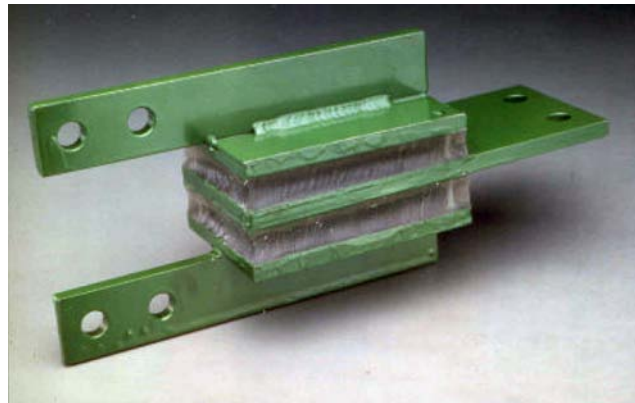


Fig. 1.8 A viscoelastic damper

Viscous Fluid Dampers Fluids can also be used for energy dissipation. Numerous configurations and materials have been considered for such type of devices. One class involves the use of a cylindrical piston immersed with viscoelastic fluid. Such systems have been studied both experimentally and analytically by Makris et al. (1993). Another device referred to as the viscous damping wall, again use viscoelastic fluid (Arima et al. 1988; Miyazaki and Mitsuaka 1992) [4].

Viscous fluid dampers widely used in aerospace and military applications recently have found applications in structural engineering (Constantinou et al. 1993). Characteristics of these devices that are of primary interest in structural applications are the linear viscous response achieved over a broad frequency range, insensitivity to temperature and compactness in terms of small stroke requirement with considerable output force.

It should be pointed out that most, if not all, viscous fluid dampers currently in use have a force-velocity relationship of the form $F = C|V|^\alpha \text{sgn}(V)$ where F is the damping force, C is dependent on ambient temperature, V is the relative velocity in between the damper, and α is an exponent in the range $0.3 \leq \alpha \leq 0.75$. Major advantages of this type of nonlinear dampers are that the force builds up fast at small velocity

and tends to flatten out at higher velocities. A typical fluid damper is shown in Fig. 1.9³.



Fig. 1.9 A Fluid Damper

Tuned Mass Dampers Tuned mass damper (TMD), first proposed by Frahm [7], as a secondary system to control the primary structure generally consists of a mass block with damping and tuning elements. The frequency of a TMD system is tuned by adjusting the stiffness of the spring (sliding type) or the arm length of the suspension cable (pendulum type) [8] to be in near-resonance with the primary structure. As a result, a considerable vibrating energy can be transferred from the primary structure to the TMD system and then dissipated via the damping mechanism of its own. In general, the TMD system is effective in the control of wind-induced structural vibrations. Many well-known skyscrapers, such as the Citibank in New York, the John Hancock Tower in Boston⁴, the CN Tower in Toronto⁵, and Taipei 101 in Taipei (Fig. 1.10) adopt TMD for wind-resistance.



(a)



(b)



(c)



(d)

Fig. 1.10 Buildings installed with TMD

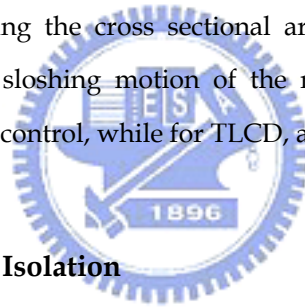
(a) John Hancock Tower in Boston (b) CN Tower
(c) TMD in Taipei 101 (d) Taipei 101

³ <http://www.e-structures.com/viscous.html>

⁴ <http://www.bluffton.edu/HomePages/FacStaff/sullivanm/peihancock/peihancock.html>

⁵ From a postcard

Tuned Liquid Dampers Conceptually similar to a TMD system, Tuned Liquid Damper (TLD) has been increasingly used in high-rise buildings for wind or earthquake induced vibration control [9,10]. The TLD can be integrated with the existing fire-suppress hydraulic tower and therefore considered a substitution of the TMD for economic reasons. The TLD can be further classified into the Tuned Sloshing Water Damper (TSWD) and the Tuned Liquid Column Damper (TLCD)[11-17]. The frequency of the TSWD is adjusted by changing the depth of the storage water as well as the geometry of the tank. Damping of the TSWD is produced via steel wire nets across the water passage, through which turbulent flow is generated and energy dissipated. While the frequency of the TLCD depends only on the total length of the water in the U-shape container, and damping of the TLCD due to headloss of the water is introduced by changing the dimension of the orifice (valve) or adjusting the cross sectional area of the U-shape container. For TSWD, only the sloshing motion of the near-surface portion of the water contributes in the control, while for TLCD, all the water is effective.



1.2.2 Seismic Isolation

Seismic isolation systems may be further classified into 3 categories: [18]

1. Elastomeric Systems
2. Sliding Systems
3. Rocking systems

Elastomeric Systems With lateral flexibility and vertical rigidity, elastomeric bearings may shift (lengthen) the natural period of the structure away from the predominant period of the ground motion (stiff soil conditions) to reduce earthquake forces. By introducing either the damping-enhanced rubber or supplemental energy dissipative components, the seismic isolation system may avoid excessive bearing displacement during severe earthquakes. The elastomeric bearings that have seen widespread applications include the lead-rubber bearing (LRB) and high-damping rubber bearing (HDRB) [19-21].

Sliding Systems Sliding systems reduce seismic forces via the friction mechanism between the sliding interfaces. The sliding-type bearings in its original form, however, are impractical due to lack of restoring capability. To overcome this problem, the friction pendulum system (FPS) introduces a spherical sliding interface to provide restoring stiffness with the friction mechanism playing the role of energy dissipation. As a result, FPS is functionally equivalent to LRB and HDRB in altering the structure's fundamental period. Made of stainless steel, the properties of FPS are less sensitive to aging and temperature. The bearing's high strength and rigidity make them compact in size, which may further reduce the installation cost. With versatile features of period-invariance, torsion-resistance, temperature-insensitivity and durability, FPS meets the diverse requirements of seismic isolation for buildings, bridges and industrial facilities [22-32].

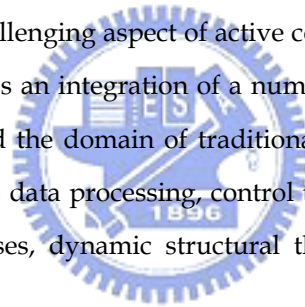
Rocking Systems Rocking mechanism is another means of seismic isolation, although it is rarely conceived this way. With a discontinuous interface between the columns and the underlying foundation, the rocking system is allowed to rock intermittently as the seismic overturning moment exceeds the restoring moment contributed by gravity. The boundary condition at the footing changes from being "fixed" to "hinging" as soon as the uplift occurs, accompanied with a sudden release from the moment-resisting status as a consequence. The earthquake load is then counteracted by the rotational inertia of the structure with respect to the supporting foot. In other words, the rocking mechanism provides a unique means to filter out earthquake energy. Rocking system is particularly effective in reducing the seismic loads and deformations of structures with heavy superstructure such as water tanks supported by tower or bridges with tall and slender pier (Priestley et al. 1996). The concept of rocking mechanism has been adopted for a railway bridge (Beck and Skinner 1974) and industrial chimney in New Zealand (Sharpe and Skinner 1983). Recently, utilization of rocking mechanism for earthquake protection of bridge structures has become a renewed interest (Mander and Cheng 1997, Wang et al. 2001).

1.2.3 Active / Semi-Active Control System

An active control system is one in which an external source powers control actuator(s) that apply forces to the structure in a prescribed manner. These forces can be used to both add and dissipate energy in the structure. In an active feedback control system, the signals sent to the control actuators are functions of the response of the system measured with vibration sensors [4].

Semi-active control systems are a class of active control system for which the external energy requirements are smaller than those for typical active control systems. Typically, semi-active control system devices do not add mechanical energy to the structural system (including the structures and the controlling actuators), therefore bounded-input bound-output stability is guaranteed. Semi-active control devices are often viewed as controllable passive devices.

The most challenging aspect of active control research in civil engineering is the fact that it is an integration of a number of diverse disciplines, some of which are beyond the domain of traditional civil engineering. These include computer science, data processing, control theory, material science, as well as stochastic processes, dynamic structural theory, and wind and earthquake engineering.



1.3 The Organization

Chapter 1 The modern structural protective systems including energy dissipation systems, control systems and seismic isolation systems have been introduced briefly.

Chapter 2 The fundamentals of the metallic yielding damper including determination of stiffness, yielding displacement, yielding load and design considerations have been introduced in this chapter.

Chapter 3 A novel methodology for measuring the moment and shear force of the metallic yielding damper based on strain measurement and Ramberg-Osgood Hysteresis Model is developed. A table searching method is proposed to overcome numerical difficulties due to the high nonlinearity of equations in this model.

Chapter 4 Component tests for both full-scale and scaled-down dampers have been tested independently. The first objective of the component tests is to investigate the characteristics of individual unit under cyclic loadings. The second one is to verify the measuring methodology for moment and shear via strain measurement. The final one is to determine the parameters of the damper for the analytical models characterizing the inelastic behavior to be used by SAP2000.

Chapter 5 In order to assess the effectiveness and feasibility of the damper through the earthquake, a series of shaking table test have been conducted. The analytical SAP2000 models are established to simulate the responses of structures under various earthquakes scenarios. The simulating results are compared with the experimental ones.

Chapter 6 Based on the testing results, the conclusions are drawn in this chapter.

2

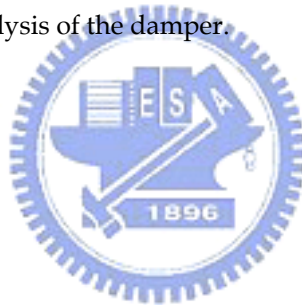
Fundamentals of Metallic Yielding Damper



2.1 Introduction

Metallic yielding damper is an earthquake protective device that dissipates earthquake energy through inelastic deformation of steel plates. Each of its plates is tailored into an optimum shape (X-shape) to maximize its energy dissipative capacity. The damper can be designed to yield at moderate deformation so as to protect the structure at early stages. If the dampers are tactfully sized and allocated, both the acceleration and displacement responses of the structure can be simultaneously reduced during severe earthquake.

In this chapter, fundamentals of the X-shaped metallic yielding damper will be introduced. These include the determination of stiffness, yielding displacement, yielding loads and design considerations. This chapter is concluded with a parametric analysis of the damper.



2.2 Theoretical Derivations

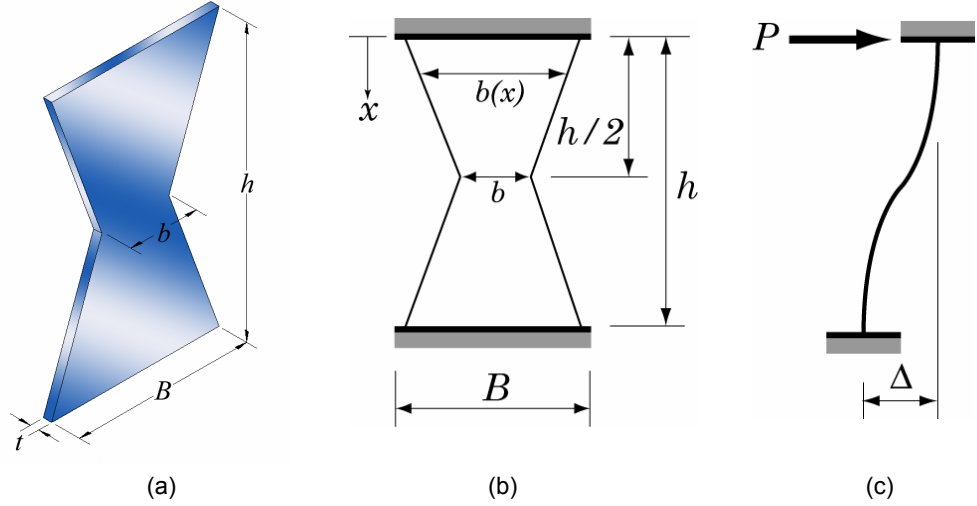


Fig. 2.1 X-shaped metallic yielding damper

(a) 3-D view of a single plate of the metallic yielding damper
 (b) Front view (c) Side view of the deformed plate

A 3-D view of a single plate of the metallic yielding damper is shown in Fig. 2.1(a) where B , h , t and b are the end width, effective height, thickness and the narrowest width (neck) of the plate, respectively. Defining the x -coordinate as in Fig. 2.1(b), one can express the cross-sectional width at any arbitrary distance x from its upper end for the upper half of the plate as

$$b(x) = B + \frac{2}{h}(b - B)x, \quad 0 \leq x \leq \frac{h}{2} \quad (2.1)$$

The corresponding cross-sectional area and moment of inertia about the neutral axis of the area are, respectively,

$$A(x) = b(x)t = \left[B + \frac{2}{h}(b - B)x \right] t, \quad 0 \leq x \leq \frac{h}{2} \quad (2.2)$$

$$I(x) = \frac{1}{12} b(x)t^3 = \frac{1}{12} \left[B + \frac{2}{h}(b - B)x \right] t^3, \quad 0 \leq x \leq \frac{h}{2} \quad (2.3)$$

The moment on the cross-section at a distance x from the upper end can be obtained from equilibrium as

$$M(x) = \frac{P}{2}(h - 2x) = \frac{Ph}{2} \left(1 - \frac{2x}{h}\right) \quad (2.4)$$

where P is the lateral force acting on the upper end.

The curvature of the plate in bending can be expressed, in accordance with mechanics of materials, as

$$\kappa(x) = \frac{M(x)}{EI(x)} = \frac{6Ph(h - 2x)}{E[Bh + 2(b - B)x]t^3} \quad (2.5)$$

where E is the Young's Modulus of the material and κ denotes the curvature. This equation shows that the curvature is directly proportional to the bending moment and inversely proportional to flexural rigidity, EI , which is a measure of the member's resistance to bending.

Idealized X-shaped Damper First we consider the idealized X-shaped plate whose neck width reduces to 0, assuming E to be constant, then Eq. (2.5) can be reduced to

$$\lim_{b \rightarrow 0} \kappa(x) = \frac{6Ph}{EBt^3} = \text{const.} \quad (2.6)$$

This equation shows that the curvature of each cross-section all over the damper is identical, meaning that the yielding initializes and develops simultaneously at all cross-sections.

Taking both the flexural and shear strain deformation into account, one can express the total strain energy in the plate as it deforms (Fig. 2.1(c)) to be

$$U = 2 \left(\frac{1}{2} \int_0^{\frac{h}{2}} \frac{[M(x)]^2}{EI(x)} dx + \frac{1}{2} \int_0^{\frac{h}{2}} \frac{[V(x)]^2}{2\beta GA(x)} dx \right) \quad (2.7)$$

in which β is the shape factor taken as $\frac{5}{6}$ for rectangular cross-section.

As the damper is subjected to the lateral force P (Fig. 2.1(b)), the deformation due to this force can be found by using Castigliano's Theorem as follow:

$$\Delta = \frac{\partial U}{\partial P} = 2 \left[\int_0^{\frac{h}{2}} \frac{[M(x)] \left[\frac{\partial M(x)}{\partial P} \right]}{EI(x)} dx + \int_0^{\frac{h}{2}} \frac{[V(x)] \left[\frac{\partial V(x)}{\partial P} \right]}{2\beta G A(x)} dx \right] \quad (2.8)$$

Carrying out the integration, one gets

$$\Delta = P \left\{ \frac{3h^3 [4Bb - 3b^2 - B^2 + 2b^2 \ln(bh) - 2b^2 \ln(Bh)]}{2Et^3 (b - B)^3} + \frac{h(\ln b - \ln B)}{2\beta Gt(b - B)} \right\} \quad (2.9)$$

Consequently, the elastic stiffness of the damper is given by

$$k_d = \frac{P}{\Delta} = \frac{1}{\frac{3h^3 [4Bb - 3b^2 - B^2 + 2b^2 \ln(bh) - 2b^2 \ln(Bh)]}{2Et^3 (b - B)^3} + \frac{h(\ln b - \ln B)}{2\beta Gt(b - B)}} \quad (2.10)$$

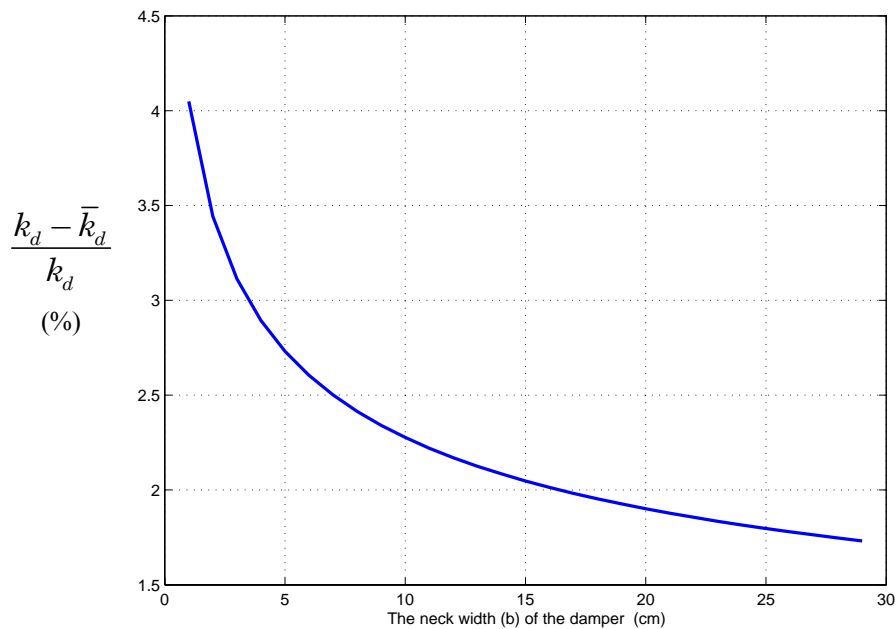
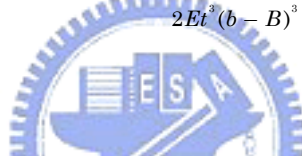


Fig. 2.2 Error of neglecting shear deformation on stiffness

If we neglect the effects of shear deformation, the right term of the dominator in Eq. (2.10) vanishes. Thus, the elastic stiffness can then be written as

$$\bar{k}_d = \frac{2Et^3(b-B)^3}{3h^3[4Bb - 3b^2 - B^2 + 2b^2 \ln(bh) - 2b^2 \ln(Bh)]} \quad (2.11)$$

For a given neck width of the damper, difference between the stiffness calculated by using the exact stiffness (Eq. (2.10)) and the simplified one (Eq. (2.11)) ranges from 1.5%~4.5%, as shown in Fig. 2.2. In other words, the effect of shear deformation on overall stiffness is insignificant and can therefore be neglected.

By further considering the neck width to be zero, for simplicity, the elastic stiffness for one single plate of the X-shaped metallic yielding damper can be simplified as

$$k'_d = \frac{2EBt^3}{3h^3} \quad (2.12)$$

The elastic stiffness for a unit consisting of N identical plates in parallel can be calculated as follows:

$$k'_d = \frac{2NEBt^3}{3h^3} \quad (2.13)$$

The yielding moment in the upper or lower end is

$$M_y = \frac{\sigma_y I_{x=0}}{\frac{h}{2}} = \frac{\sigma_y Bt^2}{6} \quad (2.14)$$

where σ_y is the yielding stress of the material of the plate. The yielding load, P_y , can then be found by dividing the yielding moment by half of the height of the damper. That is,

$$P_y = \frac{M_y}{\frac{h}{2}} = \frac{\sigma_y Bt^2}{3h} \quad (2.15)$$

The plastic moment, M_p , at the upper or lower end is 1.5 times that of the yielding moment for rectangular X-sections, and plastic load, P_p , can in turn be calculated as

$$P_p = \frac{M_p}{\frac{h}{2}} = \frac{1.5M_y}{\frac{h}{2}} = \frac{\sigma_y Bt^2}{2h} \quad (2.16)$$

Finally, the idealized yielding displacement can be calculated by the following equation:

$$\Delta'_y = \frac{P_y}{k'_d} = \frac{\sigma_y h^2}{2Et} \quad (2.17)$$

2.3 Design Considerations

To avoid undesired shear failure of the damper at the neck prior to full development of the ultimate flexural strength, a minimum width of the neck is required. If the ultimate lateral force is considered as 1.5 times the plastic load, the following inequity should be met to ensure that the shear strength of the damper is sufficient, i.e.,

$$S_s \geq P_u = 1.5P_p \quad (2.18)$$

where P_u and S_s are the ultimate load and shear strength of the damper, respectively. The shear strength equals to the cross-sectional area multiplied by the allowable stress, taken as 0.55 times the yielding stress, that is,

$$S_s = 0.55 \sigma_y bt \quad (2.19)$$

Combining Eq. (2.16), (2.18) and (2.19), the minimum neck width of the damper can be determined as follows:

$$b \geq 1.36 \frac{Bt}{h} \quad (2.20)$$

2.4 Parametric Analysis

It is observed from the analysis in the previous section that the elastic stiffness and yielding displacement of the metallic yielding damper depend on height-to-thickness ratio (h/t) of the damper. The differences between the exact stiffness, Eq. (2.11), and the idealized one, Eq. (2.13), can be revealed by performing parametric analyses.

The stiffness ratio (k_a/k'_a) with respect to the height-to-thickness ratio is plotted in Fig. 2.3 for various safety factor (SF) defined as

$$SF = \frac{b/t}{1.36 t/h} \quad (2.21)$$

The difference between the exact stiffness and idealized one decreases with height-to-thickness ratio increased.

The idealized formula underestimates the stiffness of the damper as the neck width of the damper becomes large (i.e. higher safety factor in design). Generally speaking, it is recommended to adopt a height-to-thickness ratio of 10 ~ 15 in practical design so that the stiffness ratio (k_a/k'_a) will range from 1.2 to 1.5 while the safety factor is taken as 2 to 4.

SF taken as 6, the relation between the stiffness ratio and the height-to-thickness ratio is shown in Fig. 2.4. The results show that the difference between exact stiffness and the idealized one is insignificant while the height-to-thickness ratio of the damper is larger than 10, which meets the suggested value to be adopted in practical design.

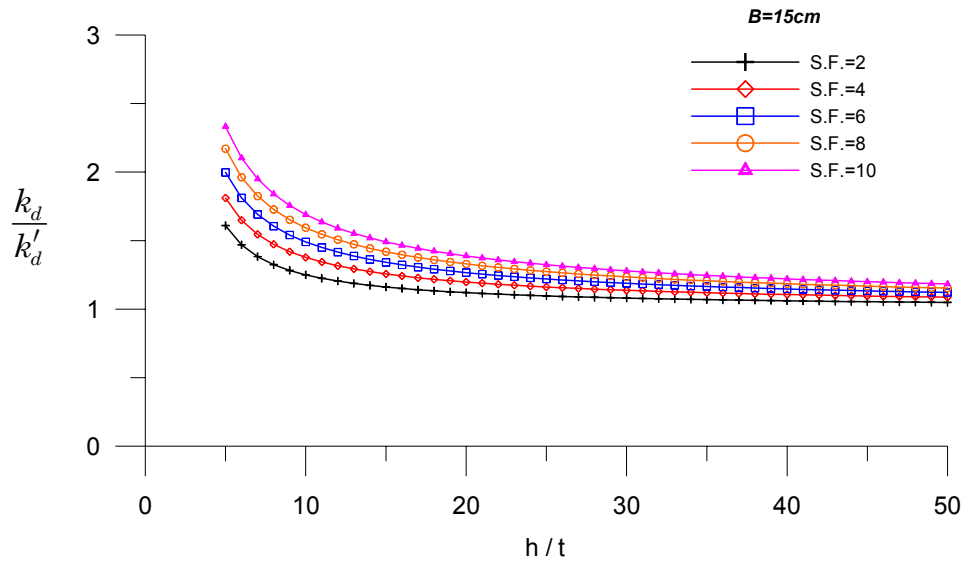


Fig. 2.3 Stiffness ratio (k_d/k'_d) with respect to height-to-thickness ratio (h/t) for various safety factors (SF)

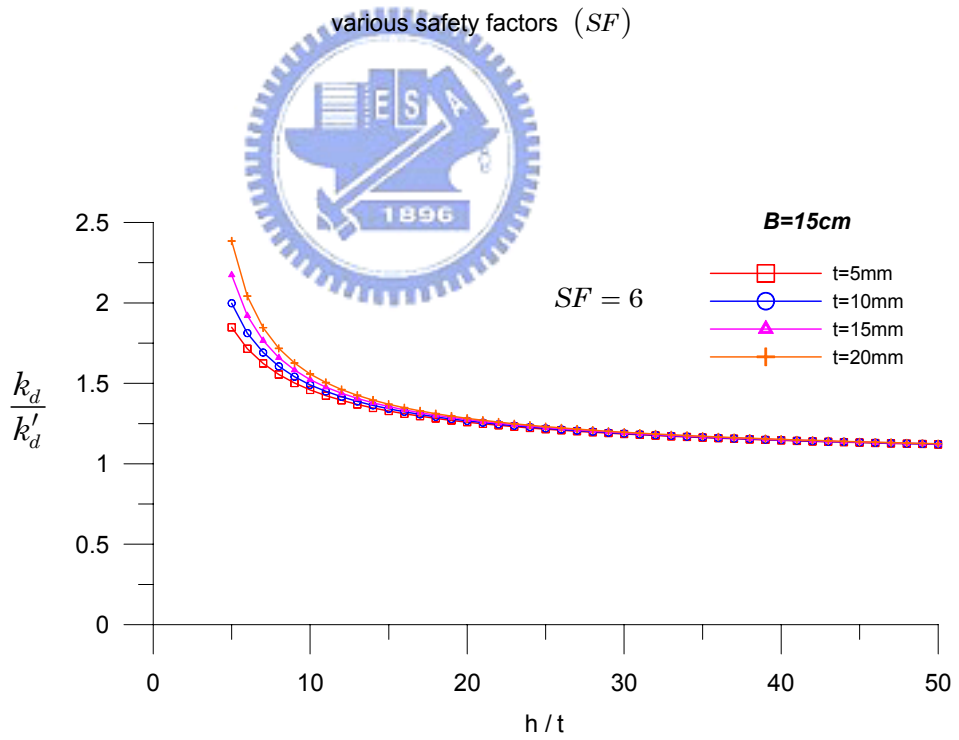


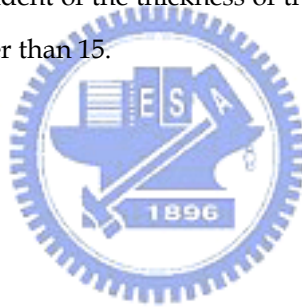
Fig. 2.4 Stiffness ratio (k_d/k'_d) with respect to height-to-thickness ratio (h/t) for various thicknesses (t)

The relationship between the yielding displacement and height-to-thickness ratio is plotted in Fig. 2.5. The results show that the yielding displacement increases as height-to-thickness ratio becomes large under a given thickness of the damper. In addition, yielding displacement depends on the height-to-thickness ratio and the height, meaning that yielding displacement is larger as the height of the damper increases for a given height-to-thickness ratio.

The exact yielding displacement is defined as

$$\Delta_y = \frac{P_y}{k_d} \quad (2.22)$$

The relationship between the yielding displacement ratio (Δ_y/Δ'_y) and height-to-thickness (h/t) ratio is shown in Fig. 2.6. It is observed that yielding displacement is independent of the thickness of the damper when the height-to-thickness ratio is greater than 15.



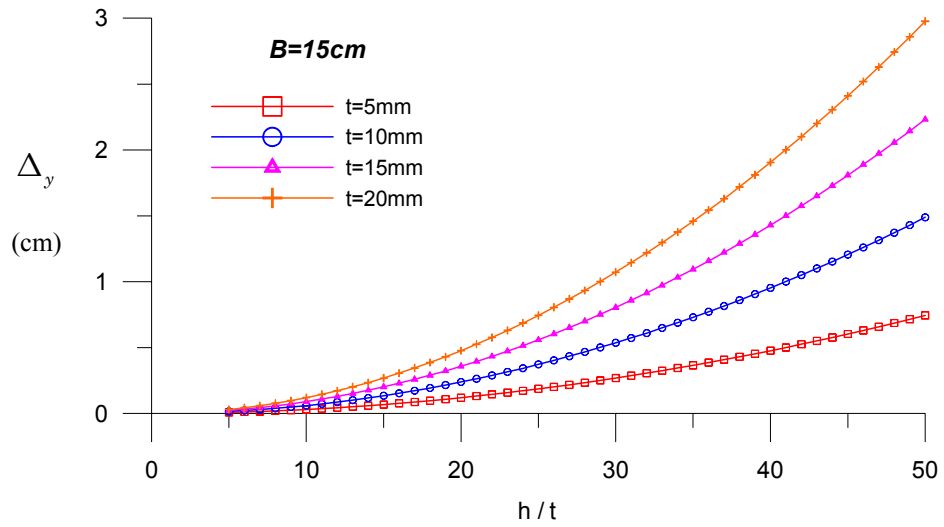


Fig. 2.5 Yielding displacement with respect to height-to-thickness ratio (h/t) for various thicknesses of the damper

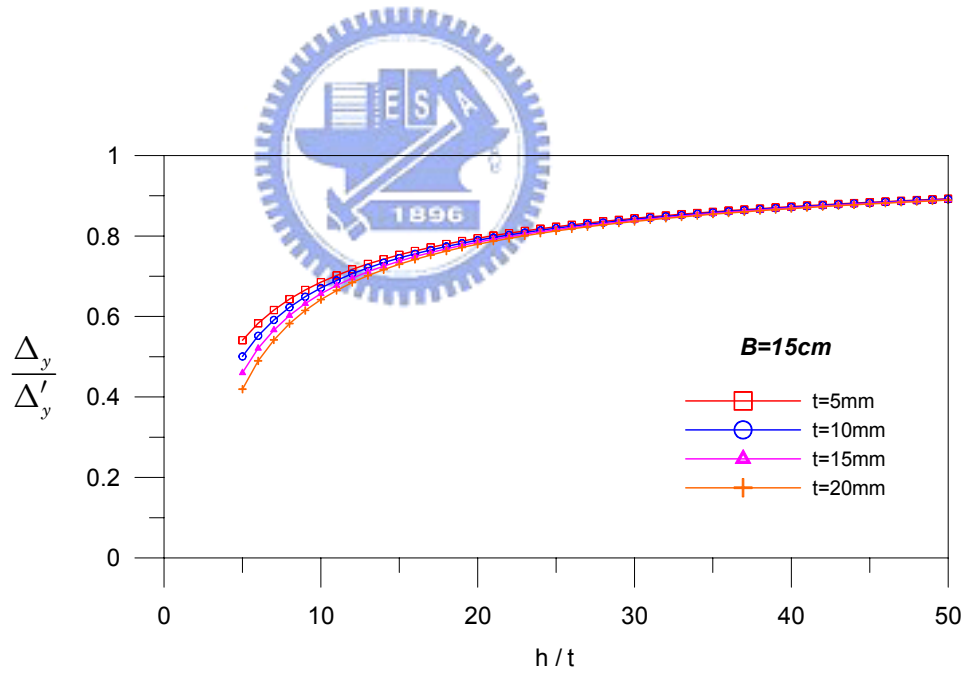


Fig. 2.6 Height-thickness ratio (h/t) with respect to yielding displacement ratio (Δ_y/Δ'_y) for various thicknesses of the damper



3

Development of Measuring Methodology for Moment and Shear via Strain Measurement



To explore the behavior of metallic energy dissipators, characterization of the inelastic stress-strain (or load-displacement) relationship of metals under cyclic loading is demanded. Several mathematical models have been introduced to describe the stress-strain relationship among which the bilinear strain hardening model, the elastoplastic model and the Ramberg-Osgood model shown in Fig. 3.1 are most commonly adopted [33]. In this study, the Ramberg-Osgood Hysteresis Model is employed to describe the stress-strain relationship of the metallic yielding damper.

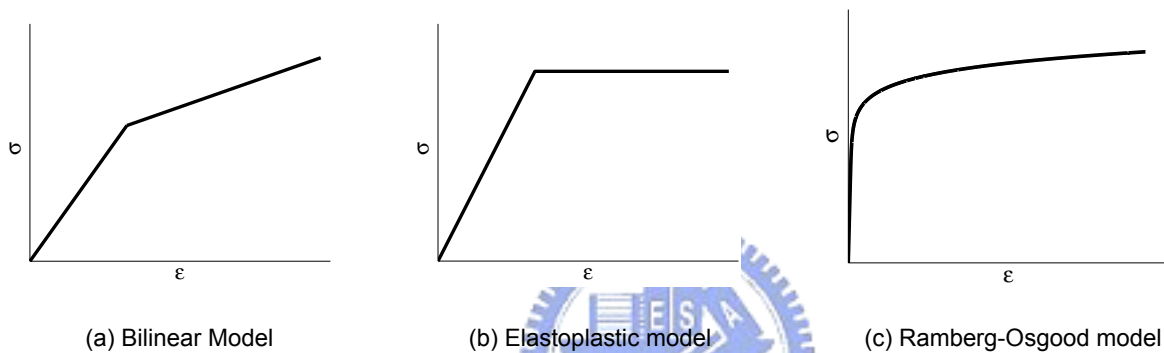


Fig. 3.1 Common mathematical models for stress-strain relationship

In deriving the hysteresis of a metallic yielding damper in component tests, usually the reacting force of the actuator is measured with a build-in loadcell from a displacement-controlled cyclic loading test. However, it is impractical to implement loadcells, regardless of axial or shear types, for monitoring the actual performance of the damper on site.

In this chapter, a methodology for estimating the moment and shear force of the metallic yielding damper based on strain measurement and Ramberg-Osgood Hysteresis Model is developed. A complete procedure for proposed methodology will be presented.

3.1 Ramberg-Osgood Hysteresis Model

3.1.1 Single-loop Model

The stress-strain relationship for several metals, including steel, aluminum and magnesium, can be accurately represented by Ramberg-Osgood equation:

$$\frac{\varepsilon}{\varepsilon_0} = \frac{\sigma}{\sigma_0} + \alpha \left(\frac{\sigma}{\sigma_0} \right)^n \quad (3.1)$$

where ε and σ are the strain and stress, respectively, and α , n , σ_0 and ε_0 are constants to be determined from tension test of the material of the device. σ_0 is the proportional (elastic) limit of the material and ε_0 is the strain corresponding to σ_0 [33].

However, Eq. (3.1) alone is not sufficient for describing the inelastic behavior in cyclic or arbitrary loading conditions where loading and unloading processes occur alternately. A more complete model that traces the unloading and reloading paths of the inelastic behavior has been proposed by Ing and Dorka [34] as

$$\frac{\varepsilon_A - \varepsilon}{2\varepsilon_0} = \frac{\sigma_A - \sigma}{2\sigma_0} + \alpha \left(\frac{\sigma_A - \sigma}{2\sigma_0} \right)^n \quad (3.2)$$

and

$$\frac{\varepsilon - \varepsilon_B}{2\varepsilon_0} = \frac{\sigma - \sigma_B}{2\sigma_0} + \alpha \left(\frac{\sigma - \sigma_B}{2\sigma_0} \right)^n \quad (3.3)$$

where ε_A and ε_B are strains of point A and B, respectively, while σ_A and σ_B are stresses at the turning point A and B, respectively (see Fig. 3.2 for a typical single-loop Ramberg-Osgood Hysteresis Model). These two equations combined with Eq. (3.1) for the initial path of the loading constitute a complete hysteresis model. The first equation (the blue line) defines the initial curve starting from the origin. The second (the red line) and third equations (the green line) define the unloading and reloading curves, respectively. These curves actually form a "loop" of the hysteresis.

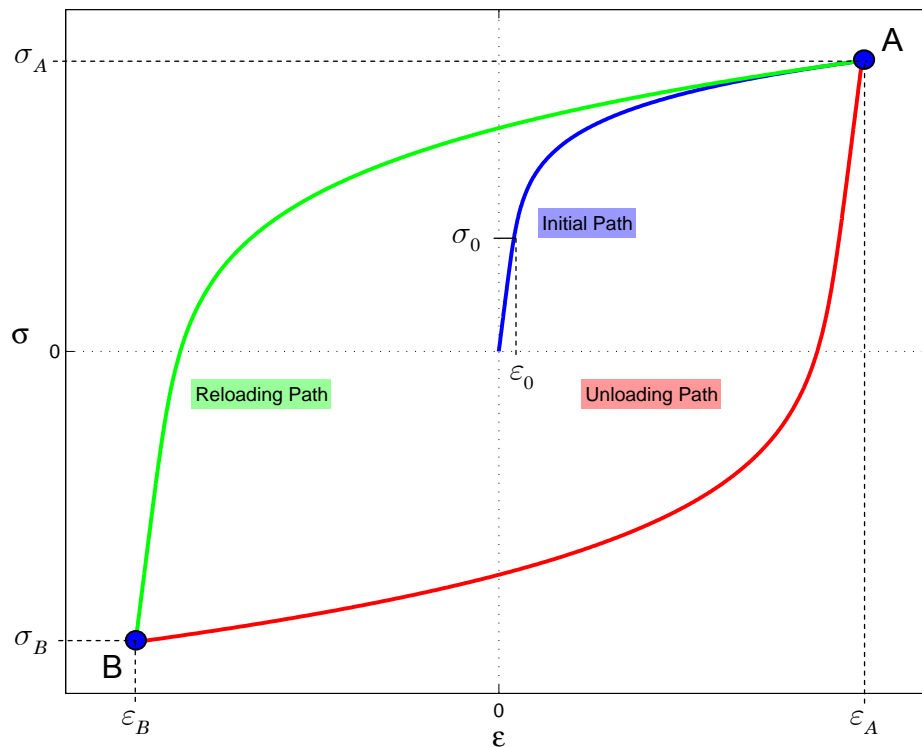


Fig. 3.2 Typical single-loop Ramberg-Osgood Hysteresis Model

Turning points of the hysteresis are points at which the consecutive governing equations intersect. They are the starting point for generating the Ramberg-Osgood Tables for the path. The strain and stress at turning points are always the local extreme values in the corresponding path.

One may encounter numerical difficulties in determining the stress for a given strain by one of Eq. (3.1)~(3.3) due to high nonlinearity of these equations. Numerical methods such as the Newton-Raphson method and the Secant Method commonly adopted fail to solve the equations for convergence problems due to significant difference in order between the stress and strain [35]. In order to overcome numerical difficulties, a table searching method is proposed in this study.

To facilitate programming by the proposed table searching method, an alternative form of the model is first derived as

$$\varepsilon = \frac{\sigma}{E} + \frac{\sigma_0 \alpha}{E} \left(\frac{\sigma}{\sigma_0} \right)^n \quad (3.4)$$

$$\varepsilon = \varepsilon_A - \frac{\sigma_A - \sigma}{E} - \frac{2\sigma_0 \alpha}{E} \left(\frac{\sigma_A - \sigma}{2\sigma_0} \right)^n \quad (3.5)$$

$$\varepsilon = \varepsilon_B + \frac{\sigma - \sigma_B}{E} + \frac{2\sigma_0 \alpha}{E} \left(\frac{\sigma - \sigma_B}{2\sigma_0} \right)^n \quad (3.6)$$

in which $E = \sigma_0 / \varepsilon_0$ is the modulus of elasticity in the initial portion of the stress-strain curve. Therefore, the strain can be obtained directly for a given stress from one of Eq. (3.4) ~ Eq. (3.6) provided that all the parameters are given and the turning points are identified. Once the turning points are specified, the Ramberg-Osgood Table for the unloading and reloading path can be generated according to Eq. (3.5) and Eq. (3.6), respectively. Note that the initial path needs no turning point for generating the table.

The inelastic relationship between strain and stress is path-dependent and not a one-to-one mapping as governed by Eq. (3.4) ~ Eq. (3.6). One can determine the corresponding stress of a given strain by searching the table only when a certain path is specified.

It has become an industrial practice to use the stress corresponding to 0.002 as the equivalent yielding stress. The stress-strain relationship takes the form [36]

$$\varepsilon = \frac{\sigma}{E} + 0.002 \left(\frac{\sigma}{\sigma_0} \right)^n \quad (3.7)$$

Comparing Eq. (3.7) with Eq. (3.4), one can write

$$\alpha = 0.002 \frac{E}{\sigma_0} \quad (3.8)$$

As an illustration, a single-loop Ramberg-Osgood Hysteresis Model is plotted in Fig. 3.3 by assigning numerical values to the parameters and specifying turning points in the equations (Table 3.1). These parameters are

supposed to be obtained from tension tests for the materials and are suggested by Rasmussen [36]. Note that the turning points depend on the loading path, not necessarily any specific values or symmetric.



Table 3.1 Parameters and turning points considered for an example of the Ramberg-Osgood Hysteresis Model

Parameters		Numerical Value
σ_0		250 MPa
E		198 GPa
α		1.584
n		6.37
Turning Points		
A	σ_A	360 MPa
	ε_A	0.022226
B	σ_B	-360 MPa
	ε_B	-0.022226

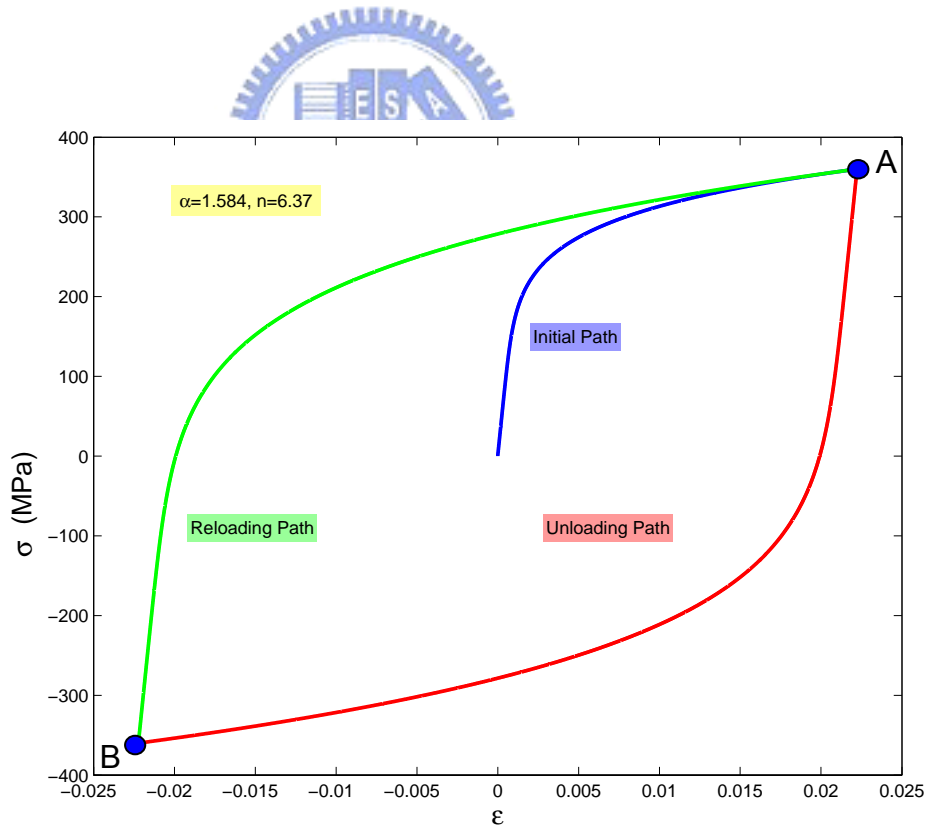


Fig. 3.3 Illustration of a single-loop Ramberg-Osgood Hysteresis Model

3.1.2 Multiple-loop Model

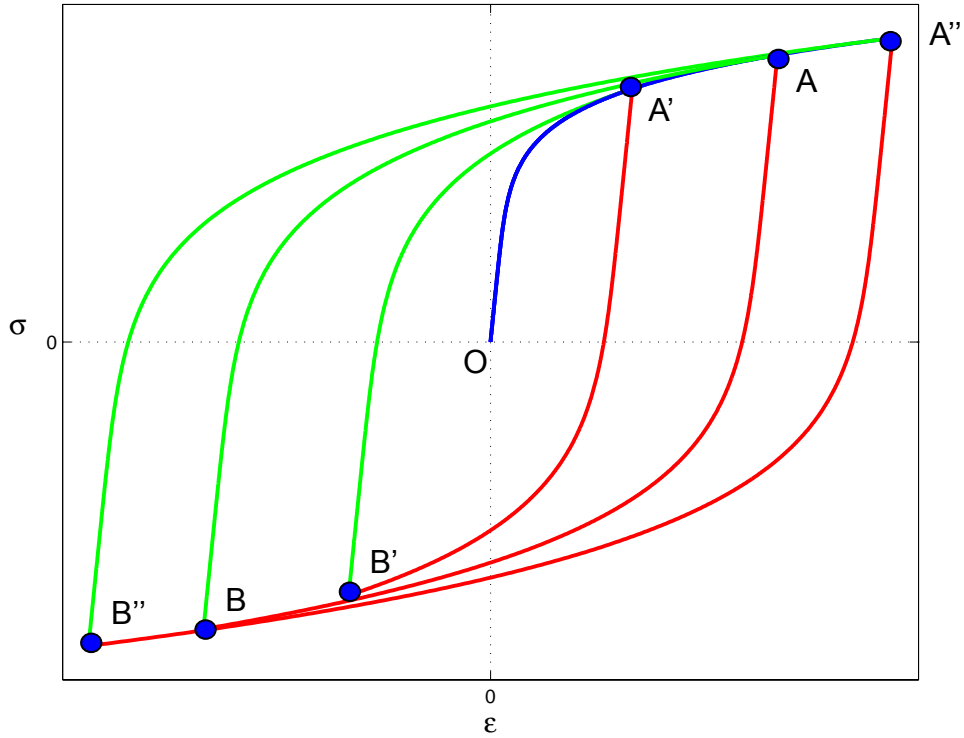


Fig. 3.4 Typical multiple-loop Ramberg-Osgood Hysteresis Model

As in a cyclic loading situation, turning points are path-dependent and the multiple-loops Ramberg-Osgood Hysteresis Model (Fig. 3.4) are generated by substituting different values of strains (ε_A 's, ε_B 's) and stresses (σ_A 's, σ_B 's) at turning points into Eq. (3.2) and (3.3). It is possible that the strain at the second turning point be larger (point A'') or smaller (point A') than that at the first turning point (point A). Therefore, assuming that B is always reached earlier than B' and B'', there would be two possible paths for the model in Fig. 3.4:

1. $O \rightarrow A \rightarrow B \rightarrow A' \rightarrow B' \rightarrow A'' \rightarrow B'' \rightarrow end$
2. $O \rightarrow A \rightarrow B \rightarrow A'' \rightarrow B' \rightarrow A' \rightarrow B'' \rightarrow end$

This illustrates the path-dependence of the relationship between strain and stress. The real path is determined by the identified turning points of the measured strain data from component tests for the damper.

3.1.3 Determining the Turning Points

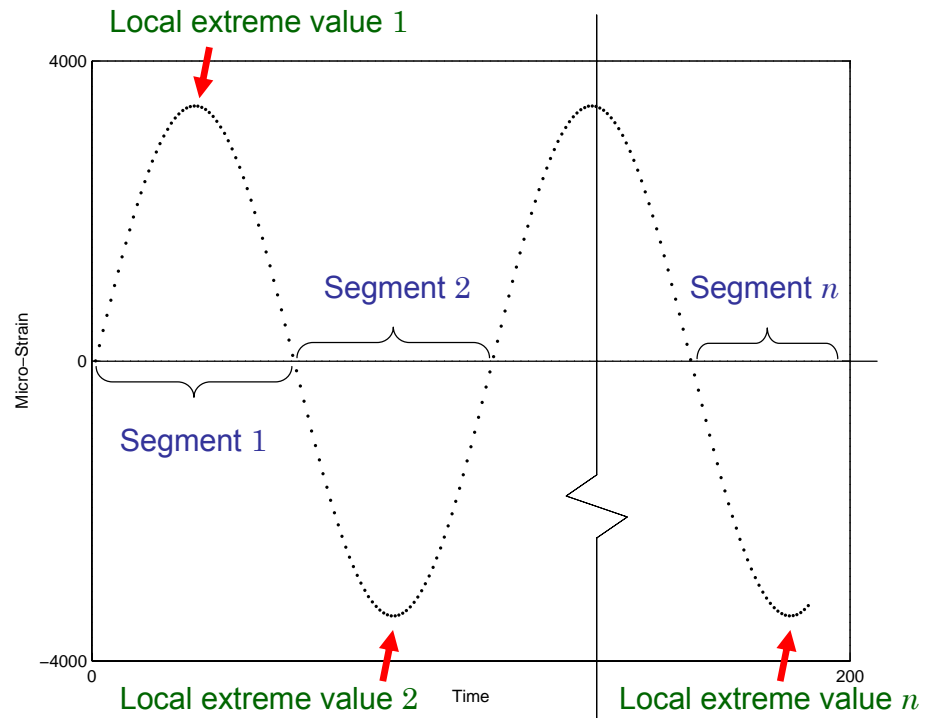


Fig. 3.5 Illustration of algorithm for determining turning points

A typical measured strain data is shown as dot-line in Fig. 3.5. The algorithm for determining whether the state of a point of the sampling strain data from component test (see section 4.1) a turning point or not is depicted as follows.

1. Find the points where the strain approaches zero (seldom equals to zero exactly). Such points will divide the total strain data into several segments.
2. Find the local extreme value in each segment. The state of the point where the local extreme value occurs is the turning point.

3.2 Derivation of Moment and Shear from Inelastic Stress-Strain Hysteresis

It is assumed that the material deforms in a stress-strain relationship that is identical in both tension and compression (i.e. symmetric stress-strain curve). Consider the rectangular cross-section $abcd$ at the position where the strain gauge is attached (Fig. 3.6(a) and (c)).

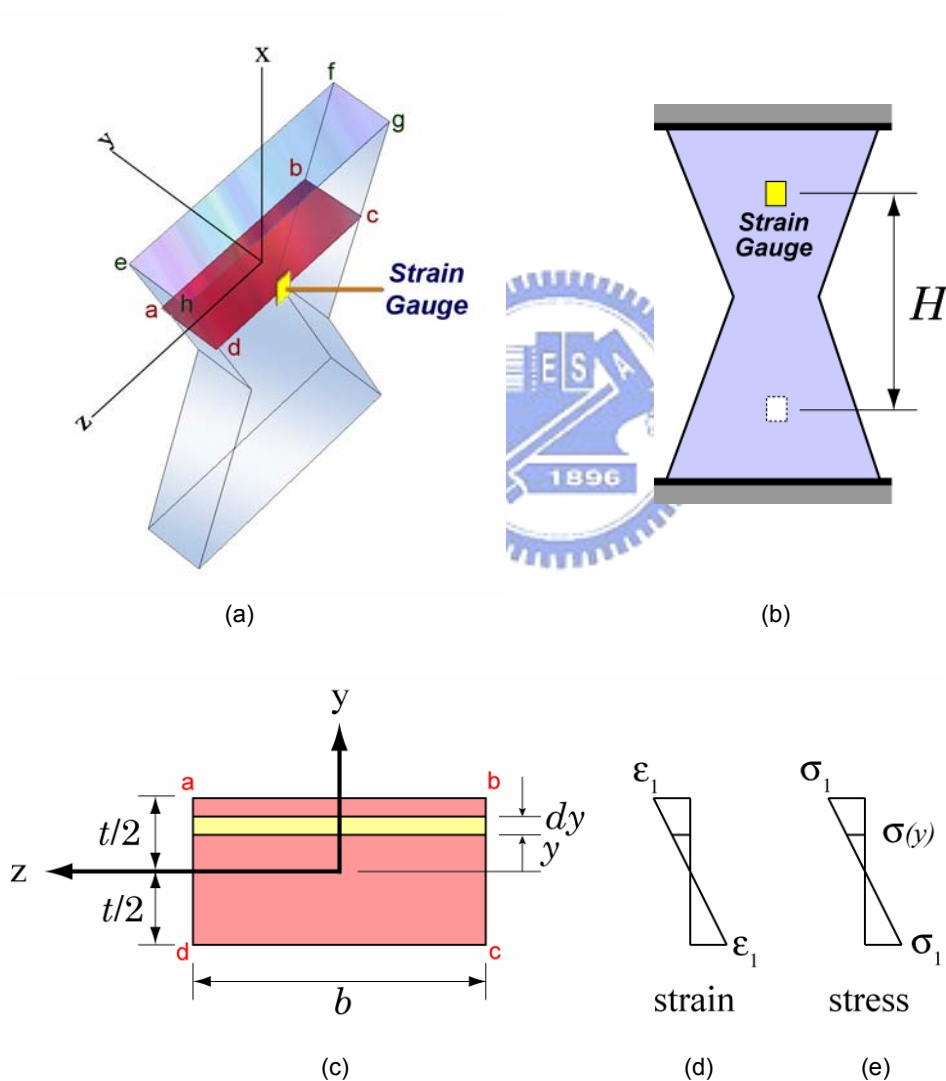


Fig. 3.6 Metallic yielding damper bonded with a piece of strain gauge
 (a) 3-D view of one simple plate of X-shaped metallic yielding damper
 (b) Position of strain gauge bounded on the damper
 (c) Section $abcd$ of the damper (d) Strains in the cross-section
 (e) Stress in the cross-section

The distribution of the normal strains in this cross section along the y -direction varies linearly as shown in Fig. 3.6(d). The strain is zero at the neutral axis and equal to ε_1 at the top and bottom of the cross-section. The corresponding stress σ_1 in a distance $\frac{t}{2}$ from the neutral axis of the steel plate (i.e. the plate surface) is in turn determined from the strain data by using the stress-strain relationship of Ramberg-Osgood Hysteresis Model (Eq. (3.4)). In component tests (section 4.1), a piece of strain gauge is bonded on the surface of the damper to measure the strain as the damper bended by the actuator. ε_1 is recorded at a specified sampling period.

Let us consider a finite strip with b and dy being the width and height, respectively (Fig. 3.6(c)). The force acting on this area is $\sigma(y)b dy$, which results in an incremental moment about the z axis of $\sigma(y)by dy$ at a given state. Thus, the overall bending moment at that particular X-section is

$$M = 2 \int_0^{t/2} \sigma(y)by dy \quad (3.9)$$

Now, assume that the stress distribution in the cross-section is linear (Fig. 3.6(e)). Due to the thin thickness of the plate, the stress at a distance y from the neutral axis can be expressed based on the geometric relation as:

$$\sigma(y) = \frac{2y\sigma_1}{t} \quad (3.10)$$

Substituting Eq. (3.10) into Eq. (3.9), it leads to

$$M = 2 \int_0^{t/2} \left(\frac{2y\sigma_1}{t} \right) by dy = \frac{bt^2}{6} \sigma_1 \quad (3.11)$$

The shear force of the steel plate with two ends fixed can be computed as follow:

$$V = \frac{2M}{H} \quad (3.12)$$

where H is twice the distance of the strain gauge from the neck of the X-shaped plate by considering the condition of symmetry as shown in Fig. 3.6(b).

3.3 Procedure for the Measuring Methodology

Step 1: Prepare a set of strain data.

Strain data (see Fig. 4.13 for an example) are obtained from the component tests (see chapter 4) in this study as well as seismic performance tests. The strain data measured may need first to be filtered by a low-pass filter to eliminate noises. \mathbf{S} contains a vector of the sampling time ($\tilde{\mathbf{t}}$) and a vector of the strain data ($\tilde{\boldsymbol{\varepsilon}}$).

$$\mathbf{S} = \begin{bmatrix} \tilde{\mathbf{t}} & \tilde{\boldsymbol{\varepsilon}} \end{bmatrix} \quad (3.13)$$

Step 2: Generate a column of turning points.

In practical applications, the damper subjected to loading and unloading alternately. The multiple-loops Ramberg-Osgood Hysteresis Model is adopted to describe the stress-strain relationship of the damper under such loadings. Meanwhile, a vector of turning point check value ($\tilde{\mathbf{p}}$) is generated prior to computing the corresponding stresses. n is the number of strain data and p_i is defined as following.

$$p_i = \begin{cases} 1 & \text{if the state of } \varepsilon_i \text{ is the turning point} \\ 0 & \text{otherwise} \end{cases} \quad i = 1, \dots, n \quad (3.14)$$

Matrix \mathbf{S} is expanded as

$$\mathbf{S} = \begin{bmatrix} \tilde{\mathbf{t}} & \tilde{\boldsymbol{\varepsilon}} & \tilde{\mathbf{p}} \end{bmatrix} = \begin{bmatrix} t_1 & \varepsilon_1 & p_1 \\ t_2 & \varepsilon_2 & p_2 \\ \vdots & \vdots & \vdots \\ t_n & \varepsilon_n & p_n \end{bmatrix} \quad (3.15)$$

Step 3: Determine the corresponding stresses by using the Ramberg-Osgood Hysteresis Model.

As mentioned before, due to the high nonlinearity of the Ramberg-Osgood equation, a table searching method is proposed to solve the equations. Whenever the turning point changes, a new Ramberg-Osgood Table needs to be generated. Matrix \mathbf{S} serves as the input for the calculation in this step.

The vector of the corresponding stress ($\tilde{\sigma}$) is the output. A pseudo code for this step is illustrated in Fig. 3.7.

```

// The Initial Path
while ( Not yet reach the turning point ) {
    Find the corresponding stress by the first
    equation of R-O Hysteresis Model.
}

Determine the number of loops.

for (i=0; i<NumberOfLoops; i++) {

    // The Unloading Path
    Generate the R-O Table according to the turning point A.
    while ( Not yet reach the turning point ) {
        Find the corresponding stress of a given strain by
        searching the R-O Table.
    }

    Reach the turning point B and switch the governing equation
    to the third equation of the R-O Hysteresis Model.

    // The Reloading Path
    Generate the R-O Table according to the turning point B.
    while ( Not yet reach the turning point ) {
        Find the corresponding stress of a given strain by
        searching the R-O Table.
    }

}

```

Fig. 3.7 The pseudo code for finding the corresponding stresses

Step 4: Compute the bending moment and shear force.

The bending moment and shear force are computed according to Eq. (3.11) and Eq. (3.12), respectively. The vector of the predicted shear force (\tilde{F}) is the output. Together with the measured displacements (\tilde{D}), the hysteresis for force-displacement relationship can be plotted.



4

Component Tests

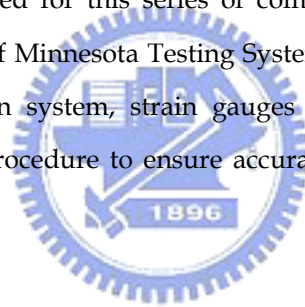


Metallic yielding damper are designed to dissipate energy through inelastic flexural deformation of the steel plates. Both full-scale and scaled-down dampers have been tested independently in the Structural Dynamic Laboratory of NCTU.

Main goals of the component test of the damper are:

- To investigate the characteristics of individual unit under cyclic loadings
- To verify the measuring methodology for moment and shear via strain measurement
- To determine the parameters of the damper for the analytical models characterizing the inelastic behavior to be used by SAP2000

The design of the damper, testing facilities and test programs will first be introduced. The instruments used for this series of component tests of the dampers include the actuators of Minnesota Testing Systems (MTS), MTS 407 controller, IMC data acquisition system, strain gauges and loadcell. Each requires a specific calibration procedure to ensure accurate and proper data collection.



4.1 Component Test of Scaled-Down Damper

4.1.1 Design of the Model Damper

Units of X-shaped metallic yielding damper consisting of four thin steel plates each are designed for the seismic performance test to be discussed in chapter 5 (Fig. 4.1(a)). These thin plates are connected in parallel at the top and bottom portions divided with separating steel stripes in between (Fig. 4.1(b)). A graphical representation of the assembly is shown in Fig. 4.1(c). The design parameters and mechanic properties of this damper calculated according to the derivation discussed in chapter 2 are summarized in Table 4.1 and Table 4.2, respectively.

Table 4.1 Numerical values of parameters for the scaled-down damper

E	210 GPa
B	3 cm
t	0.15 cm
h	5 cm
σ_y	430 MPa
N	4

Table 4.2 Calculated mechanic properties of the scaled-down damper

Δ'_y	1.7 mm
P_y	78.9 kgf
P_p	118.3 kgf
P_u	177.5 kgf

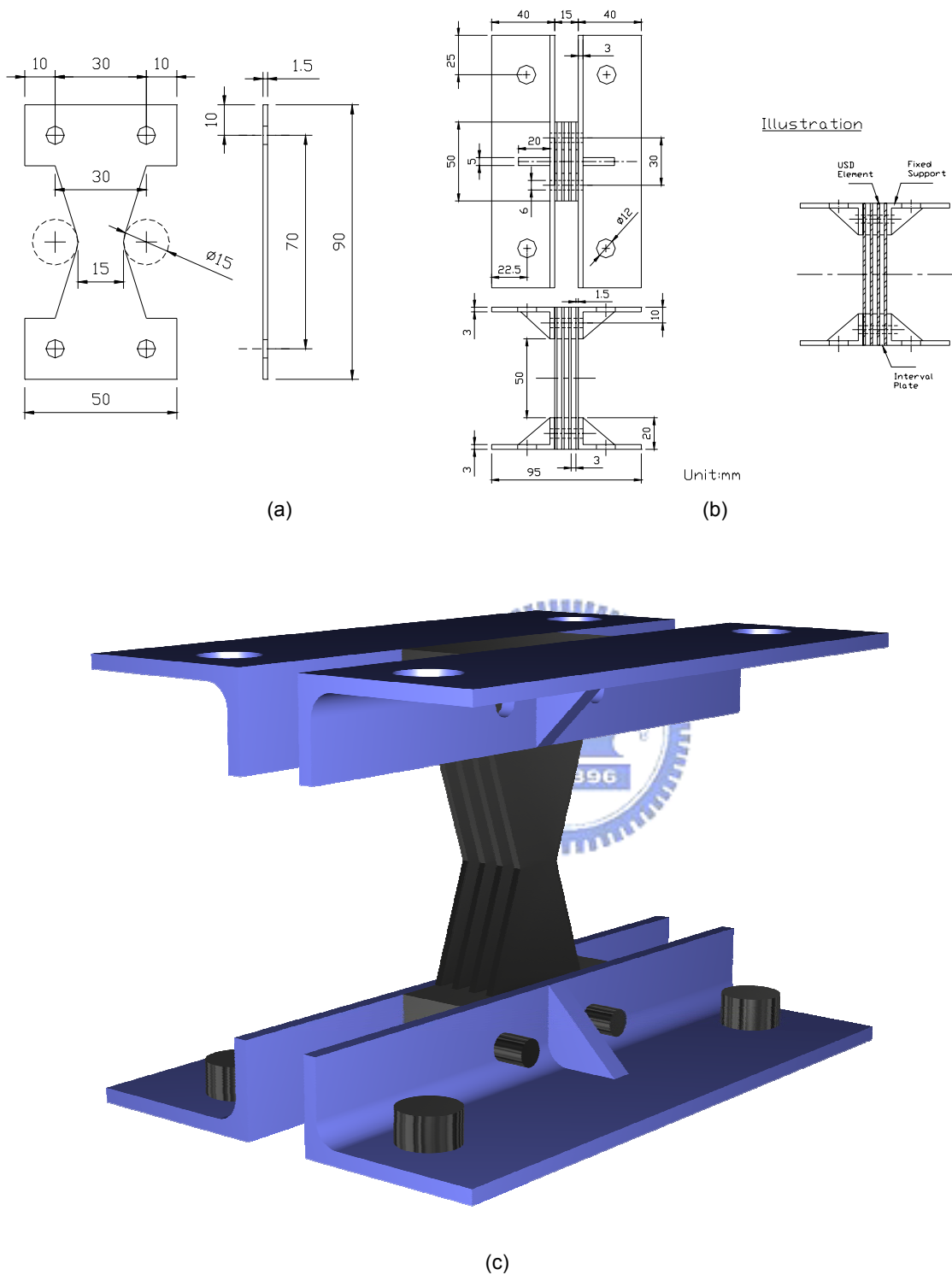


Fig. 4.1 Design of scaled-down metallic yielding damper

- (a) An element of the scaled-down damper
- (b) Assembly of the unit of the scaled-down damper
- (c) Computer graphic of a scaled-down damper unit

4.1.2 Testing Facilities

Actuator and Servo Controller A 1.5-ton dynamic actuator of MTS (Model Number: 244.11) shown in Fig. 4.3 serves as the driving source in the component tests commanded via an MTS 407 Controller (Fig. 4.2).



Fig. 4.2 MTS 407 Controller

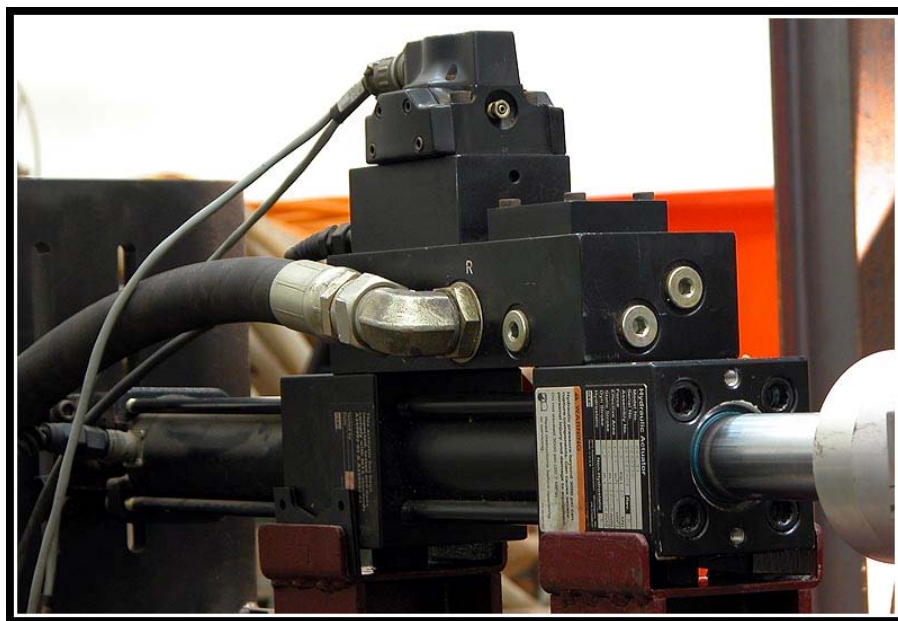


Fig. 4.3 1.5-ton actuator of MTS

Loadcell A loadcell of Jih-Sense (Model Number: S4-LD) with a capacity of 500 kgf (Fig. 4.4) is to be installed at the free end of the actuator. The output voltage of this loadcell is $\pm 10V$. It measures the force transmitting between the actuator and the upper connecting flange of the damper.

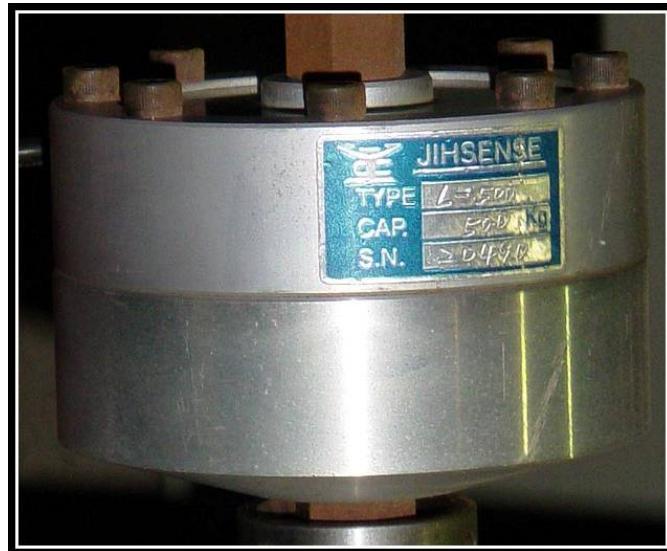


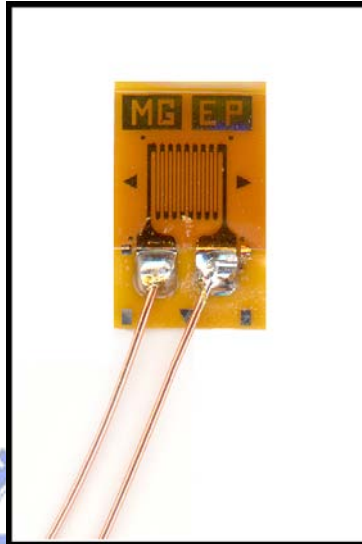
Fig. 4.4 Loadcell

Data Acquisition System An IMC Spartan-1 data acquisition system (Fig. 4.5) is adopted to acquire both the displacement in the actuator and force in the loadcell. The connecting interface of this system to the computer is 100 Mbps Ethernet.

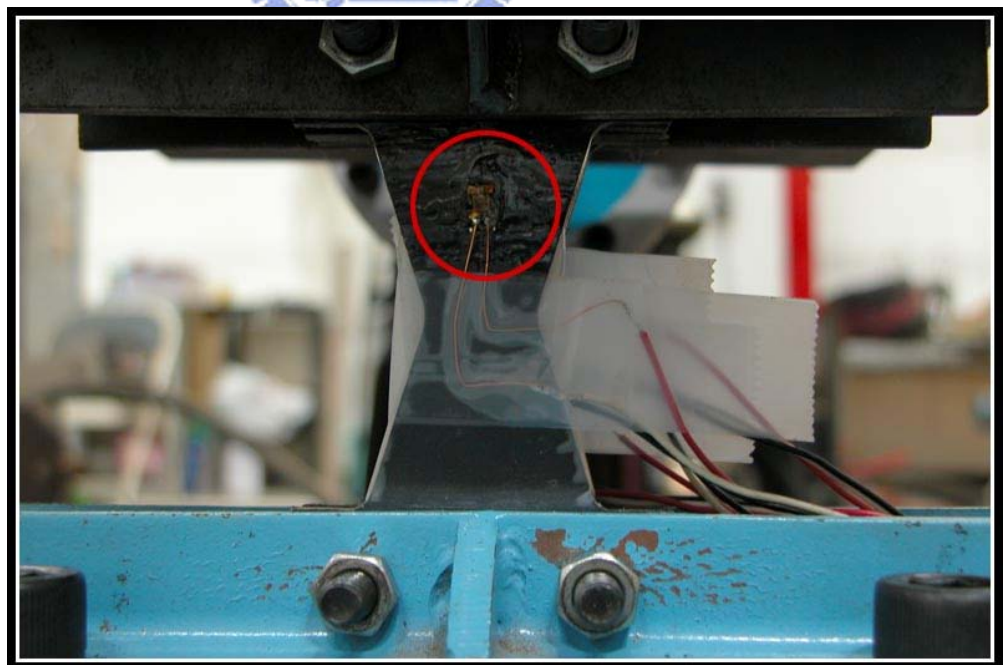


Fig. 4.5 Data acquisition system

Strain Gauge Student Strain Gauges of Micro-Measurements (Model Number: EA-13-060LZ-120) are adopted in the tests (Fig. 4.6(a)). The resistance of this gauge is 120 ohms. The strain gauge is bonded on the surface of the damper to measure the deformation (strain) of the damper in the vertical direction (Fig. 4.6(b)).



(a)



(b)

Fig. 4.6 A strain gauge for strain measurement in the tests
(a) A strain gauge (b) A strain gauge bonded on the surface of the damper

Testing Platform A full view of the experimental setup and a close-up view of the set-up are shown in Fig. 4.7 and Fig. 4.8, respectively. A detailed design sketch of the testing platform is shown in Fig. 4.9. An H-beam is fixed on the strong floor with two rods while the actuator and the damper to be tested are installed on top of the H-beam. The loadcell is installed between the free end of the actuator and the connecting angle plate which in turn is locked on top of the upper part of the damper. The damper being tested has been lifted up by a set of small frame, as shown in the picture, to minimize the rotational effects as will be discussed in section 4.1.5 where the predicaments encountered during the tests are addressed.



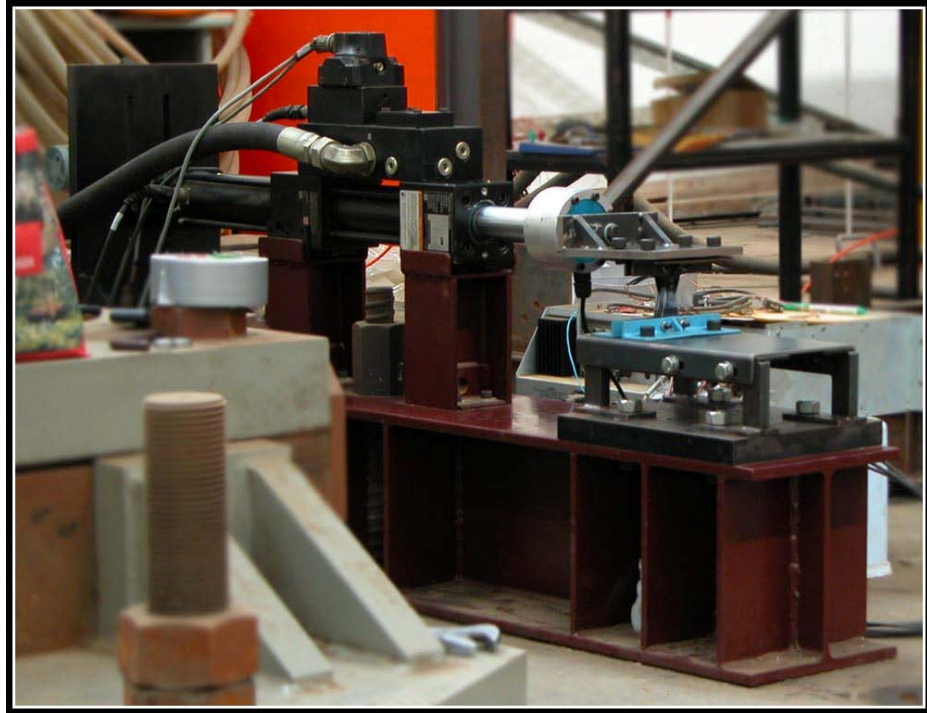


Fig. 4.7 A full view of the testing platform for component test of the scaled-down damper

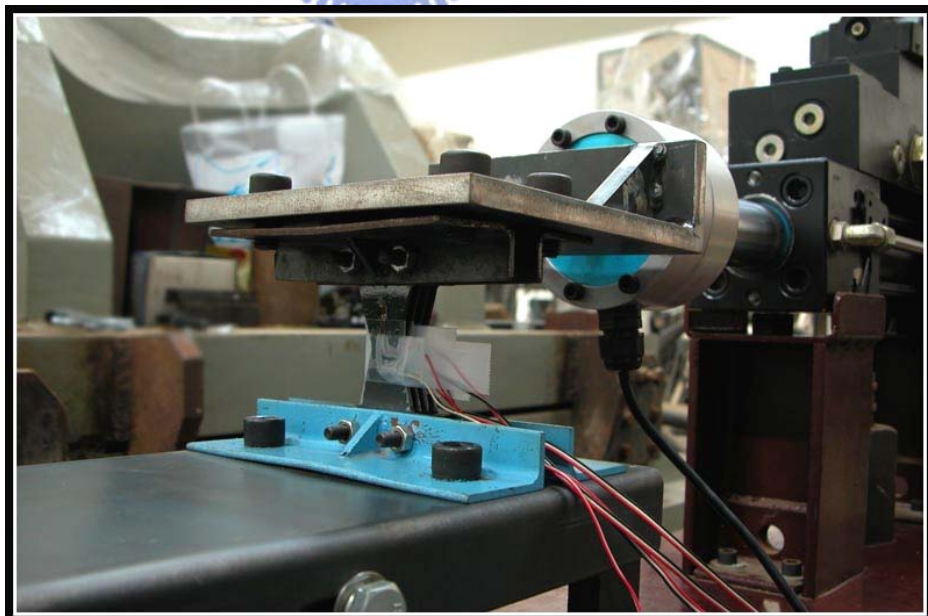


Fig. 4.8 A Close-up view of the set-up

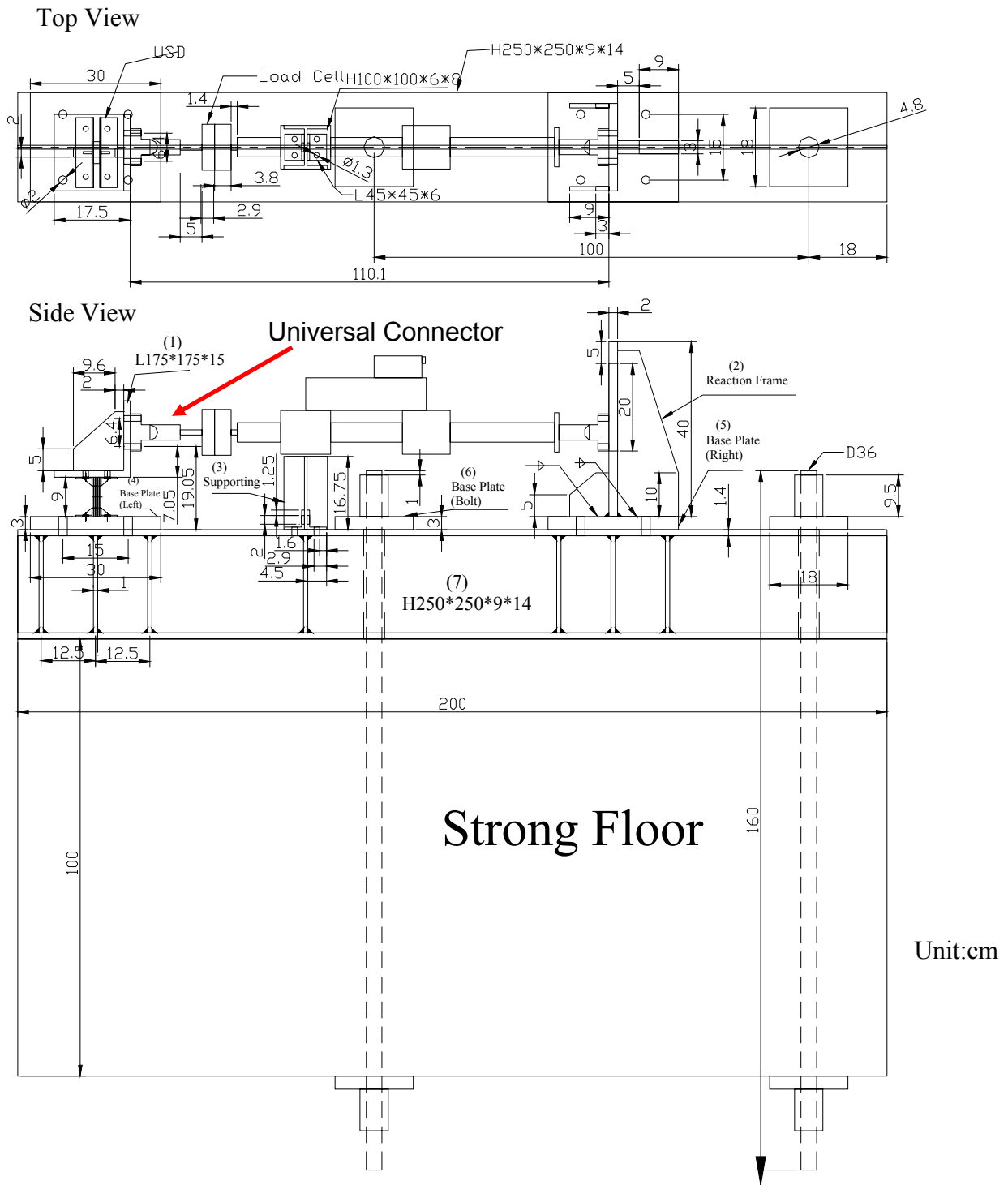


Fig. 4.9 Detailed plot of the test platform for scaled-down damper

4.1.3 Test Programs

The displacement-control command is sent by a computer to the actuator through the MTS 407 controller. The loading history with spans 3, 7, 10 and 14 mm with 3 consecutive cycles each is shown in Fig. 4.10. The sampling rate of the data acquisition system is set to be 100 Hz while the loading rate is 1 cm/sec . It takes about 10 mins to complete one test.

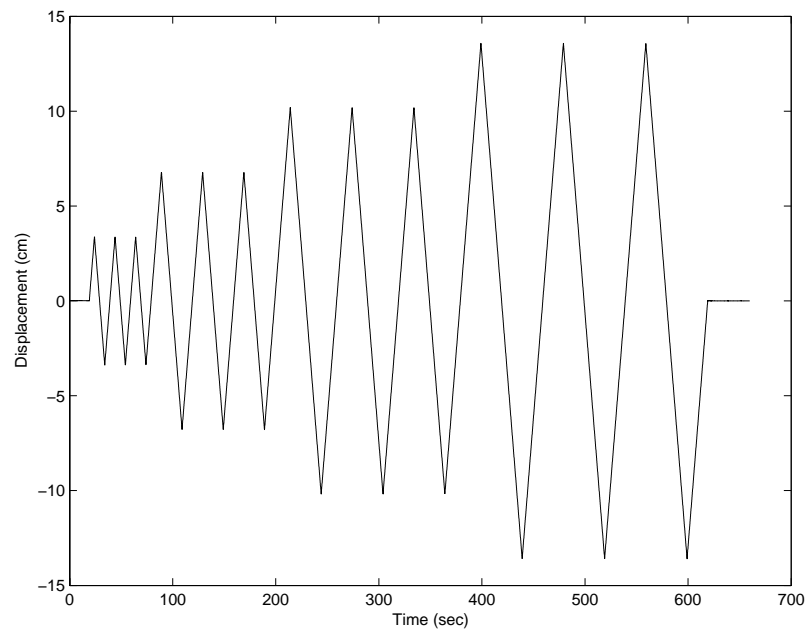


Fig. 4.10 The loading history specified for the component test of scaled-down damper

4.1.4 Testing Results

The objective of the component tests is to determine the hysteresis loop characterizing the inelastic behavior of the damper. The displacement is obtained from the built-in LVDT of the actuator while the force is directly measured from the loadcell installed.

The hysteresis of force-displacement relationship of the damper from directly measured actuator stroke and reading force is plotted in Fig. 4.11. Performing curve fitting, the elastic stiffness (k_1) and post yielding stiffness (k_2) can be extracted from the figure as shown in Fig. 4.12. The comparison between the experimental and theoretical stiffness of the damper is summarized in Table 4.3.

Table 4.3 Comparison between the experimental and theoretical stiffness for the scale-down damper

Experimental: k_1	42.07 kgf/mm
Theoretical: k'_d	46.29 kgf/mm
Difference: $\left \frac{k_1 - k'_d}{k'} \right $	9 %

Parameters of the analytical models of SAP2000 for the scale-down damper are obtained from the component tests (see Table 4.4). The post yielding stiffness ratio is defined as

$$\gamma = \frac{k_2}{k_1} \quad (4.1)$$

The yielding strength, also a required parameter for modeling by SAP2000, reads 56.4 kgf from Fig. 4.12.

Table 4.4 Parameters obtained from the component test for the analytical models of the scaled-down damper

γ	0.02
Yielding Strength	56.4 kgf

As mentioned earlier, strain of the damper in the vertical direction were also measured in the component test, which serves as the basis for estimating the moment and the shear force of the damper by using the proposed scheme discussed in chapter 3. The strain data filtered by a low-pass filter is shown in Fig. 4.13. The hysteresis for the predicted stress-strain relationship of the damper is plotted in Fig. 4.14.

To match the directly measured hysteresis and the predicted one, the parameters of the Ramberg-Osgood Hysteresis Model is adjusted. Numerical values that give the best match of the hysteretic loops are shown in Fig. 4.15 and listed in Table 4.5. Note that n controls the sharpness of the knee of the hysteresis loop and the other three parameters define the material properties. Note that from Eq. (3.8), α depends on σ_0 and E . The suggested values for E and n by Rasmussen [36] are adopted while the value of σ_0 are changed to 430 MPa.

Table 4.5 Numerical values of parameters in the Ramberg-Osgood Hysteresis Model for the methodology of measuring shear force

Parameters	Numerical Value
σ_0	430 MPa
E	210 GPa
α	0.9767
n	5.33

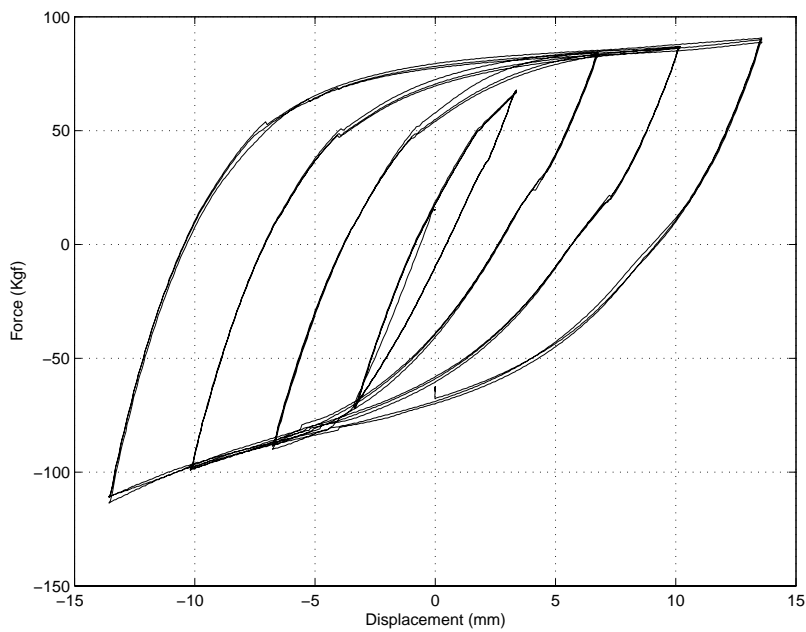


Fig. 4.11 Hysteresis for directly measured force-displacement relationship of the scaled-down damper

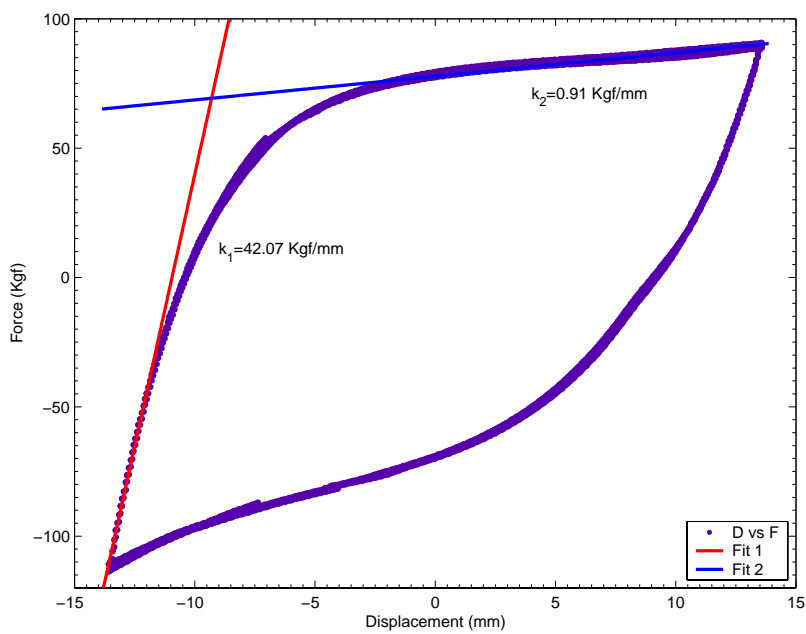


Fig. 4.12 Curve fitting for determining the experimental stiffness of the scaled-down damper

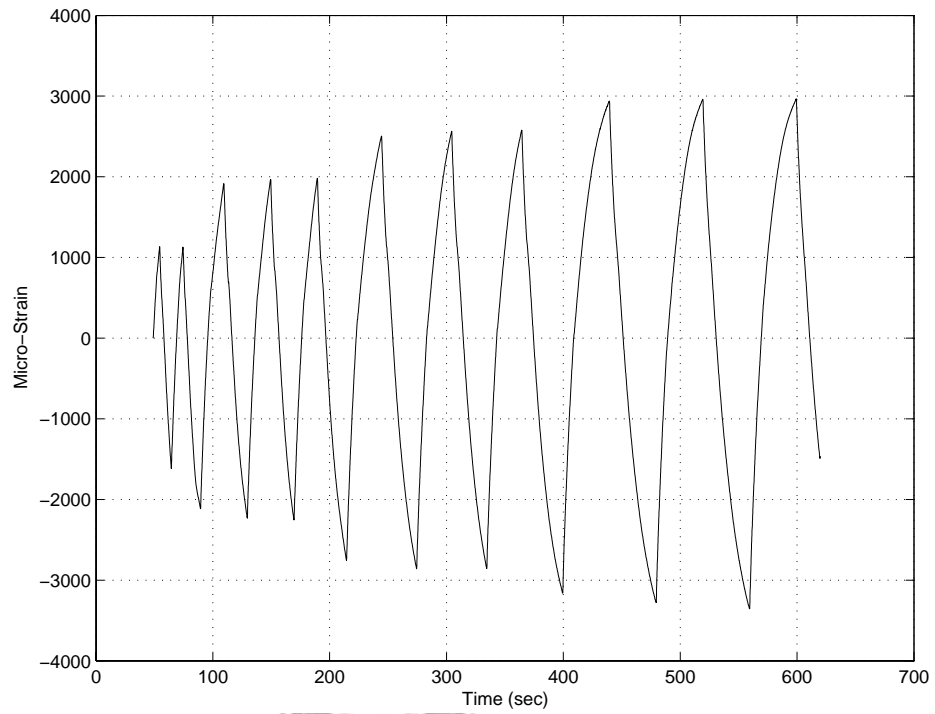


Fig. 4.13 Measured strain data from component test of scaled-down damper

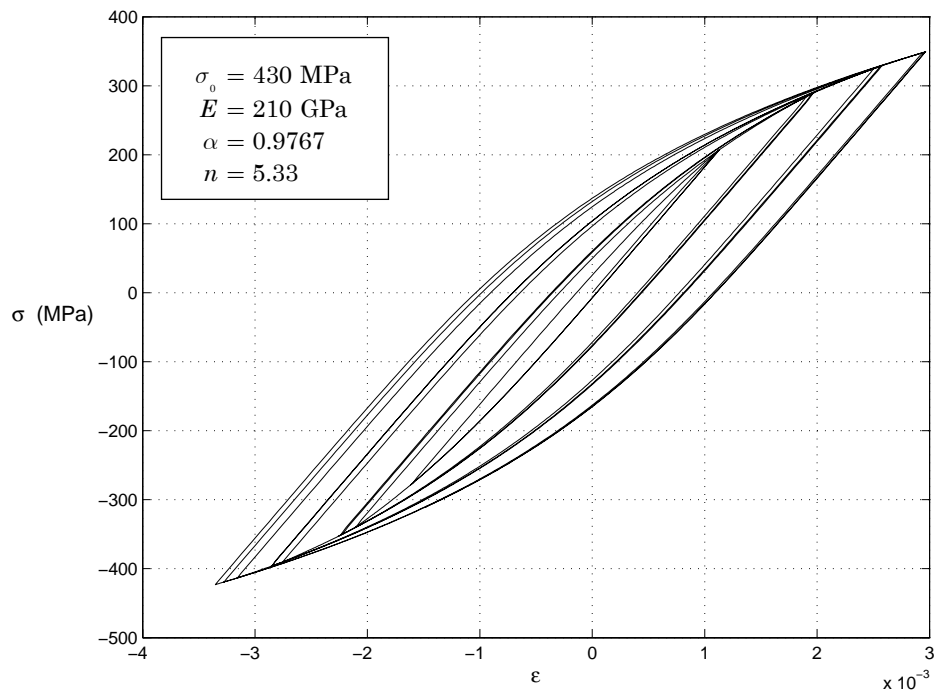


Fig. 4.14 Predicted stress-strain hysteresis of the scaled-down damper

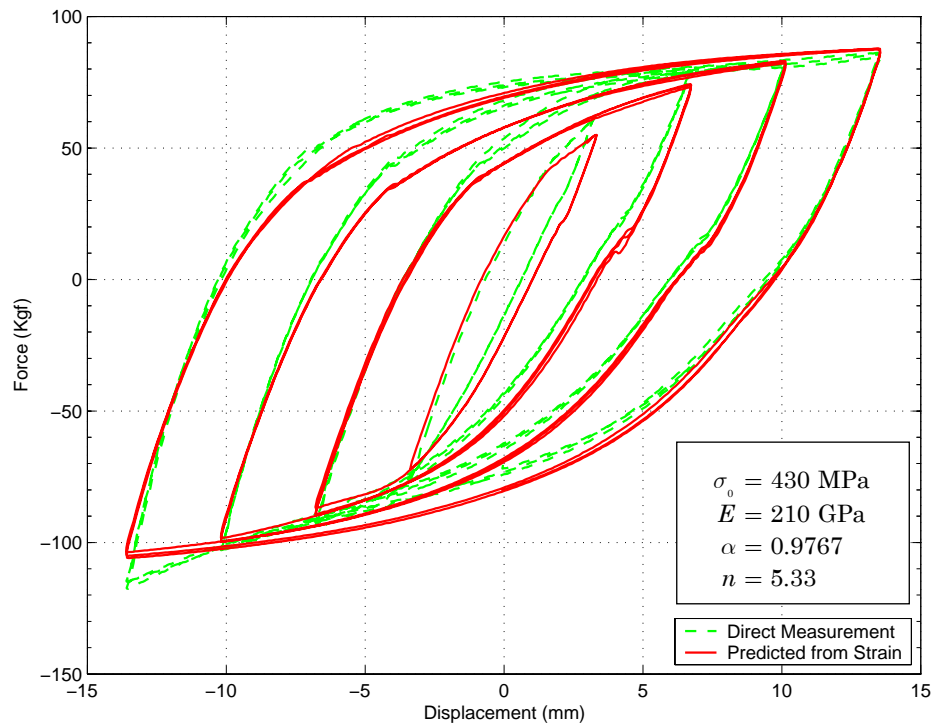


Fig. 4.15 Comparison of the hystereses for force-displacement relationship between directly measured and predicted results



4.1.5 Discussion

Predicaments encountered during the tests and the solutions

By the original design of the testing setup shown in Fig. 4.9, the connecting interface between the free end of the actuator and the angle plate of the damper was a universal connector found rotating during the tests. These undesired rotation lead to erroneous and unrealistic hysteresis. In order to eradicate the unsatisfactory rotating effects, modifications of the testing platform have been considered.

The major modifications were to discard the universal connector and lift up the damper. By getting rid of the universal connector, the interface between the free end of the actuator and the angle plate of the damper becomes more rigid, with a risk of damaging the actuator if the transverse shear force is excessive. Fortunately, the maximum axial force in the test is only about 120 kgf that can not damage the actuator. Lifting up the damper decreases the moment arm of rotation about the upper edge of the damper so that rotation is minimized. These modifications have shown to improve significantly the testing results. The final testing platform used in the component tests is shown in Fig. 4.7 and Fig. 4.8.

The possible reason for obtaining non-symmetric hysteresis

In the test setup, the actuator is lifted by a set of supporting stages with its rear end fixed on an angle plate. However, the actuator is not fixed on the supporting stage. When the actuator was pushing the damper in the + direction, as shown in the Fig. 4.16, it was also moving a little bit in the Z-direction as shown blurringly in the same figure. Conversely, when the actuator was pulling the damper (i.e. in the opposite direction) the stage prevents it from moving in the Z-direction. It is clearly that the boundary conditions differ in the Z-direction between the back and forth movements of the actuator, resulting in a non-symmetric force record.

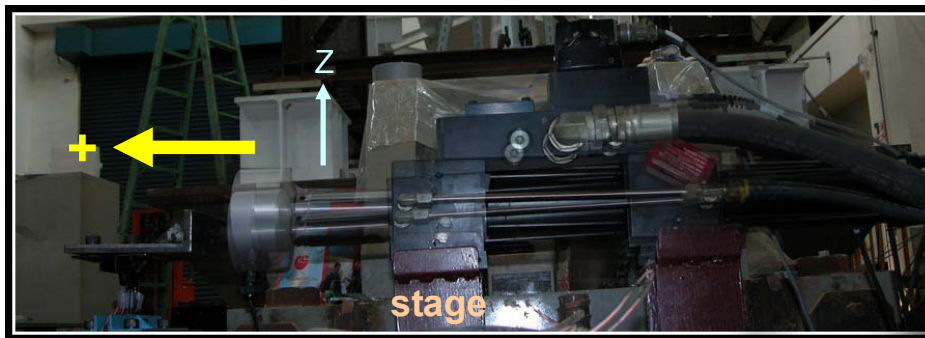


Fig. 4.16 Illustration of the movement of the actuator

4.2 Component Test of Full-Scale Damper

4.2.1 Design of the Model Damper

Units of X-shaped metallic yielding damper consists 15 steel plates ((Fig. 4.7(a)). These plates are connected in parallel at the top and bottom portions divided with separating steel stripes in between. The design parameters and mechanic properties of this damper calculated according to the derivation discussed in chapter 2 are listed in Table 4.6 and Table 4.7, respectively. A graphical representation of the assembly is shown in Fig. 4.17(b).

Table 4.6 Numerical values of parameters for the full-scale damper

E	2.04+E07 ton/m ²
B	0.15 m
t	0.01 m
h	0.15 m
σ_y	25000 ton/m ²
N	15

Table 4.7 Calculated mechanic properties of the full-scale damper

Δ'_y	2.9 mm
P_y	8.5 ton
P_p	12.8 ton
P_u	19.2 ton

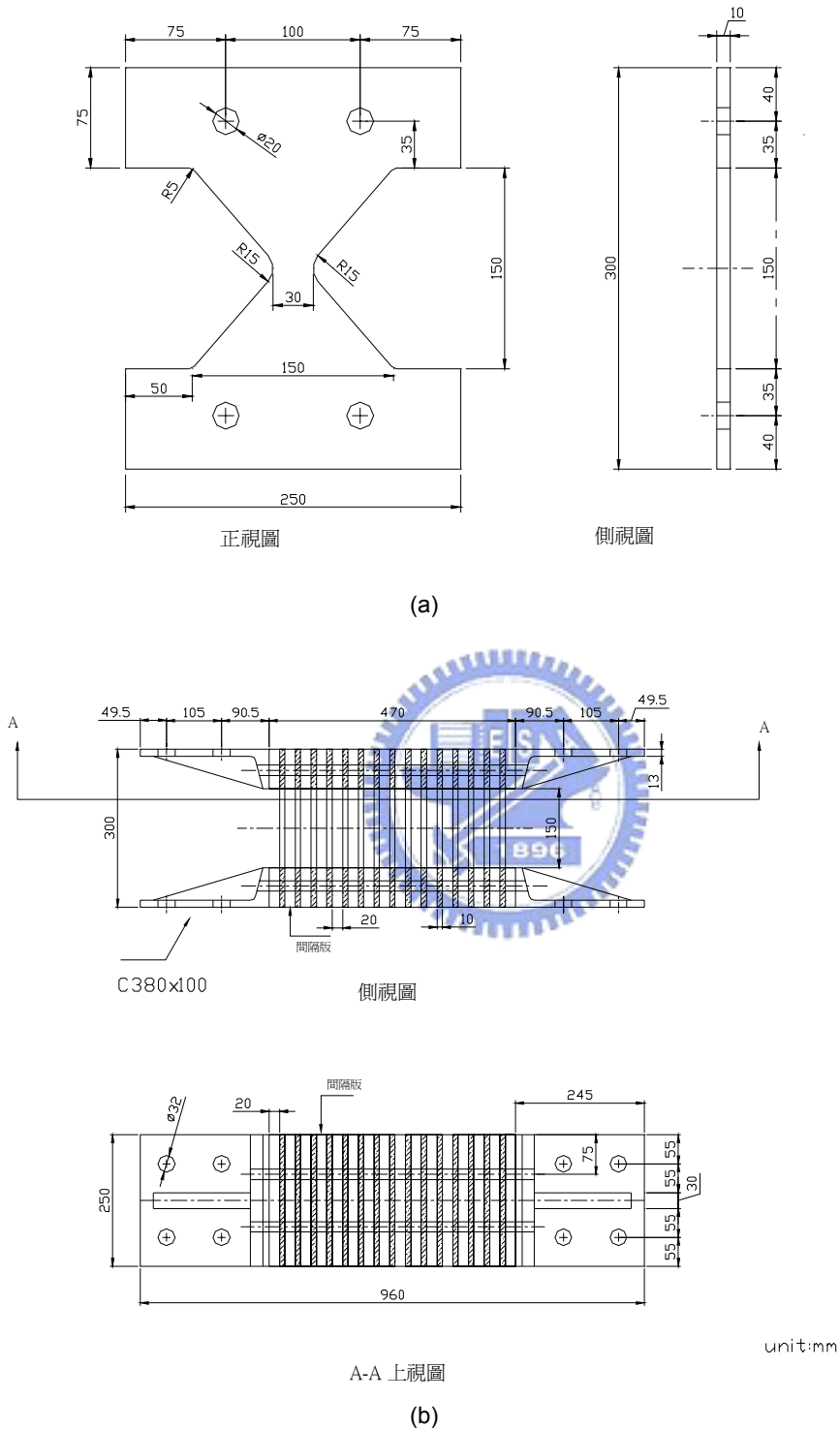


Fig. 4.17 Design of the full-scale metallic yielding damper
 (a) A single plate of the full-scale damper
 (b) Assembly of the full-scale damper

4.2.2 Testing Facilities

Actuator and MTS Control System A 50-ton dynamic actuator of MTS (Model Number: 244.41S) serves as the driving source in the component tests. This actuator is fixed on the reaction wall. The displacement-controlled commands are sent by an MTS Test Star controller from the control room (Fig. 4.18).



Fig. 4.18 MTS control system in the control room

Testing Platform A detailed design sketch of the testing platform for component tests of full-scale damper is shown in Fig. 4.20. The unit of damper to be tested is mounted on an H-beam (Fig. 4.19) which in turn is fixed on the strong floor. The actuator is installed on the reaction wall. Another H-beam on the top of the damper serves as the connector transmitting the loading of actuator to the damper. The interfaces between the ends of the H-beam and the supporting stage are coated with Teflon pads to reduce friction.

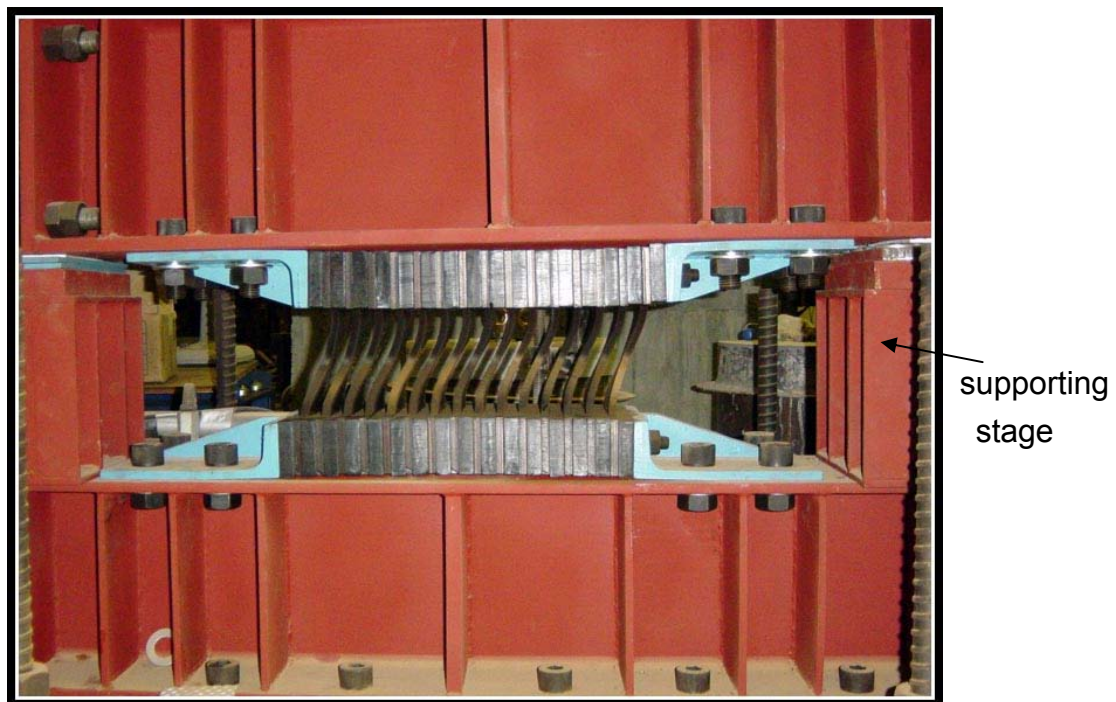


Fig. 4.19 A close-up view of the full-scale damper in testing

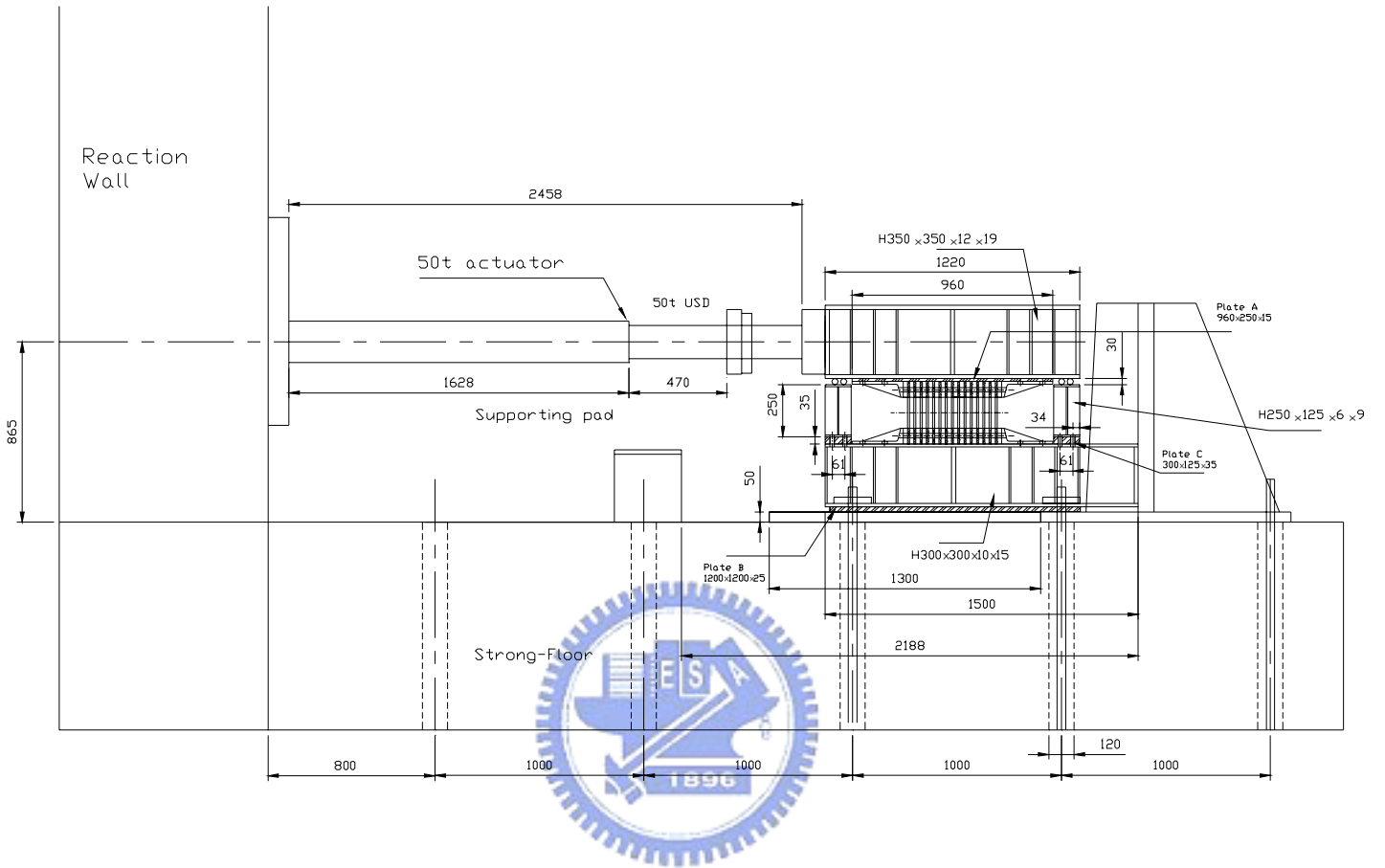


Fig. 4.20 Design sketch of the testing platform for component test of a full-scale damper (Unit: mm)

4.2.3 Test Programs

The loading history with spans of 10, 20, 30 and 40 mm with 3 consecutive cycles each is shown in Fig. 4.21. The sampling rate of the data acquisition system is set to be 1 Hz while the loading rate is 0.3 cm/sec . It takes about 70 mins to complete one test.

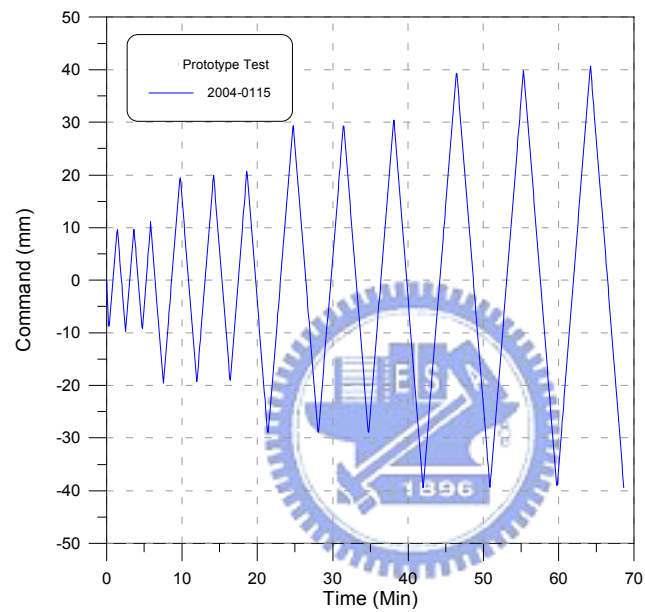


Fig. 4.21 The loading history specified for component test of full-scale damper

4.2.4 Testing Results

The objective of the component tests is to determine the hysteresis loop characterizing the inelastic behavior of the damper. The displacement and force are obtained from the built-in LVDT and the loadcell of the actuator, respectively.

The experimental hysteresis of the full-scale damper is plotted in Fig. 4.22 which shows a stable behavior of the damper. Curve fitting was performed on this hysteresis to determine the elastic stiffness of the damper for the hysteresis (Fig. 4.23). It is observed that the boundary conditions of the damper are not completely fixed. A reduction factor ϕ (Table 4.8) can be taken to modify the stiffness calculated according to Eq. (2.13). If the upper and lower boundaries are considered as completely fixed, ϕ takes 1. In the component test of the full-scale damper, ϕ takes 0.75. The comparison between experimental and theoretical stiffness is summarized in Table 4.9.

Table 4.8 The reduction factor and stiffness of the full-scale damper

ϕ	0.75
$\phi k'_d$	2242 t/m

Table 4.9 Comparison between the experimental and theoretical stiffness for the full-scale damper

Experimental: k_1	2097 t/m
Theoretical: $\phi k'_d$	2242 t/m
Difference: $\left \frac{k_1 - \phi k'_d}{\phi k'_d} \right $	6 %

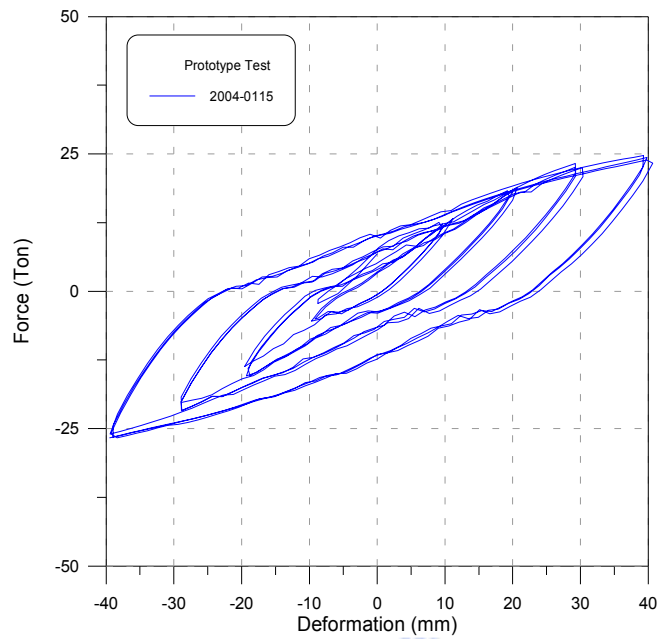


Fig. 4.22 Experimental hysteresis loop of the full-scale damper

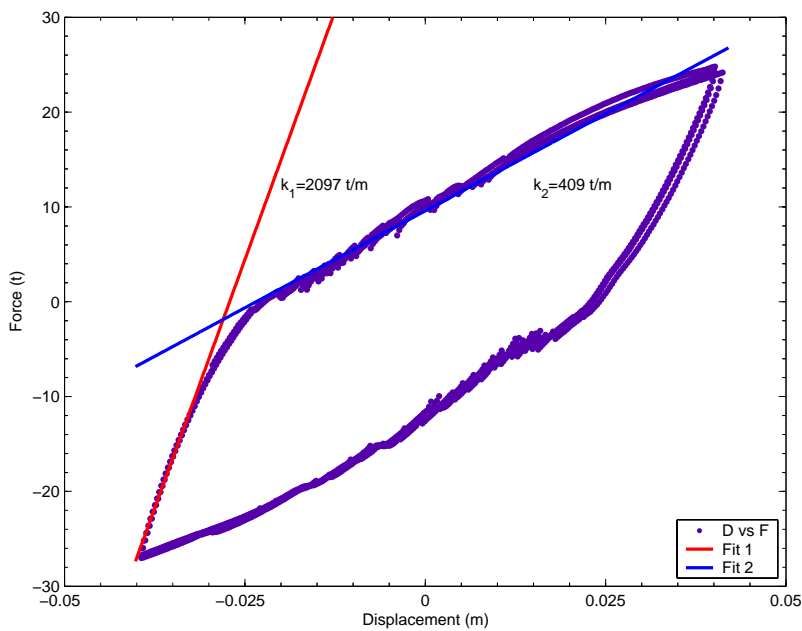


Fig. 4.23 Curve fitting for determining the experimental stiffness of the full-scale damper

5

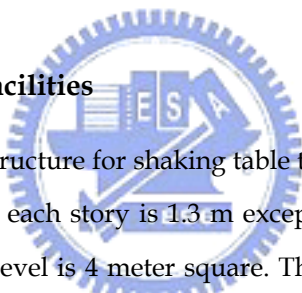
Seismic Performance Tests



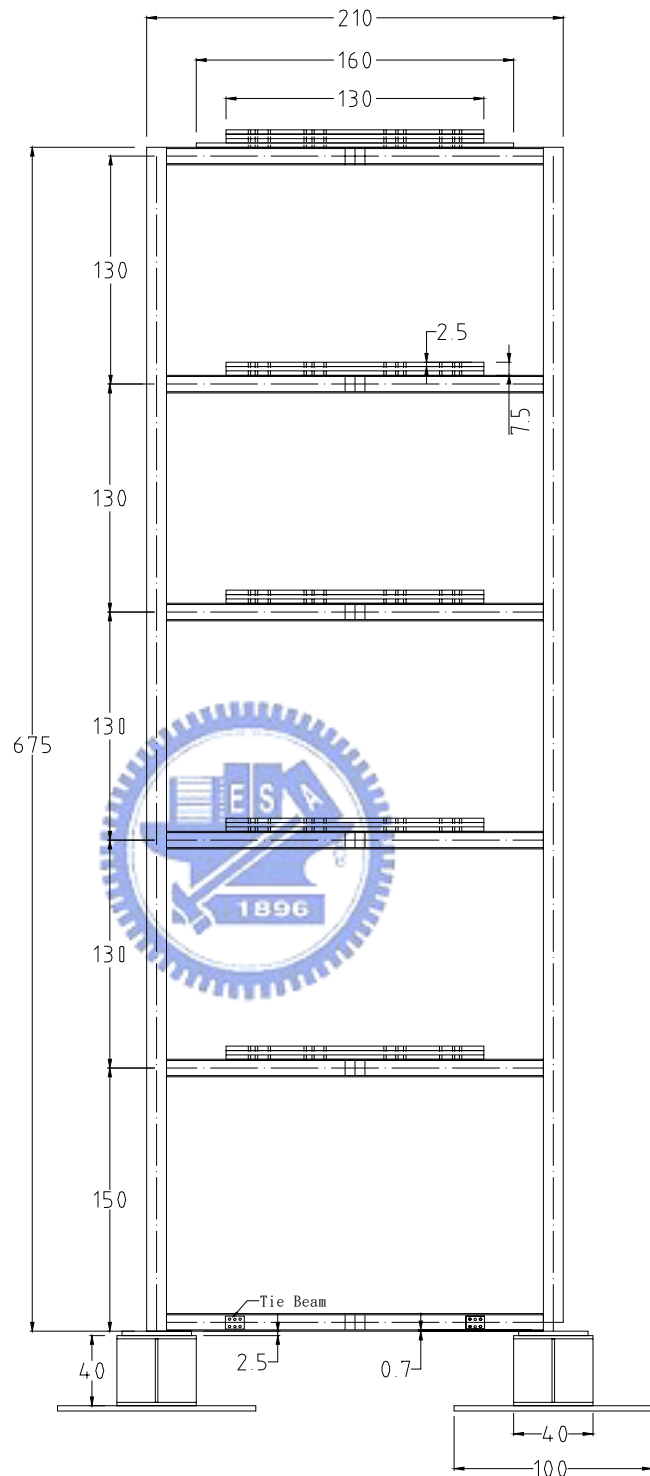
In order to assess the effectiveness and feasibility of the damper through the earthquake, a series of shaking table test simulating the real earthquake scenario have been conducted in the Structural Dynamic Laboratory. In section 5.1, the experimental setup including the 5-story steel model structure, seismic shaking table and instrumentations are introduced concisely. The design of the metallic yielding damper for this structure is summarized. The assessment of seismic performance of the damper follows. In section 5.2, the commercial software, SAP2000, is used to simulate the responses of the 5-story model under various earthquake scenarios and compared the results with the experimental ones.

5.1 Shaking Table Tests

5.1.1 Description of Test Facilities



Model Structure The model structure for shaking table test is a 5-story steel building (Fig. 5.1). The height of each story is 1.3 m except for the first story which is 1.5 m. The area of one level is 4 meter square. The smallest H-Beam (H100x50x5x7) commercially available is used to form the main frames of the building. Besides, two mass blocks (332 kg each) are installed on each floor to simulate the floor weight. The total weight of the model structure is about 4.14 ton, including the frame. Detailed properties of the model building are tabulated in table 5.1. System parameters that are listed in table 5.2 are obtained by using the processes of system identification [37].



Scale: 1/30
Unit: cm

Fig. 5.1 The model structure for shaking table test

Table 5.1 Detailed properties of the model structure

Length (m)	2
Width (m)	2
Height of 2~5 floors (m)	1.3
Height of 1 st floor (m)	1.5
m_5 ($kg - sec^2 / m$)	82.28
m_4 ($kg - sec^2 / m$)	84.75
m_3 ($kg - sec^2 / m$)	84.75
m_2 ($kg - sec^2 / m$)	84.75
m_1 ($kg - sec^2 / m$)	85.13
Cross section of the column ($m m$)	100×50×5×7
Cross section of the beam ($m m$)	100×50×5×7
Cross-sectional area of the column (m^2)	0.0011
Cross-sectional area of the beam (m^2)	0.0011

Table 5.2 Natural Frequency and Damping Ratio of the Model Structure Extracted from System Identification Analysis

<i>Mode</i>	1	2	3	4	5
<i>Frequency (Hz)</i>	1.46	4.57	7.85	11.01	13.47
<i>Damping Ratio(%)</i>	0.51	0.32	4.14	4.33	5.83

Earthquake Simulator The earthquake simulator designed by Prof. Yen-Po Wang of National Chiao-Tung University (Fig. 5.2) is the first “made-in-Taiwan” product of similar testing facility. It is primarily integrated from a 15-ton dynamic actuator of MTS (Model 244.23s, see Fig. 5.3) with a stainless steel table fabricated by a local supplier. The effective operating frequency of the hydraulic actuator is 50 Hz in accordance with the MTS specification. Therefore, a fundamental frequency higher than 100 Hz is desired for the table body to assure performance of the actuator. The ratio of the weight between the tested model and the table is suggested to be 2:1, at most, to avoid model-table interactions during the tests. Accordingly, a 3m×3m table of hollow box-like structure reinforced with ribs of steel plates is devised. The body is rigid enough against bending and torsion loads while with its weight minimized to 5 ton. As a result, the shaking table can accommodate a payload as much as 10-ton at a peak acceleration of 1.0 g. The maximum stroke of the shaking table is ±12.5 cm limited by the capacity of the actuator. With a piston area of 89 cm^2 , the actuator operating under a 210 kg/cm^2 working pressure can afford a maximum control force of 18.7 ton, which is greater than what is required by driving the table in full loads at 1g acceleration. The flow rate required by driving the table at a speed of 60 cm/sec is 320 lpm , which can be accommodated by the 3-stage servo valve (MTS Model 256.09) with a flow rate of 90 gpm (340 lpm). The shaking table system is facilitated with a 75 gpm (283 lpm) hydraulic pump (MTS Model 506.62), which is sufficient for an average flow requirement of 204 lpm estimated by $\frac{2}{\pi}$ times the peak requirement (320 lpm). The difference between the required and the average flow is supplemented or reserved by the accumulators (MTS Model 111).



Fig. 5.2 Earthquake simulator -- shaking table system



Fig. 5.3 15-ton dynamic actuator of MTS

Control and Data Acquisition System The MTS 407 Controller is adopted as the control system of the shaking table. The 407 Controller accepts built-in waveforms as well as external input digital signals such as earthquake ground motion, which is converted into analog signals that, in turn, commands the hydraulic actuator to drive the shaking table via the servo valve. The shaking table system is also facilitated with a μ -Musyacs system of IMC Corporation, German for data acquisition, by which at most synchronous measurement of 32 channels is available. The test data is recorded via a personal computer implemented with an Ethernet interface which allows for rapid data transfer and post processing on computers elsewhere.

Accelerometers Seven accelerometers of Crossbow (CXL04M1) with a dynamic range of $\pm 4g$ were used to measure the acceleration responses of the model structure in the direction of input ground motion during the tests. The accelerometers were implemented on each floor as well as the foundation beam.

Linear Variable Displacement Transducers LVDT of Kyowa (DLT-300AS) with a dynamic range of ± 30 cm was installed to measure the storydrift of the first floor during the tests.

5.1.2 Description of the Dampers

Totally 10 identical units of the metallic yielding damper (see Fig. 5.4 and Fig. 5.5) have been installed in the model structure in seismic performance tests, two for each story on the side frames parallel to the direction of earthquake ground motion (see Fig. 5.4). It is noted that over-design of the dampers will lead to amplification of the acceleration responses despite the displacement can be drastically reduced, while under-design of the dampers will provide only limited controlling effects, which may not be sufficient in severe earthquakes. Optimal design of the damping system for a prescribed structure is still a state-of-the-art.

The dimension of the damper was determined, based on preliminary parametric studies via computer simulations, to meet the design goal of suppression the acceleration and displacement responses of the structure simultaneously. Each unit of the damper consists of four X-shaped steel plates (1.5 mm thick each) as shown in Fig. 4.1. The plates with separation steel strips in between and two confining angle plates from the outside are bolted together through the preserved holes by a set of rods. The horizontal legs of the angle plates in turn serve as the interfaces for connecting the damper with the bracing system and the beam.





Fig. 5.4 Seismic performance test of the damper on a model structure via shaking table

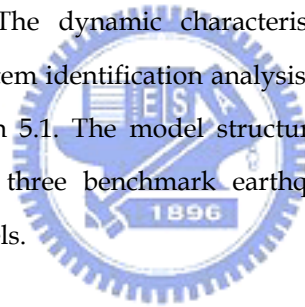


Fig. 5.5 A close-up view of a unit of the damper on the model structure

5.1.3 Test Programs

The El Centro, Hachinohe earthquake and Kobe earthquake, that are selected as benchmark earthquake by the International Structural Control Society for earthquake engineering research, were considered in this series of tests as the input excitations with their intensity (in terms of Peak Ground Acceleration, PGA) scaled to various levels. The time histories of these earthquake records in full-scale is illustrated in Fig. 5.6, Fig. 5.7 and Fig. 5.8, respectively.

The model structure without implementation of the damper was first tested with the minimum earthquake intensity (PGA=0.1g) for each earthquake scenario. The seismic responses are then recorded as the basis for system identification of the model structure as well as comparison with those facilitated with the damper. The dynamic characteristics of the model structure extracted from the system identification analysis have been listed in Table 5.1 and 5.2 in the section 5.1. The model structure protected by the dampers was tested with the three benchmark earthquakes scaled from moderate to severe intensity levels.



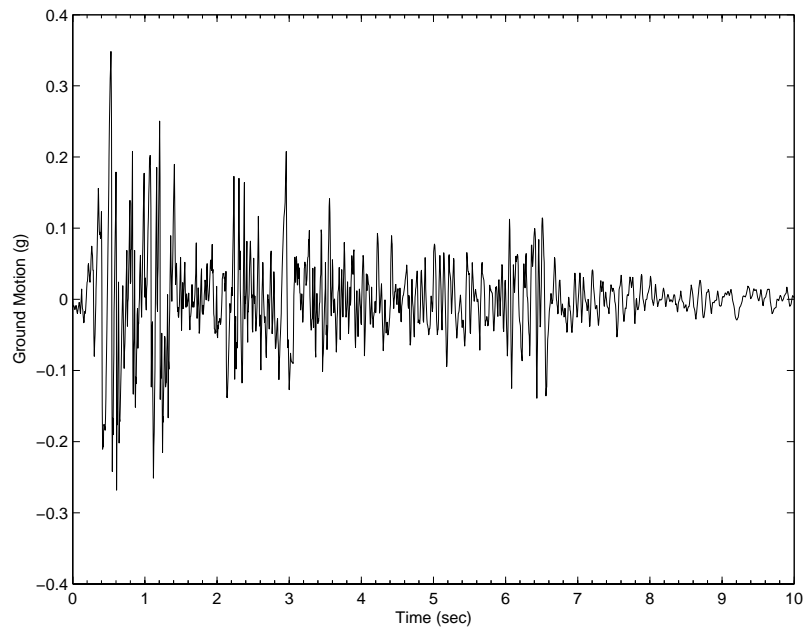


Fig. 5.6 Time history of El Centro earthquake

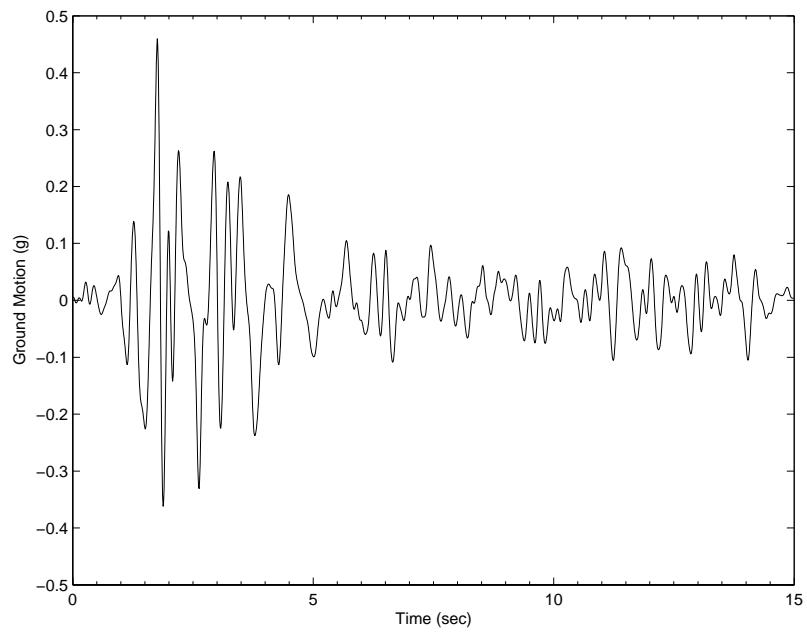


Fig. 5.7 Time history of Hachinohe earthquake

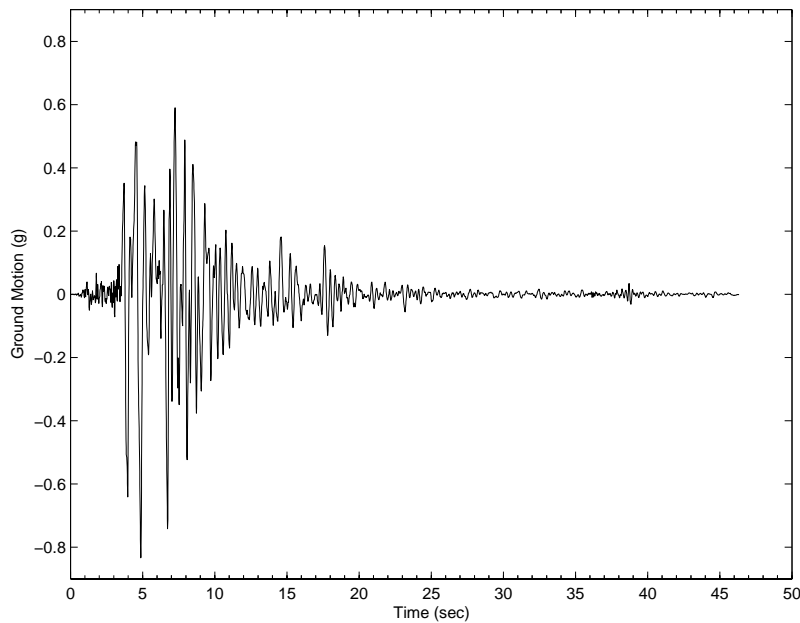


Fig. 5.8 Time history of Kobe earthquake

5.1.4 Assessments of Seismic Performance

To prevent damage of the model structure, no tests with intensity larger than 0.1g have been conducted on the bare frame (i.e. without damper). The responses of the bare frame at greater intensities (PGA=0.2g, 0.3g and 0.4g for El Centro, PGA=0.15g, 0.2g and 0.25g for both Hachinohe and Kobe) presented in this section were obtained by linear extrapolation from the recorded results for PGA=0.1g. The testing results for the damper-protected structure were recorded directly.

El Centro Earthquake The comparisons of floor acceleration responses under the El Centro earthquake are illustrated in Fig. 5.9 ~ 5.12 for intensities of 0.1g, 0.2g, 0.3g and 0.4g, respectively. As protected with damper, evident reductions of all the floor accelerations at various earthquake intensities have been observed. The peak floor responses at each testing scenario are summarized in Table 5.3. The peak accelerations are reduced except for 5F of PGA=0.1g, 0.2g, 0.3g and 0.4g, 2F of PGA=0.1g. The reduction of the 1st floor peak acceleration in the case of PGA=0.1g is 16% and increased to 38% in the case of PGA=0.4g. The controlling effects of the damper system is even more pronounced as we look into the root-mean-squares (RMS) responses of the floor accelerations, as summarized in Table 5.4. The RMS responses are reduced except for 5F of PGA=0.1g. The reduction of the 5th floor RMS acceleration in the case of PGA=0.2g is 18%, and increased to over 40% for higher intensities.

The comparison of the storydrift of the 1st floor under the El Centro earthquake are illustrated in Fig. 5.13 ~ 3.16 for intensities of 0.1g, 0.2g, 0.3g and 0.4g, respectively. The controlling effects of the damper on the displacement responses have been achieved to a greater extent. The comparison of the root-mean-squares responses of the 1st floor storydrift is summarized in Table 5.5. The reduction of the RMS response is 62% in the case of PGA=0.1g and increases for higher intensities.

The dynamic characteristics of the model structure in terms of the equivalent natural frequency and damping ratio of each mode under each testing scenario were determined, using the system identification technique from the test results, and summarized in Table 5.6. It is noted that the equivalent natural frequencies of the model structure decrease as the earthquake intensity increased, while the model damping ratios increase with the earthquake intensity. This is due to involvement of more inelastic behavior of the dampers for stronger earthquake. The natural frequencies of the structure have been increased as compared with those for the bare frame from Table 5.2 due to the added stiffness by the damper. The damping ratio of the 1st mode was increased from 0.51% to 2.89% for PGA=0.1g and up to 7.49% for PGA=0.4g. Similar trends have been observed for the other modes.

Hachinohe Earthquake The comparisons of floor acceleration responses under the Hachinohe earthquake are illustrated in Fig. 5.17 ~ 5.20 for intensities of 0.1g, 0.15g, 0.2g and 0.25g, respectively. As protected with damper, evident reductions of all the floor accelerations at various earthquake intensities have been observed, without exception. The peak floor responses at each testing scenario are summarized in Table 5.7. The reduction of the 5th floor peak acceleration in the case of PGA=0.1g is 46%, and increased slightly for higher intensities. The reduction of the 1st floor peak acceleration in the case of PGA=0.1g is 31% and increased to 49% in the case of PGA=0.25g. The controlling effects of the damper system is even more pronounced as we look into the root-mean-squares (RMS) responses of the floor accelerations, as summarized in Table 5.8. The reduction of the 5th floor RMS acceleration in the case of PGA=0.1g is 54%, and increased to over 70% for higher intensities. The comparison of the storydrift of the 1st floor under the Hachinohe earthquake are illustrated in Fig. 5.21~3.24 for intensities of 0.1g, 0.15g, 0.2g and 0.25g, respectively. The controlling effects of the damper on the displacement responses have been achieved to a greater extent. The comparison of the root-mean-squares responses of the 1st floor storydrift is summarized in Table 5.9. The reduction of the RMS response is 72% in the case of PGA=0.1g and 81% for higher intensities.

The dynamic characteristics of the model structure in terms of the equivalent natural frequency and damping ratio of each mode under each testing scenario were determined, using the system identification technique from the test results, and summarized in Table 5.10. It is noted that the equivalent natural frequencies of the model structure decrease as the earthquake intensity increased, while the model damping ratios increase with the earthquake intensity. This is due to involvement of more inelastic behavior of the dampers for stronger earthquake. The natural frequencies of the structure have been increased as compared with those for the bare frame from Table 5.2 due to the added stiffness by the damper. The damping ratio of the 1st mode was increased from 0.51% to 4.79% for PGA=0.1g and up to 10.34% for PGA=0.25g. Similar trends have been observed for the other modes.

Kobe Earthquake The comparisons of floor acceleration responses under the Kobe earthquake are illustrated in Fig. 5.25 ~ 5.28 for intensities of 0.1g, 0.15g, 0.2g and 0.25g, respectively. Similarly, as protected with damper, evident reductions of all the floor accelerations at various earthquake intensities have been observed, without exception. The peak floor responses at each testing scenario are summarized in Table 5.11. The reduction of the 5th floor peak acceleration in the case of PGA=0.1g is 45%, and increased slightly for higher intensities. The reduction of the 1st floor peak acceleration in the case of PGA=0.1g is 21% and increased to 28% in the case of PGA=0.2g. The controlling effects of the damper system is even more pronounced as we look into the root-mean-squares (RMS) responses of the floor accelerations, as summarized in Table 5.12. The reduction of the 5th floor RMS acceleration in the case of PGA=0.10g is 72%, and increased to 75% in the case of PGA=0.25g.

The comparison of the storydrift of the 1st floor under the Hachinohe earthquake are illustrated in Fig. 3.29~3.32 for intensities of 0.1g, 0.15g, 0.2g and 0.25g, respectively. The controlling effects of the damper on the displacement responses have been achieved to a greater extent. The comparison of the root-mean-squares responses of the 1st floor storydrift is summarized in Table 5.13. The reduction of the RMS response is 85% in the case of PGA=0.1g and 81% for higher intensities.

The dynamic characteristics of the model structure in terms of the equivalent natural frequency and damping ratio of each mode under each testing scenario were determined, using the system identification technique from the test results, and summarized in Table 5.14. It is noted that the equivalent natural frequencies of the model structure decrease as the earthquake intensity increased, while the modal damping ratios increase with the earthquake intensity. This again is due to involvement of more inelastic behavior of the dampers for stronger earthquake. The natural frequencies of the structure have been increased as compared with those for the bare frame from Table 2.2 due to the added stiffness by the damper. The damping ratio of the 1st mode was increased from 0.51% to 7.56% for PGA=0.1g and up to 9.26% for PGA=0.25g. Similar trends have been observed for the 2nd mode.

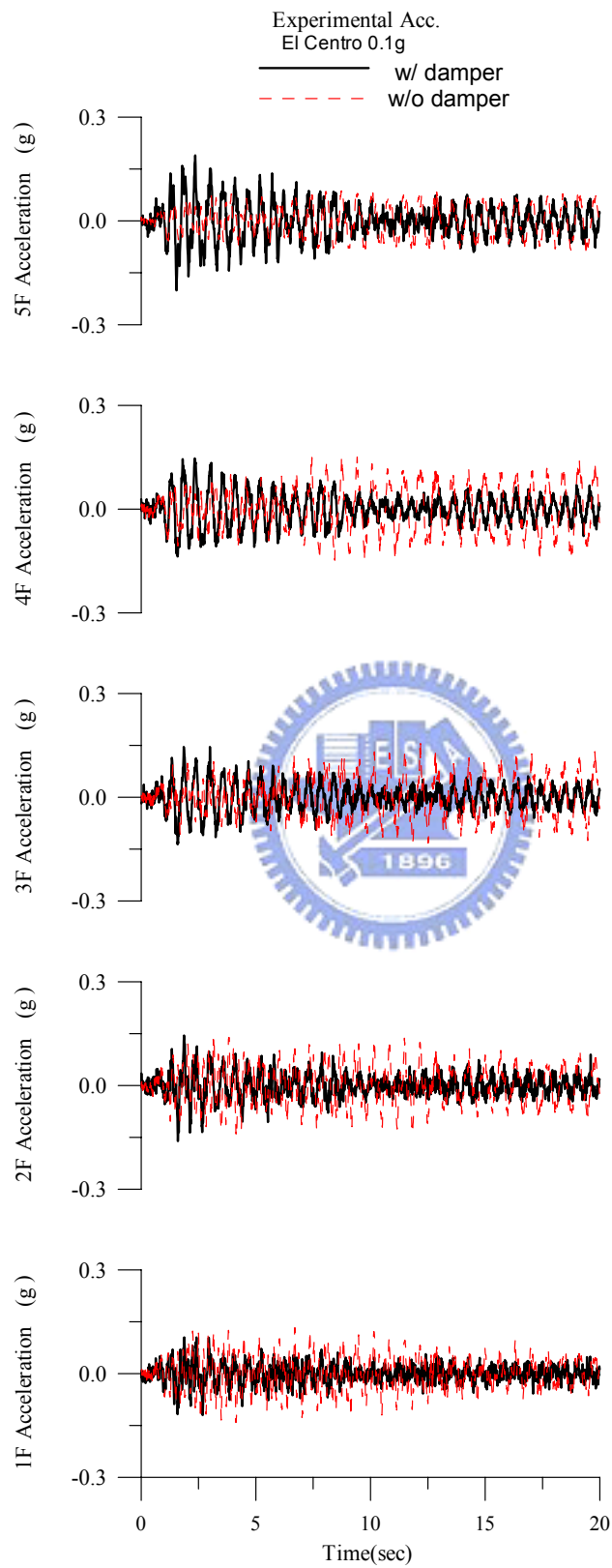


Fig. 5.9 Comparison of floor acceleration responses (El Centro, PGA=0.1g)

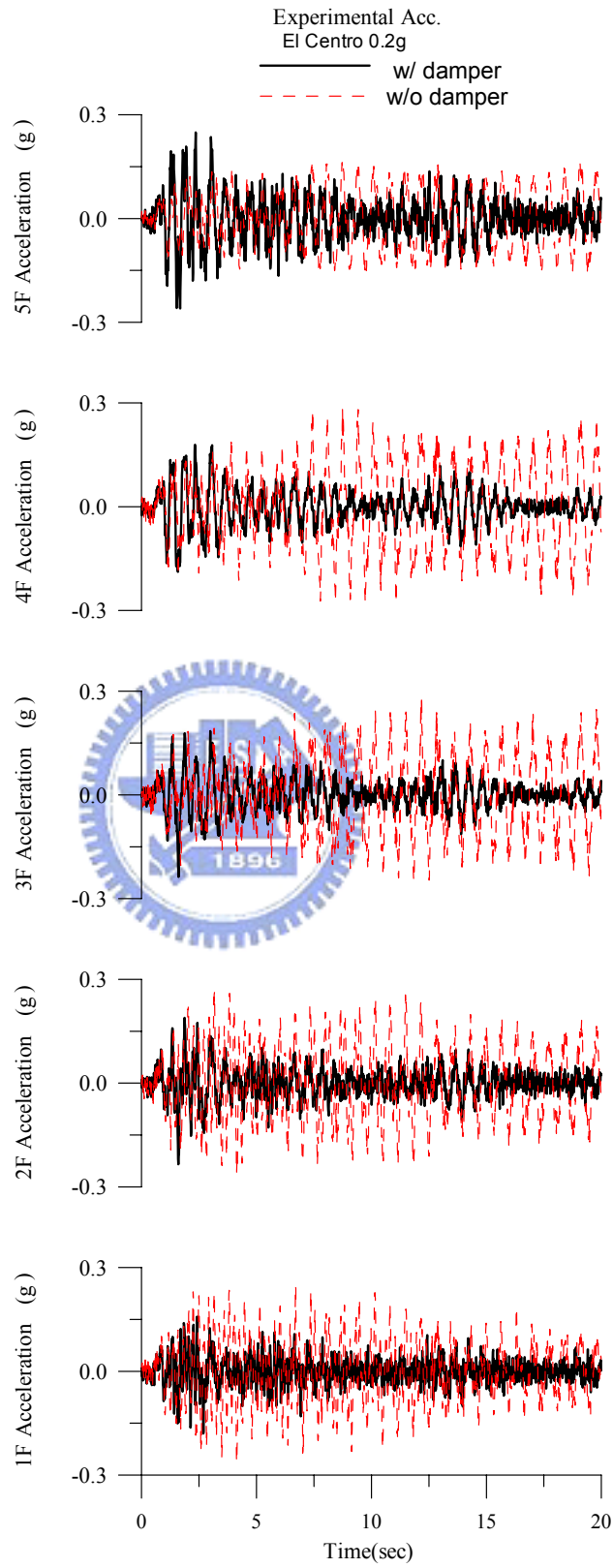


Fig. 5.10 Comparison of floor acceleration responses (El Centro, PGA=0.2g)

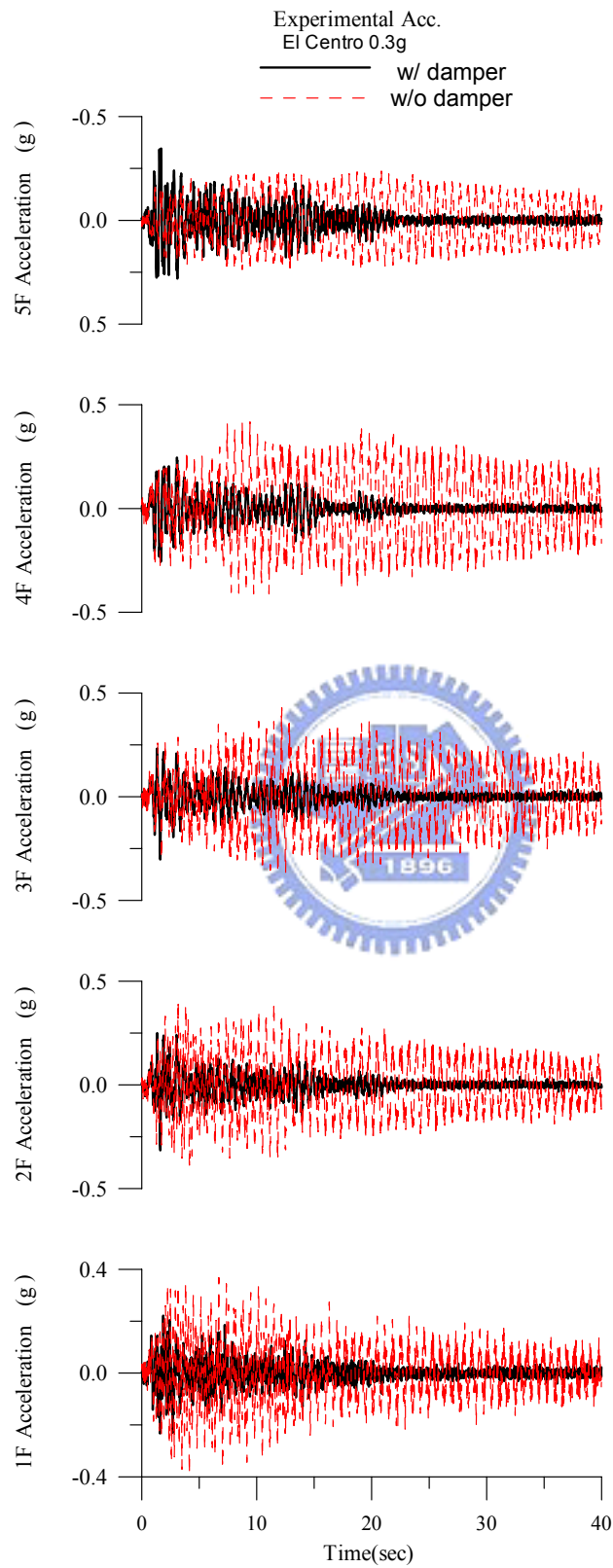


Fig. 5.11 Comparison of floor acceleration responses (El Centro, PGA=0.3g)

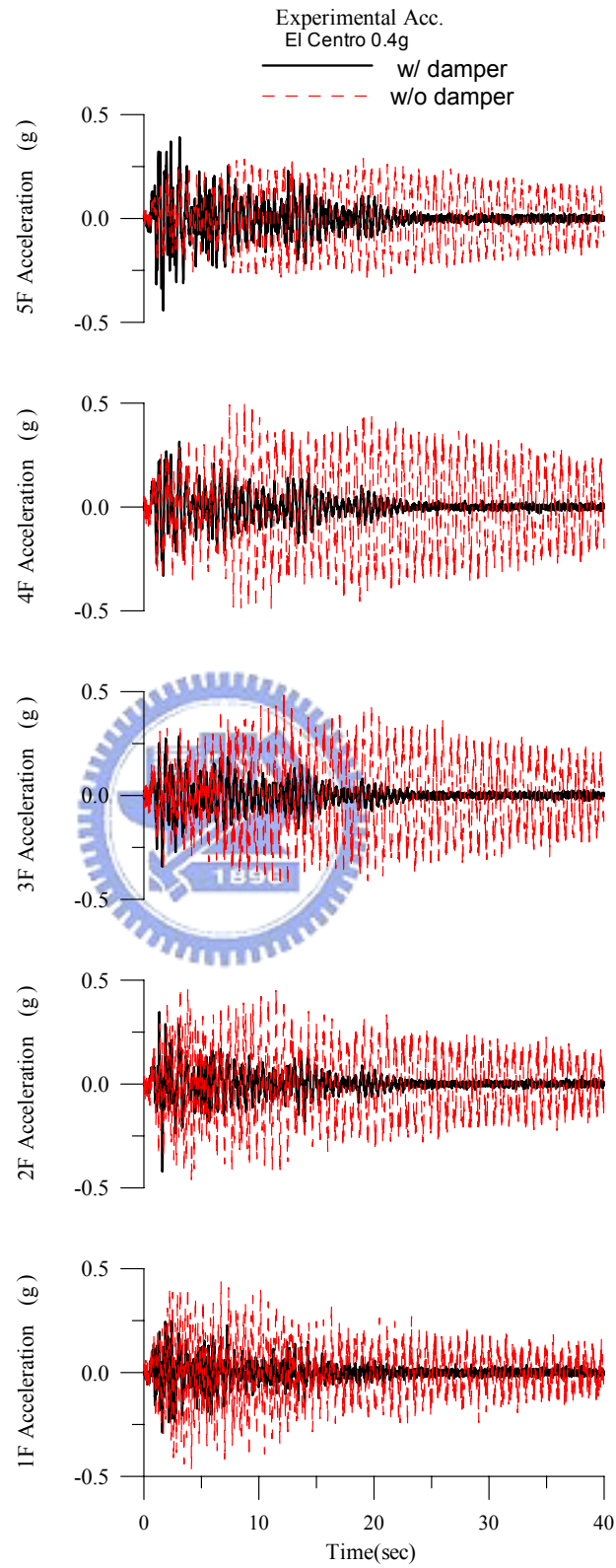


Fig. 5.12 Comparison of floor acceleration responses (El Centro, PGA=0.4g)

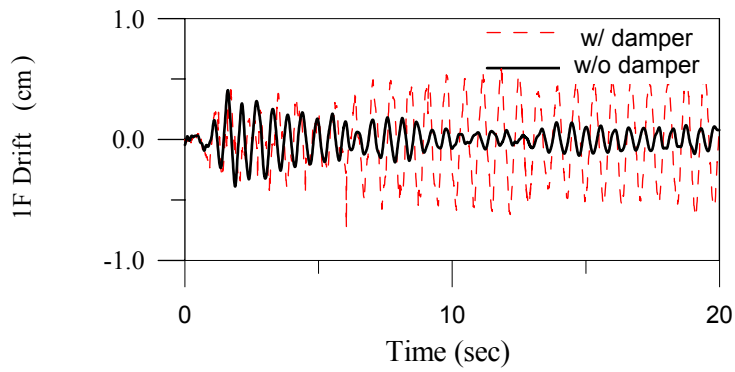


Fig. 5.13 Comparison of storydrift of the 1st Floor
(El Centro, PGA = 0.1g)

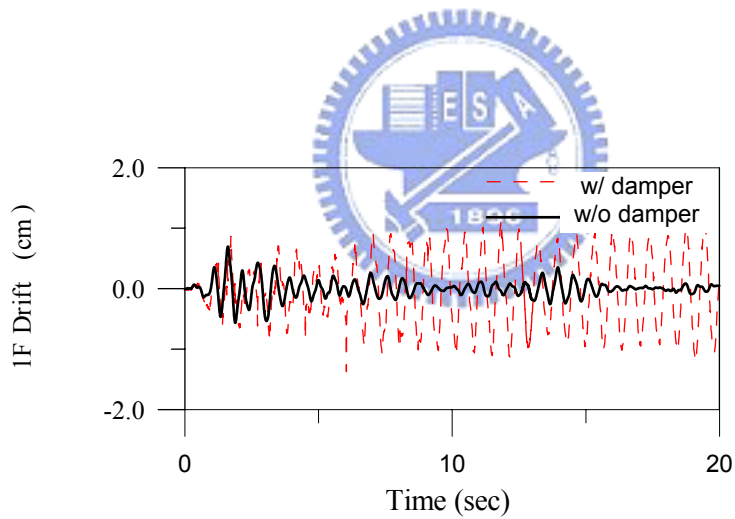


Fig. 5.14 Comparison of storydrift of the 1st Floor
(El Centro, PGA = 0.2g)

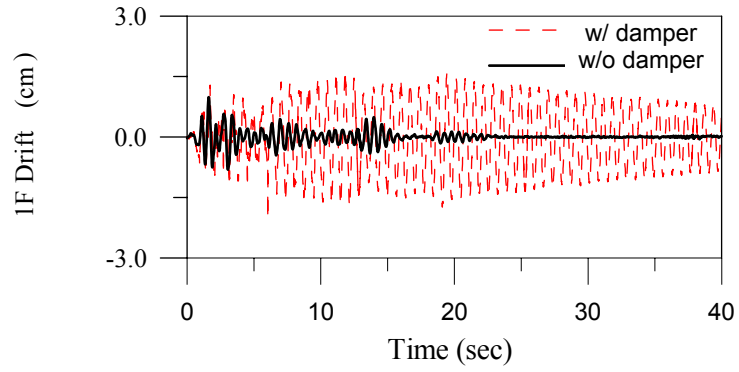


Fig. 5.15 Comparison of storydrift of the 1st Floor
(El Centro, PGA = 0.3g)

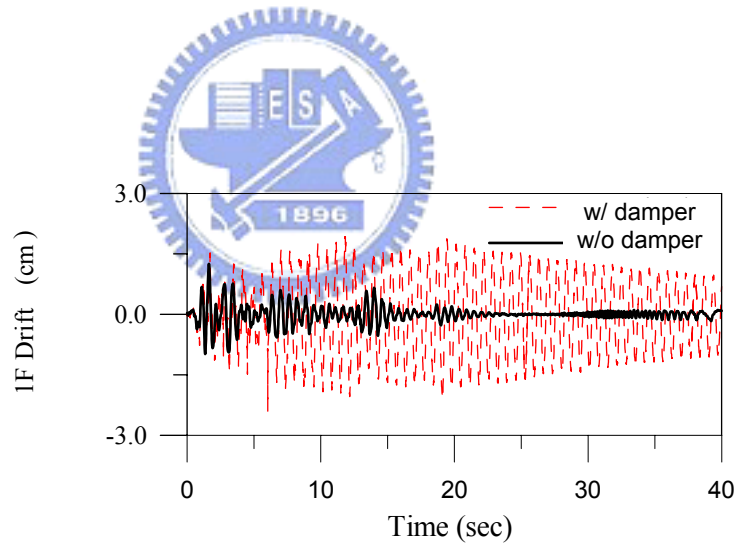


Fig. 5.16 Comparison of storydrift of the 1st Floor
(El Centro, PGA = 0.4g)

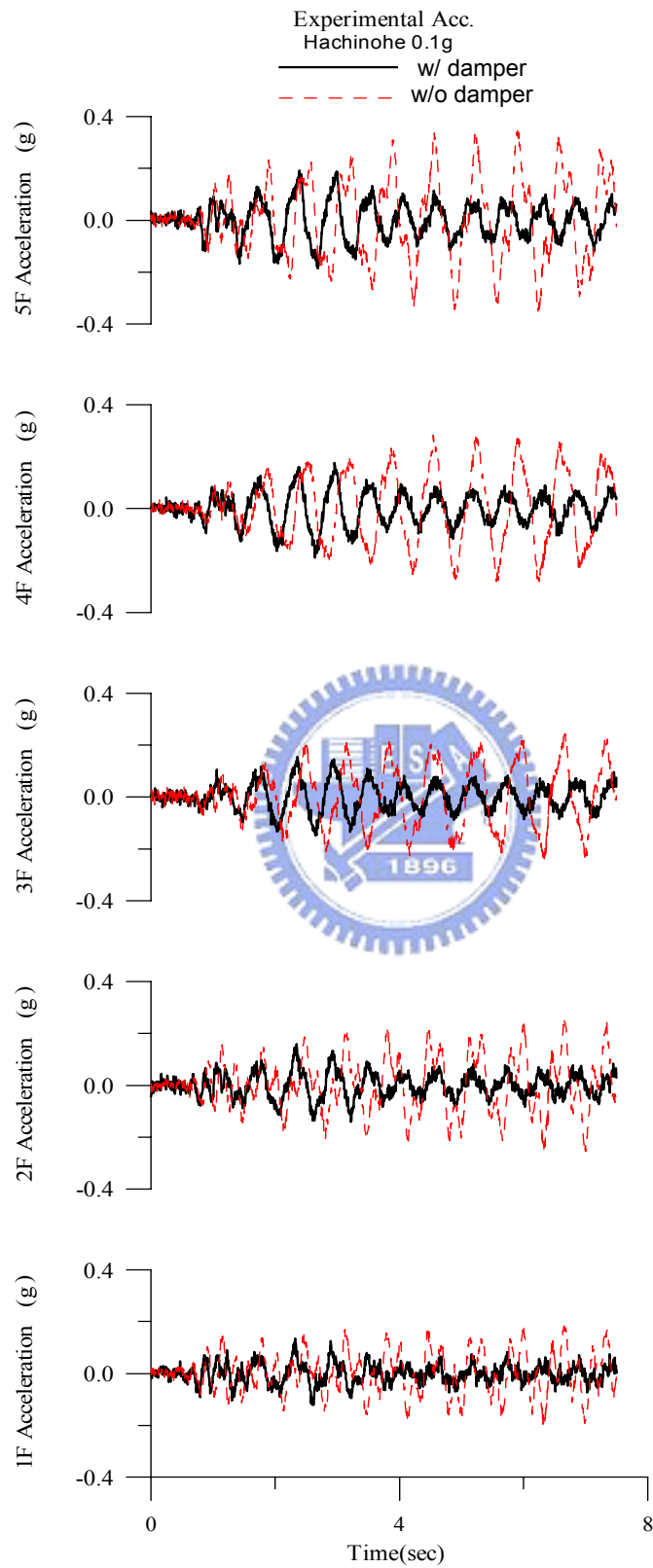


Fig. 5.17 Comparison of Floor Acceleration Responses (Hachinohe, PGA = 0.1g)

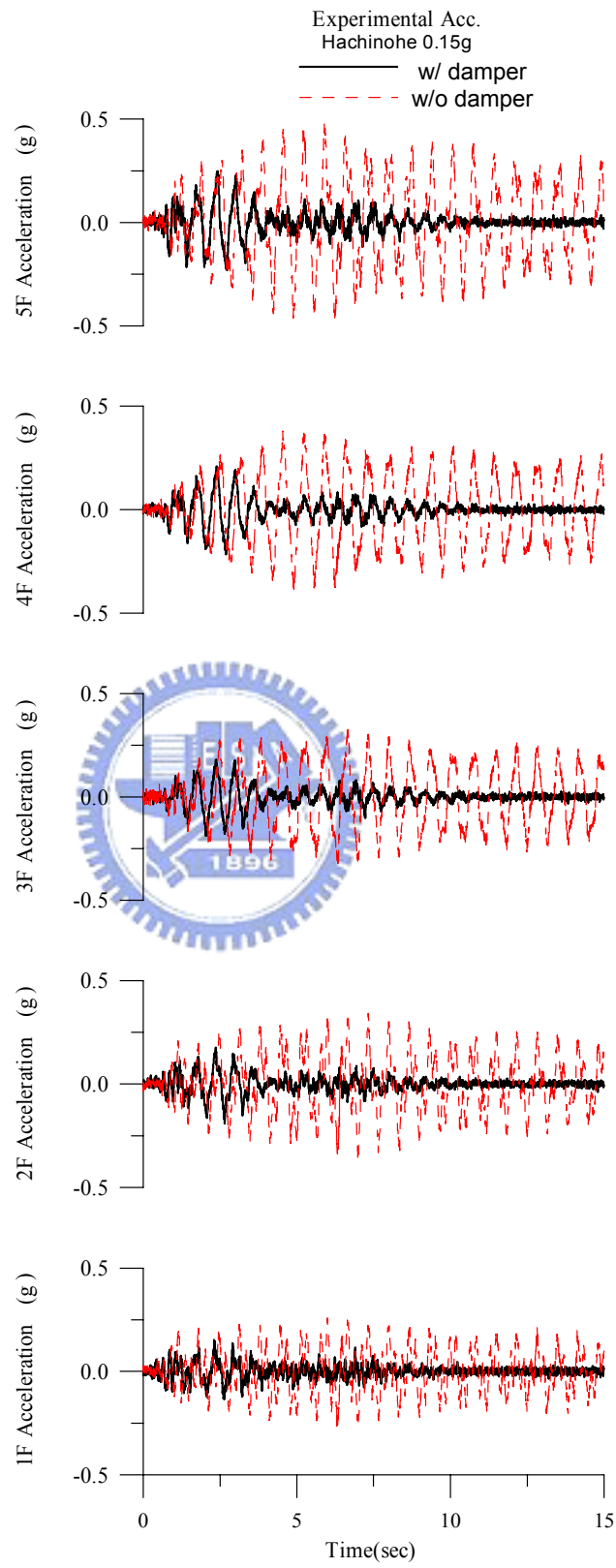


Fig. 5.18 Comparison of Floor Acceleration Responses (Hachinohe, PGA = 0.15g)

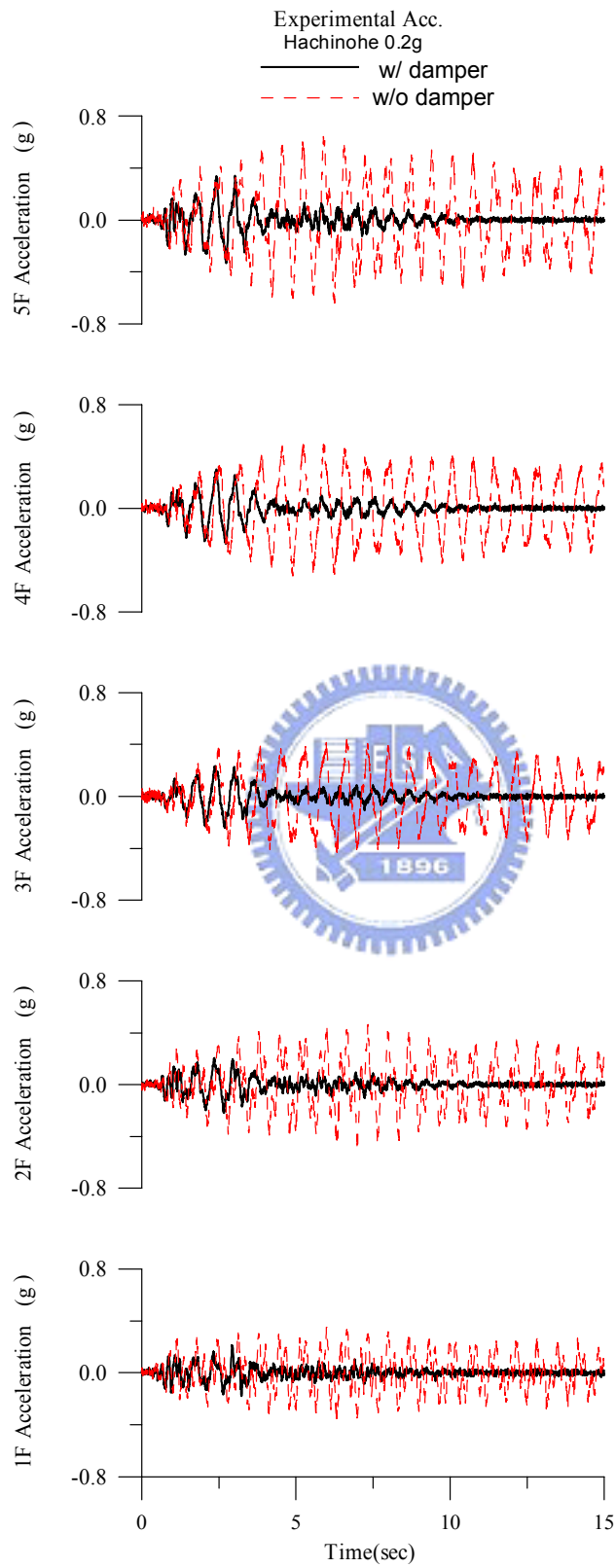


Fig. 5.19 Comparison of Floor Acceleration Responses (Hachinohe, PGA = 0.20g)

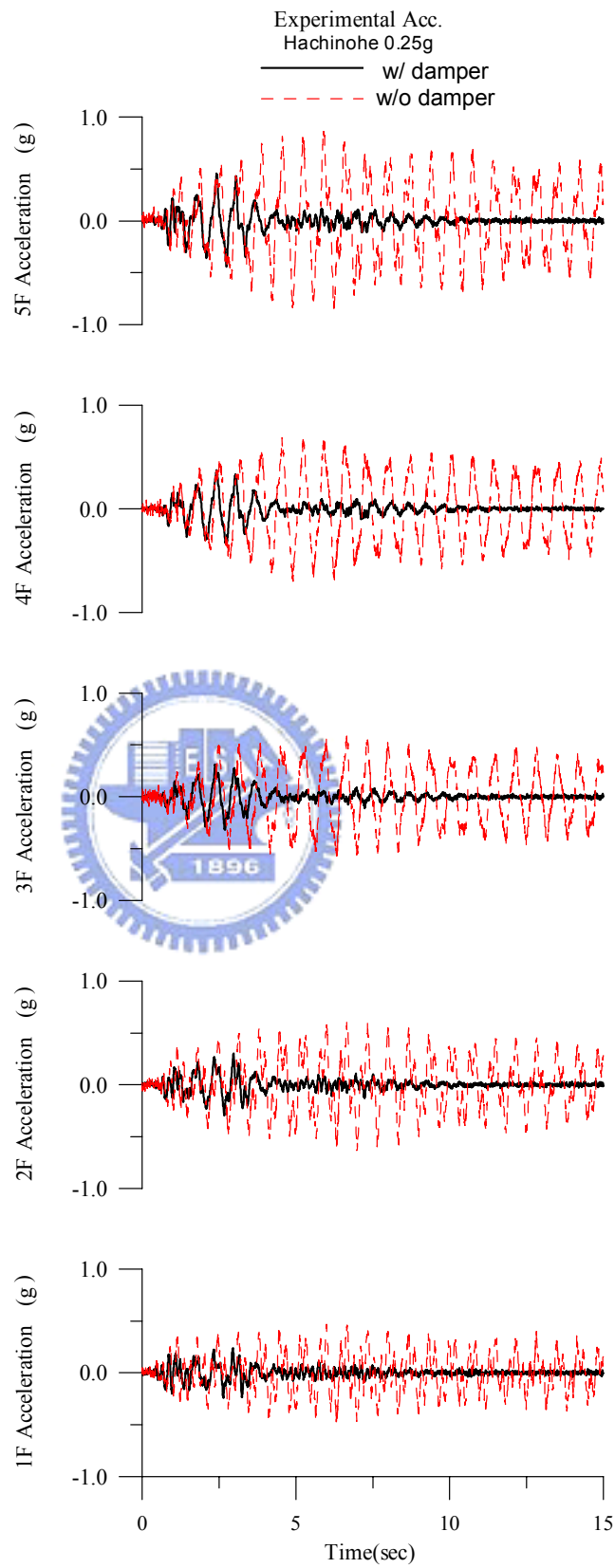


Fig. 5.20 Comparison of Floor Acceleration Responses (Hachinohe, PGA = 0.25g)

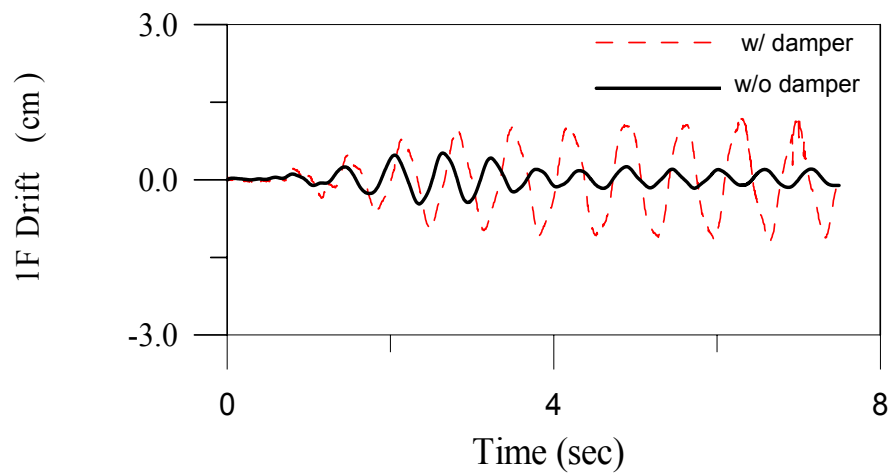


Fig. 5.21 Comparison of Storydrift of the 1st Floor (Hachinohe, PGA = 0.1g)

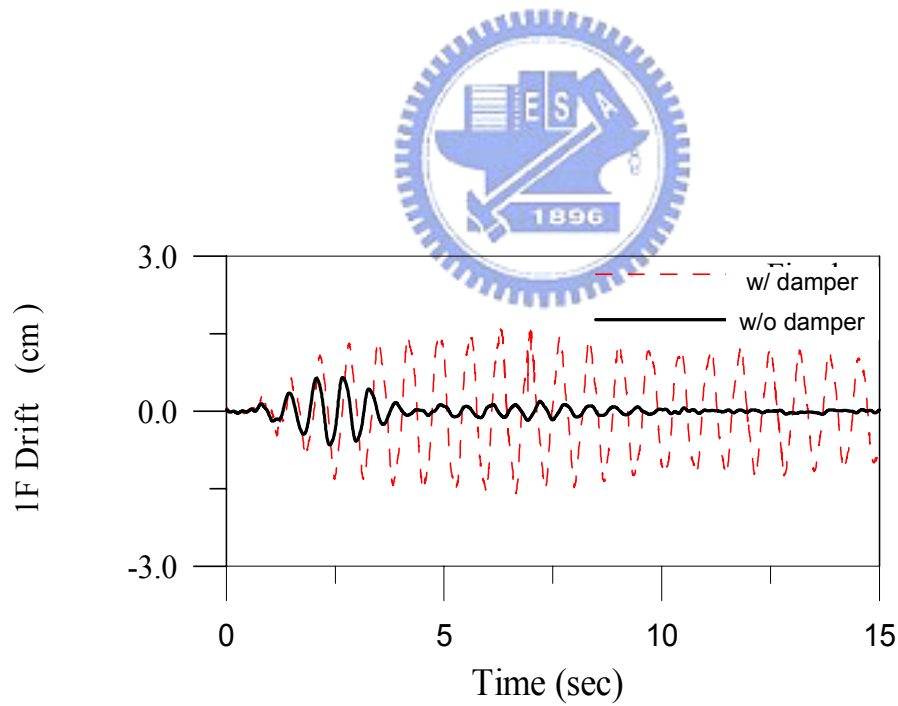


Fig. 5.22 Comparison of Storydrift of the 1st Floor (Hachinohe, PGA = 0.15g)

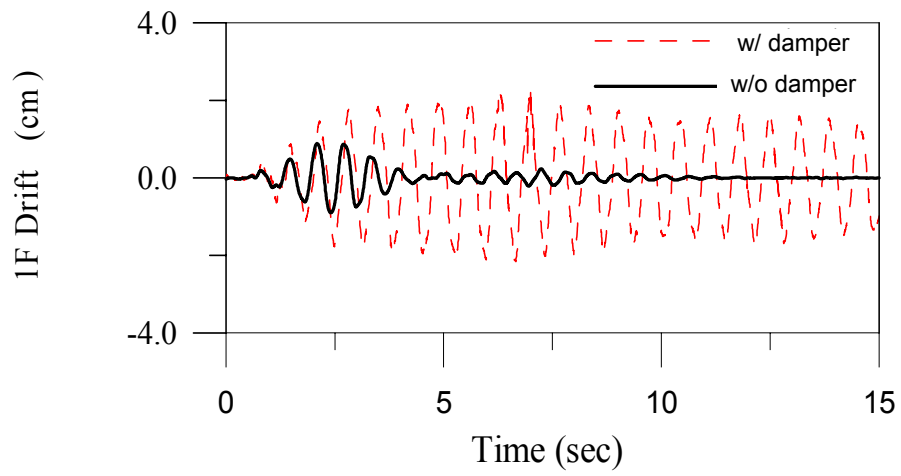


Fig. 5.23 Comparison of Storydrift of the 1st Floor (Hachinohe, PGA = 0.2g)

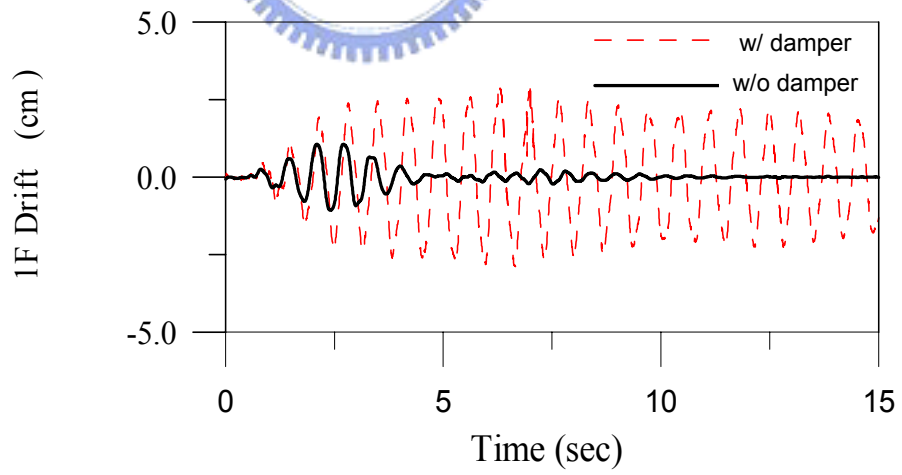


Fig. 5.24 Comparison of Storydrift of the 1st Floor (Hachinohe, PGA = 0.25g)

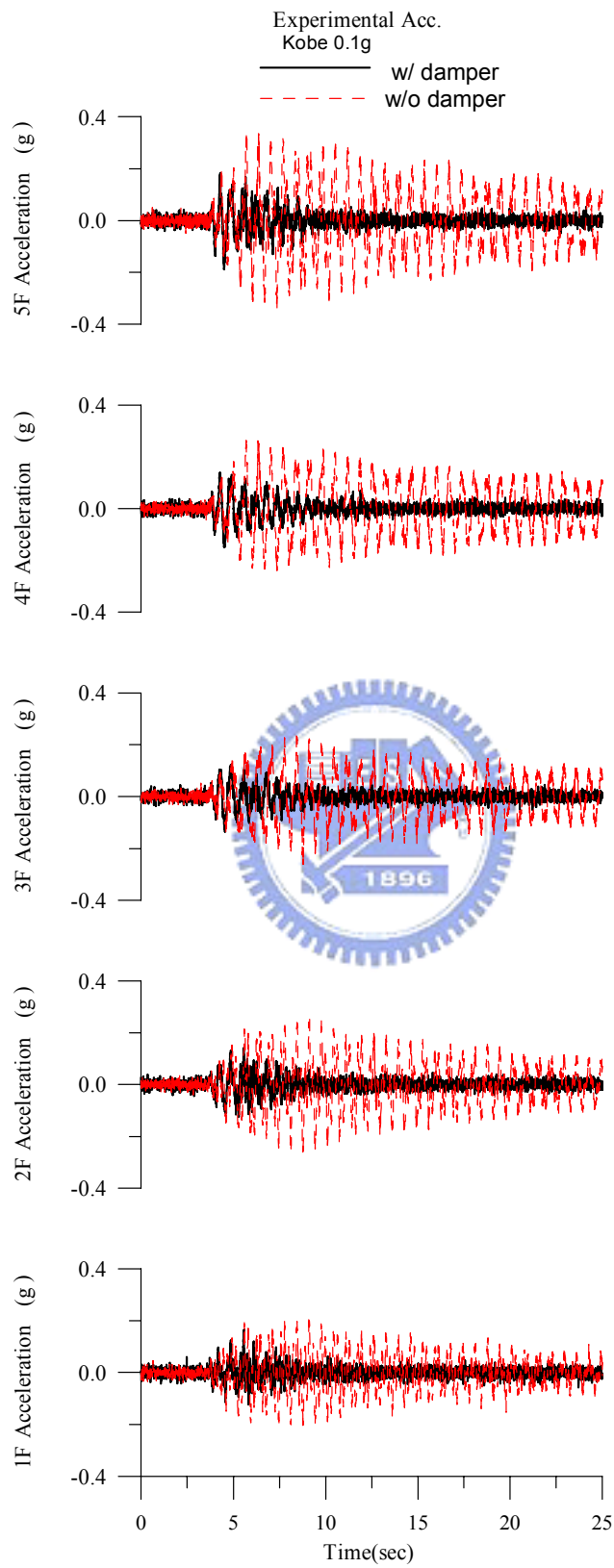


Fig. 5.25 Comparison of Floor Acceleration Responses (Kobe, PGA = 0.1g)

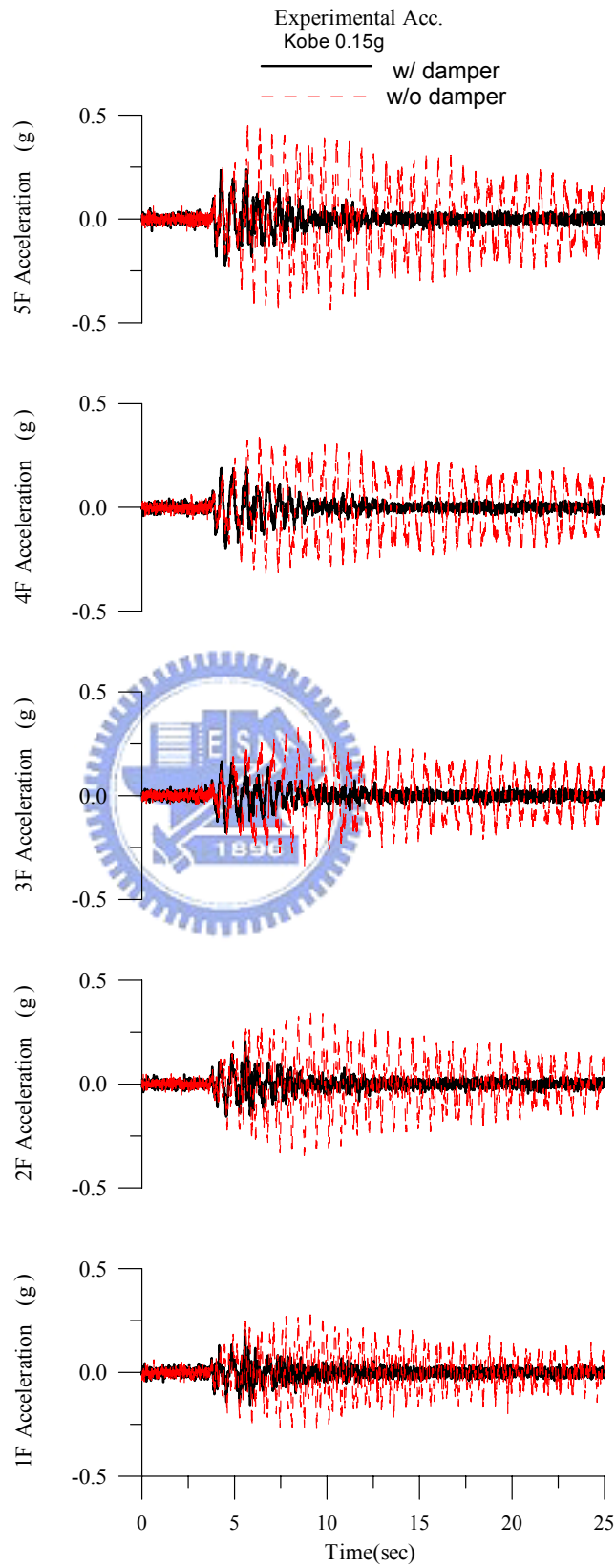


Fig. 5.26 Comparison of Floor Acceleration Responses (Kobe, PGA = 0.15g)

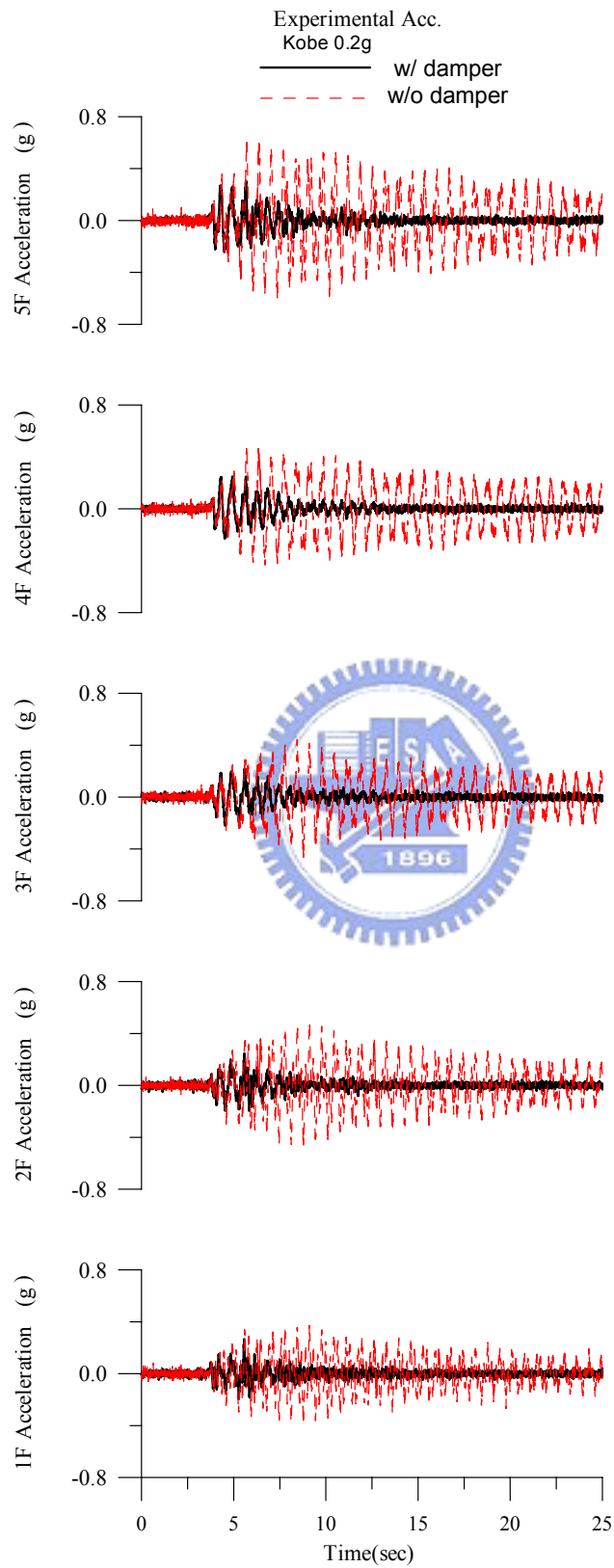


Fig. 5.27 Comparison of Floor Acceleration Responses (Kobe, PGA = 0.2g)

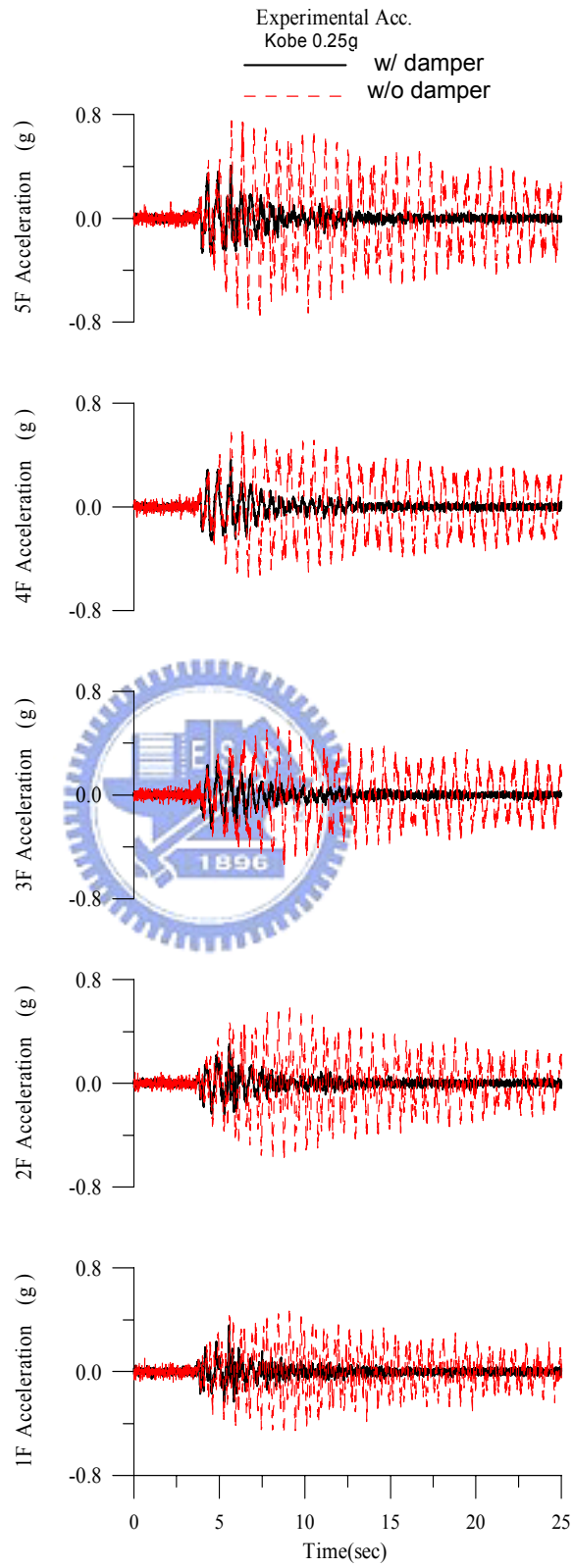


Fig. 5.28 Comparison of Floor Acceleration Responses (Kobe, PGA = 0.25g)

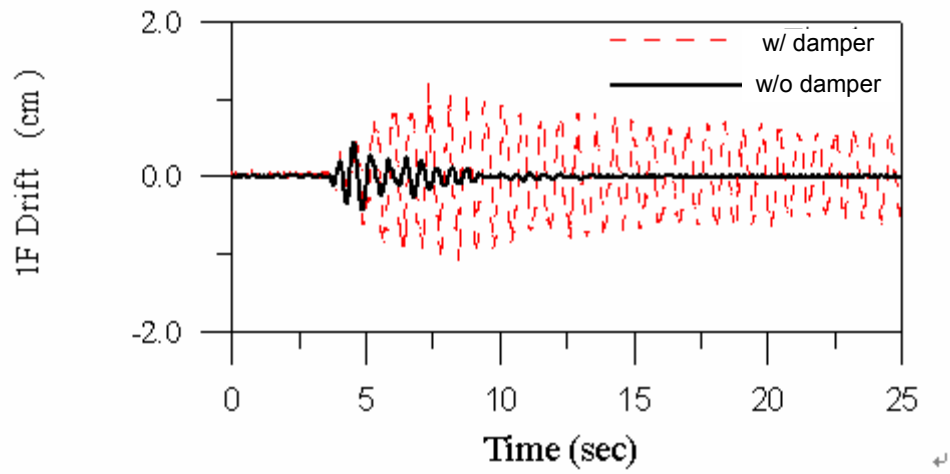


Fig. 5.29 Comparison of Storydrift of the 1st Floor
(Kobe, PGA = 0.1g)

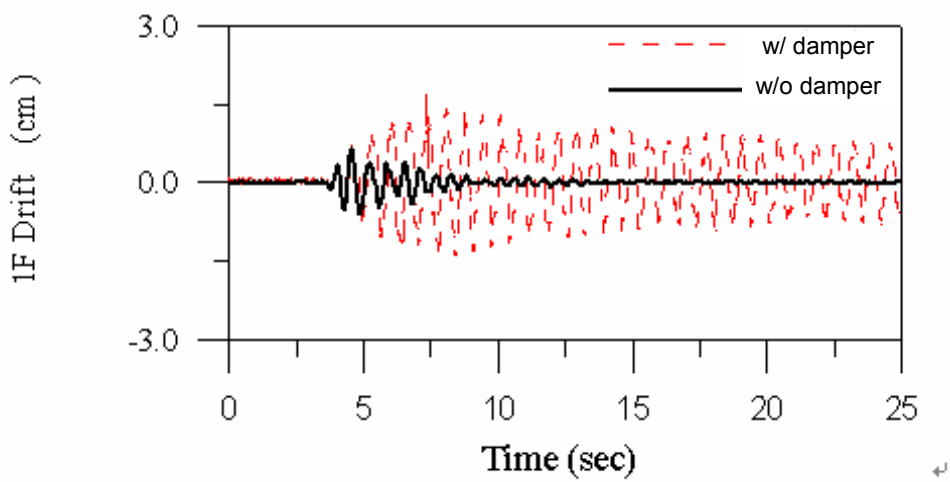


Fig. 5.30 Comparison of Storydrift of the 1st Floor
(Kobe, PGA = 0.15g)

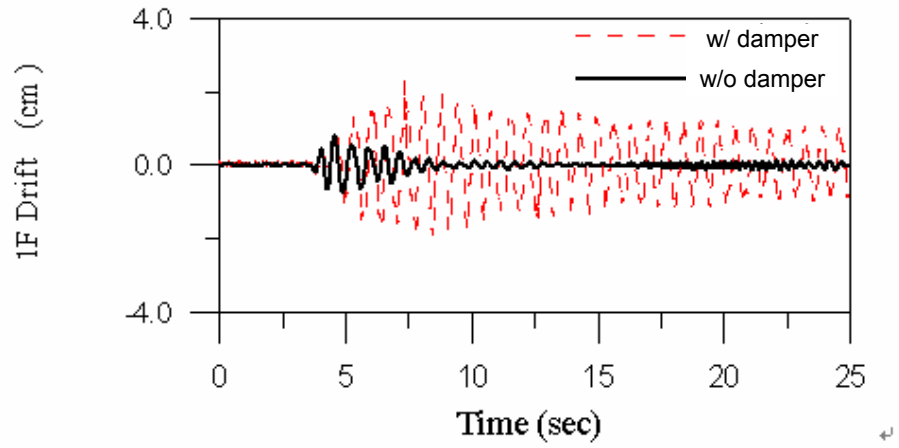


Fig. 5.31 Comparison of Storydrift of the 1st Floor
(Kobe, PGA = 0.2g)

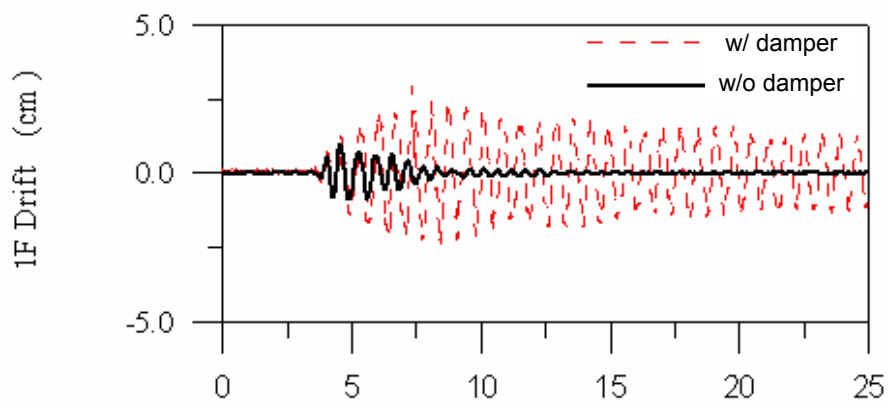


Fig. 5.32 Comparison of Storydrift of the 1st Floor
(Kobe, PGA = 0.25g)

Table 5.3 Comparison of Peak Floor Acceleration Responses in the El Centro Series of Tests

<i>Input = El Centro Earthquake</i>						
	PGA = 0.1g			PGA = 0.2g		
Floor	w/o damper (g)	w/ damper (g)	Reduction (%)	w/o damper (g)	w/ damper (g)	Reduction (%)
5F	0.088	0.2	-127	0.164	0.259	-58
4F	0.152	0.147	3	0.283	0.179	3
3F	0.155	0.146	6	0.289	0.237	37
2F	0.141	0.161	-14	0.262	0.235	10
1F	0.141	0.119	16	0.264	0.179	32
	PGA = 0.3g			PGA = 0.4g		
Floor	w/o damper (g)	w/ damper (g)	Reduction (%)	w/o damper (g)	w/ damper (g)	Reduction (%)
5F	0.244	0.346	-42	0.289	0.443	-53
4F	0.419	0.547	39	0.499	0.331	34
3F	0.429	0.302	30	0.51	0.343	33
2F	0.388	0.316	19	0.462	0.422	9
1F	0.391	0.233	40	0.464	0.289	38

Table 5.4 Comparison of Root-Mean-Squares Floor Acceleration In the El Centro Series of Tests

<i>Input = El Centro Earthquake</i>						
	PGA = 0.1g			PGA = 0.2g		
Floor	w/o <i>damper</i> (g)	w/ <i>damper</i> (g)	Reduction (%)	w/o <i>damper</i> (g)	w/ <i>damper</i> (g)	Reduction (%)
5F	0.042	0.050	-19	0.077	0.063	18
4F	0.061	0.044	28	0.155	0.051	56
3F	0.054	0.038	30	0.101	0.046	54
2F	0.048	0.034	29	0.09	0.043	52
1F	0.039	0.027	31	0.072	0.039	46
	PGA = 0.3g			PGA = 0.4g		
Floor	w/o <i>damper</i> (g)	w/ <i>damper</i> (g)	Reduction (%)	w/o <i>damper</i> (g)	w/ <i>damper</i> (g)	Reduction (%)
5F	0.015	0.060	48	0.136	0.074	46
4F	0.169	0.049	71	0.202	0.062	69
3F	0.149	0.044	70	0.178	0.054	70
2F	0.134	0.041	69	0.159	0.051	68
1F	0.107	0.038	64	0.128	0.046	64

Table 5.5 Root-Mean-Squares of 1st Floor Storydrift In the El Centro Series of Tests

<i>Input= El Centro Earthquake</i>			
PGA	RMS Response of Storydrift (cm)		Reduction (%)
	w/o damper	w/ damper	
0.1g	0.29	0.11	62
0.2g	0.55	0.15	73
0.3g	0.81	0.16	80
0.4g	0.97	0.21	78

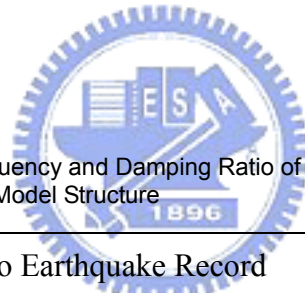


Table 5.6 Equivalent Natural Frequency and Damping Ratio of the damper-Protected Model Structure

El Centro Earthquake Record								
Mode	PGA = 0.1g		PGA = 0.2g		PGA = 0.3g		PGA = 0.4g	
	Fre. (Hz)	Damping Ratio (%)	Fre. (Hz)	Damping Ratio (%)	Fre. (Hz)	Damping Ratio (%)	Fre. (Hz)	Damping Ratio (%)
1	1.84	2.89	1.77	6.90	1.69	8.04	1.73	7.49
2	5.78	1.46	5.72	2.11	5.68	3.34	5.71	2.66
3	9.55	2.50	9.42	2.10	9.39	3.43	9.29	3.25
4	12.49	2.80	12.43	1.23	12.20	1.44	12.30	1.65
5	15.64	2.87	14.49	2.30	14.29	3.14	14.55	3.14

Table 5.7 Comparison of Peak Floor Acceleration Responses in the Hachinohe Series of Tests

<i>Input = Hachinohe Earthquake</i>						
	PGA = 0.10g			PGA = 0.15g		
Floor	w/o <i>damper</i> (g)	w/ <i>damper</i> (g)	Reduction (%)	w/o <i>damper</i> (g)	w/ <i>damper</i> (g)	Reduction (%)
5F	0.355	0.193	46	0.476	0.248	48
4F	0.288	0.188	35	0.386	0.214	45
3F	0.243	0.154	37	0.326	0.188	42
2F	0.262	0.159	39	0.352	0.192	45
1F	0.196	0.135	31	0.262	0.151	42
	PGA = 0.20g			PGA = 0.25g		
Floor	w/o <i>damper</i> (g)	w/ <i>damper</i> (g)	Reduction (%)	w/o <i>damper</i> (g)	w/ <i>damper</i> (g)	Reduction (%)
5F	0.643	0.340	47	0.860	0.455	47
4F	0.522	0.299	43	0.698	0.376	46
3F	0.441	0.241	45	0.589	0.320	46
2F	0.475	0.219	54	0.635	0.303	52
1F	0.354	0.211	40	0.474	0.242	49

Table 5.8 Comparison of Root-Mean-Squares Floor Acceleration In the Hachinohe Series of Tests

<i>Input = Hachinohe Earthquake</i>						
	PGA = 0.10g			PGA = 0.15g		
Floor	w/o damper (g)	w/ damper (g)	Reduction (%)	w/o damper (g)	w/ damper (g)	Reduction (%)
5F	0.148	0.068	54	0.199	0.055	72
4F	0.128	0.062	52	0.172	0.049	72
3F	0.111	0.054	51	0.149	0.043	71
2F	0.101	0.047	53	0.135	0.038	72
1F	0.176	0.036	53	0.102	0.032	69
	PGA = 0.20g			PGA = 0.25g		
Floor	w/o damper (g)	w/ damper (g)	Reduction (%)	w/o damper (g)	w/ damper (g)	Reduction (%)
5F	0.269	0.071	74	0.359	0.088	75
4F	0.232	0.063	73	0.311	0.077	75
3F	0.201	0.055	73	0.269	0.067	75
2F	0.182	0.049	73	0.244	0.061	75
1F	0.138	0.041	70	0.185	0.051	72

Table 5.9 Root-Mean-Squares of 1st Floor Storydrift In the Hachinohe Series of Tests

<i>Input= Hachinohe Earthquake</i>			
PGA	RMS Response of Storydrift (cm)		Reduction (%)
	<i>w/o damper</i>	<i>w/ damper</i>	
0.10g	0.64	0.18	72
0.15g	0.86	0.16	81
0.20g	1.16	0.22	81
0.25g	1.51	0.28	81

Table 5.10 Equivalent Natural Frequency and Damping Ratio of the damper-Protected Model Structure

Hachinohe Earthquake Record								
Mode	PGA = 0.1g		PGA = 0.15g		PGA = 0.2g		PGA = 0.25g	
	Fre. (Hz)	Damping Ratio (%)	Fre. (Hz)	Damping Ratio (%)	Fre. (Hz)	Damping Ratio (%)	Fre. (Hz)	Damping Ratio (%)
1	1.79	4.79	1.72	8.24	1.67	9.42	1.65	10.34
2	5.59	2.71	5.53	2.65	5.39	3.51	5.25	3.38
3	9.26	5.99	9.05	5.95	8.61	6.17	8.29	6.65
4	12.73	3.59	12.43	3.50	12.32	4.12	11.96	5.41
5	21.02	1.67	20.76	6.13	20.49	7.29	19.96	6.32

Table 5.11 Comparison of Peak Floor Acceleration Responses in the Kobe series Tests

<i>Input = Kobe Earthquake</i>						
	PGA = 0.10g			PGA = 0.15g		
Floor	w/o damper	w/ damper	Reduction (%)	w/o damper	w/ damper	Reduction (%)
5F	0.339	0.188	45	0.449	0.239	47
4F	0.262	0.148	44	0.347	0.201	42
3F	0.260	0.136	48	0.345	0.177	49
2F	0.262	0.141	46	0.347	0.204	40
1F	0.209	0.165	21	0.278	0.204	27
	PGA = 0.20g			PGA = 0.25g		
Floor	w/o damper	w/ damper	Reduction (%)	w/o damper	w/ damper	Reduction (%)
5F	0.602	0.305	49	0.752	0.406	46
4F	0.465	0.248	47	0.581	0.365	37
3F	0.462	0.219	53	0.577	0.266	54
2F	0.465	0.248	47	0.581	0.305	48
1F	0.372	0.267	28	0.465	0.358	23

Table 5.12 Comparison of Root-Mean-Squares Floor Acceleration for Kobe Series of Tests

<i>Input = Kobe Earthquake</i>						
	PGA = 0.1g			PGA = 0.15g		
Floor	w/o <i>damper</i> (g)	w/ <i>damper</i> (g)	Reduction (%)	w/o <i>damper</i> (g)	w/ <i>damper</i> (g)	Reduction (%)
5F	0.133	0.032	72	0.150	0.043	71
4F	0.094	0.027	71	0.124	0.037	70
3F	0.082	0.025	70	0.109	0.032	71
2F	0.083	0.025	70	0.109	0.032	71
1F	0.066	0.023	65	0.088	0.028	68
	PGA = 0.2g			PGA = 0.25g		
Floor	w/o <i>damper</i> (g)	w/ <i>damper</i> (g)	Reduction (%)	w/o <i>damper</i> (g)	w/ <i>damper</i> (g)	Reduction (%)
5F	0.201	0.053	74	0.256	0.065	75
4F	0.167	0.046	72	0.212	0.056	74
3F	0.146	0.040	73	0.185	0.049	74
2F	0.147	0.039	73	0.187	0.046	75
1F	0.118	0.033	72	0.149	0.041	72

Table 5.13 Root-Mean-Squares of 1st Floor Storydrift for Kobe Series of Tests

<i>RMS of 1F Drift for Kobe Earthquake Record (cm)</i>			
PGA	RMS of 1F Drift (cm)		Reduction (%)
	w/o damper	w/ damper	
0.1g	0.48	0.07	85
0.15g	0.63	0.12	81
0.2g	0.84	0.16	81
0.25g	1.02	0.19	81

Table 5.14 Equivalent Natural Frequency and Damping Ratio of the damper-Protected Model Structure

Kobe Earthquake Record								
Mode	PGA = 0.1g		PGA = 0.15g		PGA = 0.2g		PGA = 0.25g	
	Fre. (Hz)	Damping Ratio (%)	Fre. (Hz)	Damping Ratio (%)	Fre. (Hz)	Damping Ratio (%)	Fre. (Hz)	Damping Ratio (%)
1	1.75	7.56	1.71	8.05	1.68	8.92	1.67	9.26
2	5.68	2.86	5.57	2.92	5.50	3.04	5.44	4.03
3	9.26	5.94	9.32	5.23	9.08	4.25	8.92	4.14
4	13.31	5.11	12.76	3.06	12.50	3.92	12.26	2.97
5	24.78	1.24	24.80	1.2	24.80	1.15	24.76	1.06

5.2 Numerical Simulation Using SAP2000

SAP2000 is a powerful analysis software widely used in structural engineering. It offers the following analysis features [38]:

- Static and dynamic analysis
- Linear and nonlinear analysis
- Dynamic seismic analysis and static pushover analysis
- Frame and shell structural elements
- Two-dimensional plane and axisymmetric solid elements
- Three-dimensional solid elements
- Nonlinear link and spring elements
- Multiple coordinate systems
- Many types of constraints
- A wide variety of loading options

In addition to those analysis features, SAP2000 also provides a friendly graphical user interface which helps users to establish the analytical models both accurately and efficiently. The integration of these advantages makes SAP2000 superior to simulate the responses of the 5-story model structure under the various earthquake scenarios.

5.2.1 An Analytical Model in SAP2000

Two analytical models of the 5-story model structure, one for the bare frame (Fig. 5.33) and the other for the damper-implemented frame (Fig. 5.34) are established by SAP2000. These two models are completely identical except that the metallic yielding dampers are added to the later one. These models are established according to the real dimensions as shown in Fig. 5. 1 except that the height of every floor is subtracted from 28 cm. This is because stiffeners are added to the joints of the columns and the beams to increase the strength of the structure, which also reduces the effective length of the columns. The three elements used in these analytical models include:

The frame/cable element This element is used to model the beam-column and truss behavior in planar and three-dimensional structures. The frame/cable element uses a general, three-dimensional, beam-column formulation which includes the effects of biaxial bending, torsion, axial deformation, and biaxial shear deformation. Such an element is modeled as a straight line connecting two points and has its local coordinate system for defining section properties and loads. The section of the beams and the columns of the 5-story model structure is identical (Fig. 5.35) and that of the bracing systems is smaller (Fig. 5.36). Note that the material of the structural members can also be assigned for automatic dealing with the mass of the members.

The shell element The shell element is used to model shell, membrane, and plate behavior in planar and three-dimensional structures. The shell element is one type of area object. Depending on the type of section properties assigned to an area (Fig. 5.37), the object could also be used model the floor in the model structure. The thickness of the element is calculated according the weight, volume and density of the mass blocks installed in the 5-story model structure.

The plastic (Wen) link element This plasticity model, based on the hysteretic behavior proposed by Wen (1976), is used to model the inelastic behavior of the metallic damper installed on the model structure. Definition of parameters for this Wen Plasticity Property is shown in Fig. 5.39. The numerical values for these parameters as shown in Fig. 5.38 can be obtained from the fundamental of the damper (for stiffness, see section 2.2) and the component test of the scaled-down damper (for post yielding stiffness ratio and yielding strength, see section 4.1.4).

An analysis case in SAP2000 defines how the loads are to be applied to the structure (e.g., statically or dynamically), how the structure responds (e.g., linearly or nonlinearly), and how the analysis is to be performed (e.g., modally

or by direct-integration). SAP2000 provides the ability of defining several analysis cases to one model. The analysis cases that were defined in this study are summarized in Table 5.15. Three of these nine cases are defined for the bare-frame model while another six cases are defined for the damper-implemented frame model. In each of the nine cases, the type of loads and the structural responses are set to be earthquake and nonlinearity, respectively. Note that the input time-histories of the earthquakes to the SAP2000 models are the acceleration responses of the base of the 5-story model structure recorded in the shaking table tests.

The method of the nonlinear time-history analysis performed in these cases is an extension of the Fast Nonlinear Analysis (FNA) method developed by Wilson (Ibrahimbegovic and Wilson, 1989; Wilson, 1993). The method is extremely efficient and is designed to be used for structural systems which are primarily linear elastic, but which have a limited number of predefined nonlinear elements. The 5-story model structure on which has 10 sets of damper installed meets this condition.

Table 5.15 Analysis cases defined in SAP2000

Bare Frame		Damper-Implemented Frame		
Case	Earthquake	Case	Earthquake	
1	El Centro PGA = 0.1g	4	El Centro	PGA = 0.1g
		5		PGA = 0.4g
2	Hachinohe PGA = 0.1g	6	Hachinohe	PGA = 0.1g
		7		PGA = 0.25g
3	Kobe PGA = 0.1g	8	Kobe	PGA = 0.1g
		9		PGA = 0.25g

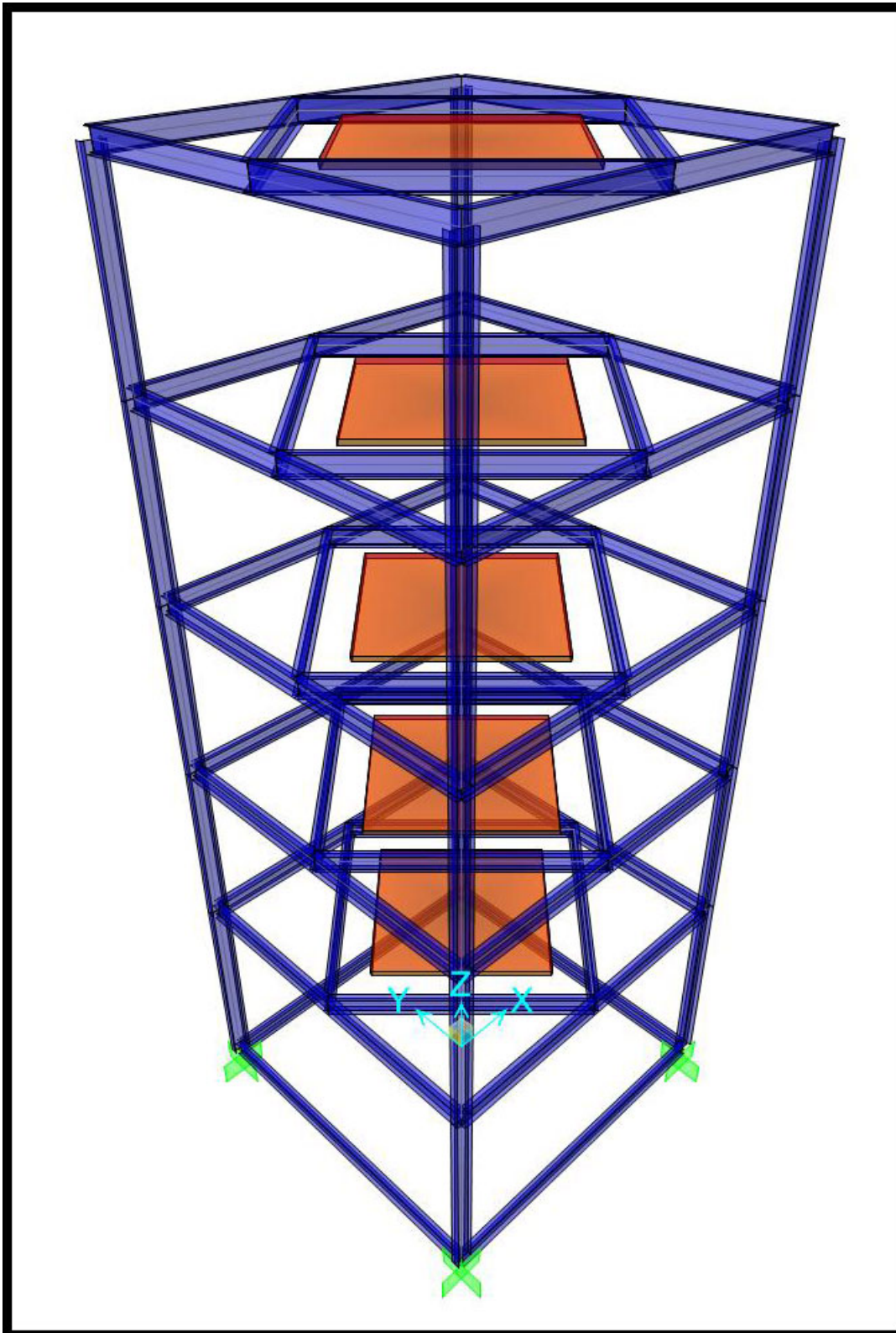


Fig. 5.33 The analytical model of the 5-story model structure (bare frame) established by SAP2000

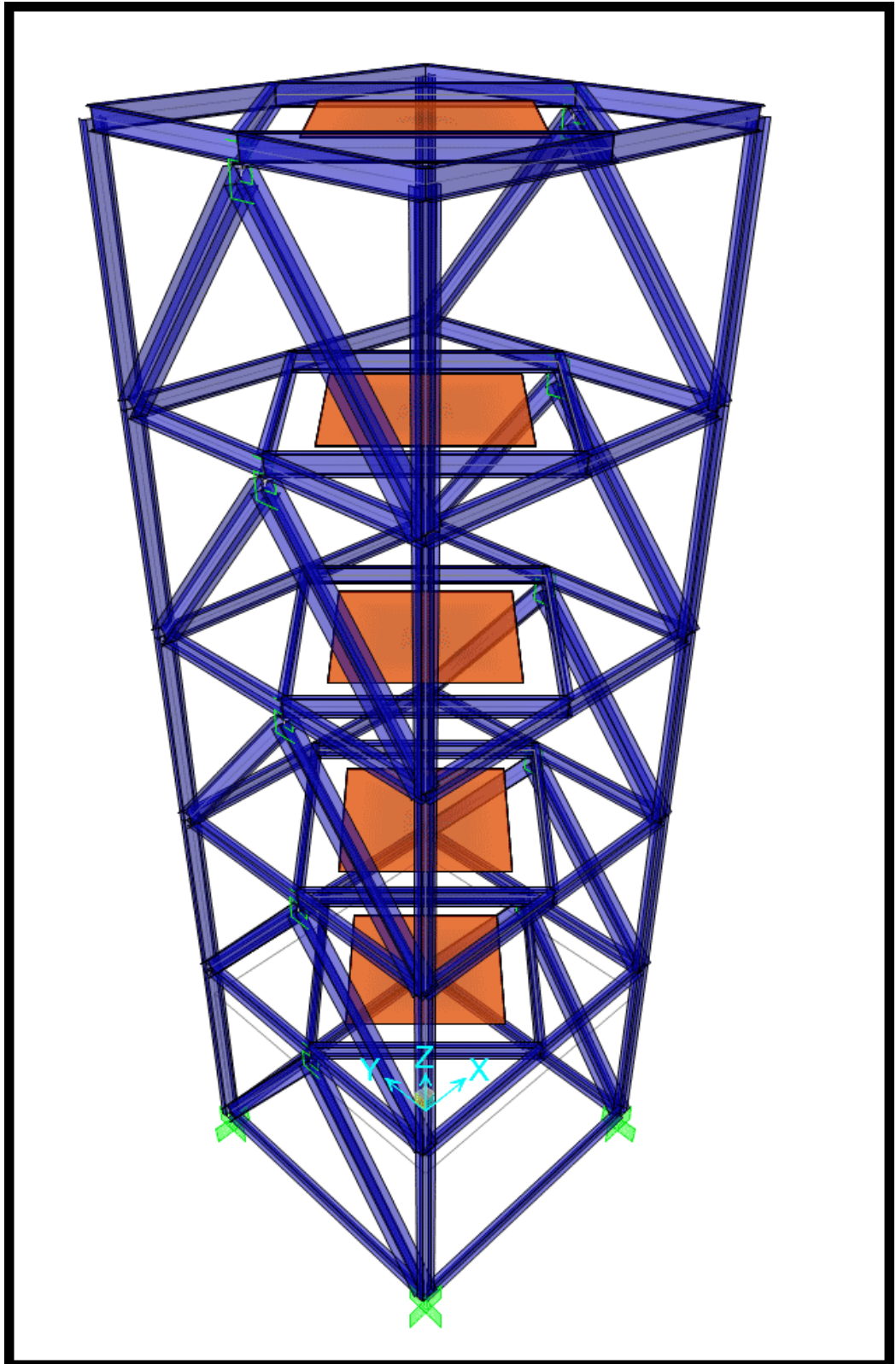


Fig. 5.34 The analytical model of the 5-story model structure (damper-implemented frame) established by SAP2000

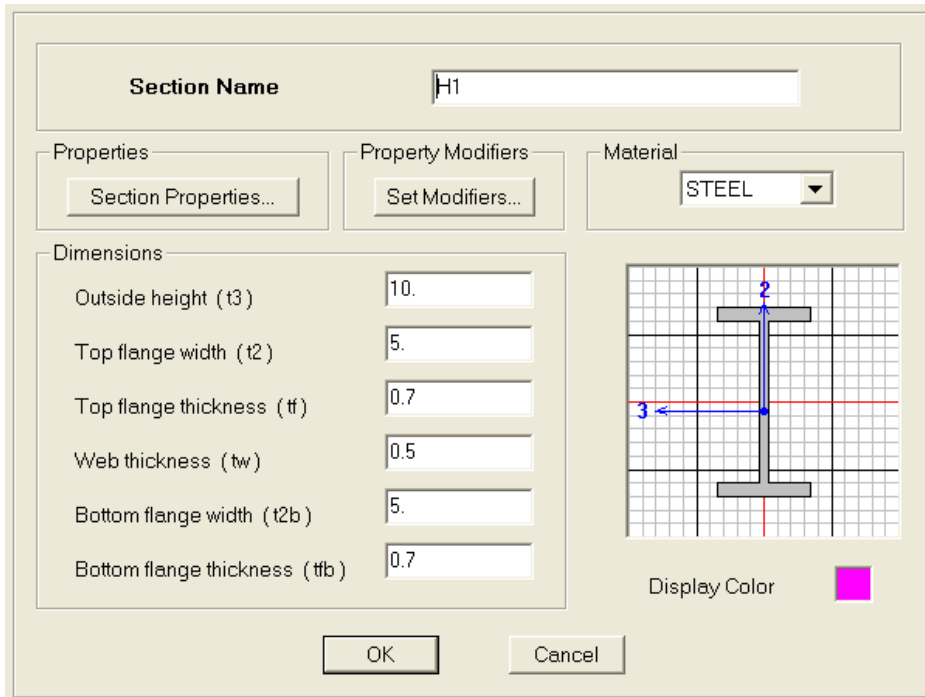


Fig. 5.35 The parameters for the frame/cable element specified for the beams and columns in the model structure (Unit: cm)

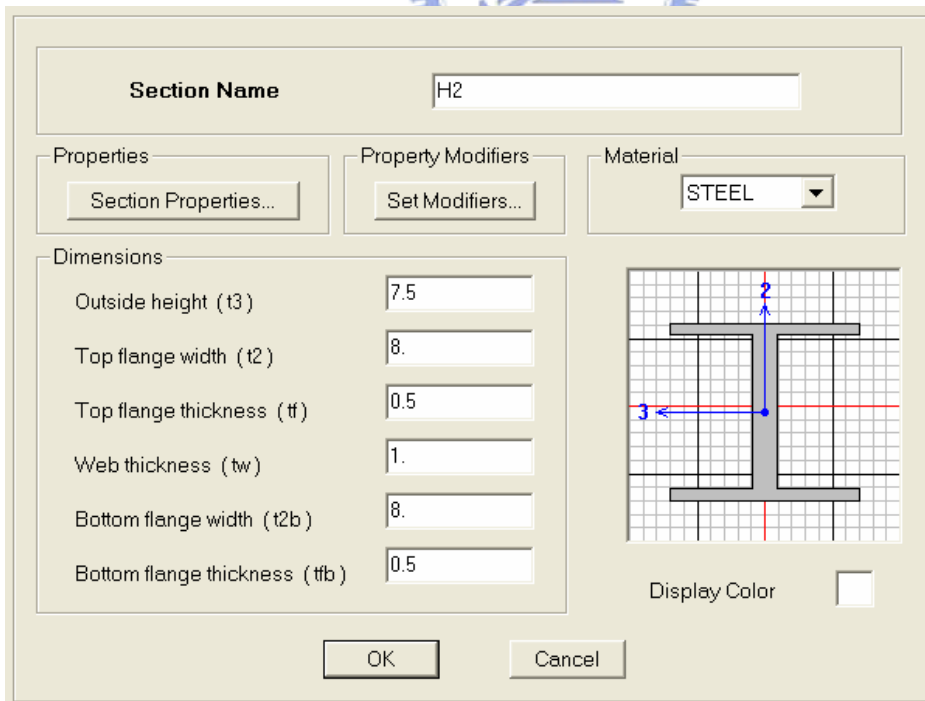


Fig. 5.36 The parameters for the frame/cable element specified for the bracing system in the model structure (Unit: cm)

Fig. 5.37 The parameters for the shell element in the model structure (Unit: cm)

Fig. 5.38 The parameters for the plastic (Wen) element in the model structure (Unit: mm, Kgf)

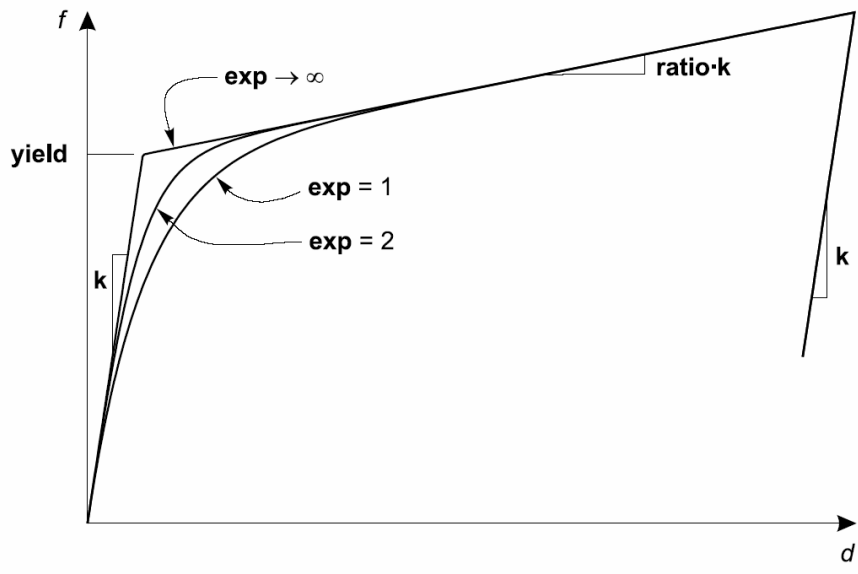


Fig. 5.39 The definition of parameters for the Wen's Plasticity Property



5.2.2 Simulating Results

The acceleration responses of the base of the 5-story model structure in shaking table tests serves as the inputs to the analytical models of SAP2000. In every analysis cases defined in Table 5.15, the responses of the each story are obtained by performing the nonlinear time-history analysis on the analytical models.

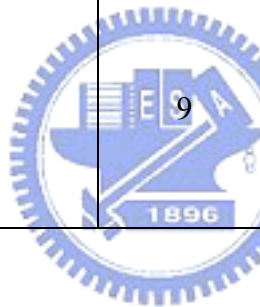
Bare Frame The simulating results are compared with experimental ones obtained from the shaking table tests as shown in Fig. 5.40 ~ 5.42 for case 1 ~ 3. Results show that the bare frame model of SAP2000 can predict the acceleration responses accurately except for the acceleration response of bare-frame on 5F under El Centro PGA = 0.1g.

Damper-Implemented Frame The simulating results are compared with experimental ones obtained from the shaking table tests as shown in Fig. 5.43 ~ 5.51 for case 4 ~ 9 including the figures of hysteresees of the damper for the largest PGA in each earthquake record.

Assessments of Seismic Performance The assessments of seismic performance of the damper are plotted in Fig. 5.52 ~ 5.57 for case 4 ~ 9. The root-mean-square reductions are summarized in Table 5.16. Results show that the dampers can suppress the acceleration responses on a large scale.

Table 5.16 Root-mean-square reduction of acceleration responses

Case	Root-Mean-Square Reduction (%)		Case	Root-Mean-Square Reduction (%)	
4	1F	69.7	7	1F	85.6
	2F	63.1		2F	86.8
	3F	48.1		3F	85.4
	4F	46.1		4F	85.3
	5F	54.8		5F	86.2
5	1F	64.1	8	1F	68.4
	2F	53.3		2F	71.4
	3F	28.9		3F	70.8
	4F	25.9		4F	70.8
	5F	41.8		5F	71.3
6	1F	64.7	9	1F	87.9
	2F	68.5		2F	88.3
	3F	69.0		3F	86.7
	4F	69.0		4F	86.5
	5F	69.4		5F	87.3



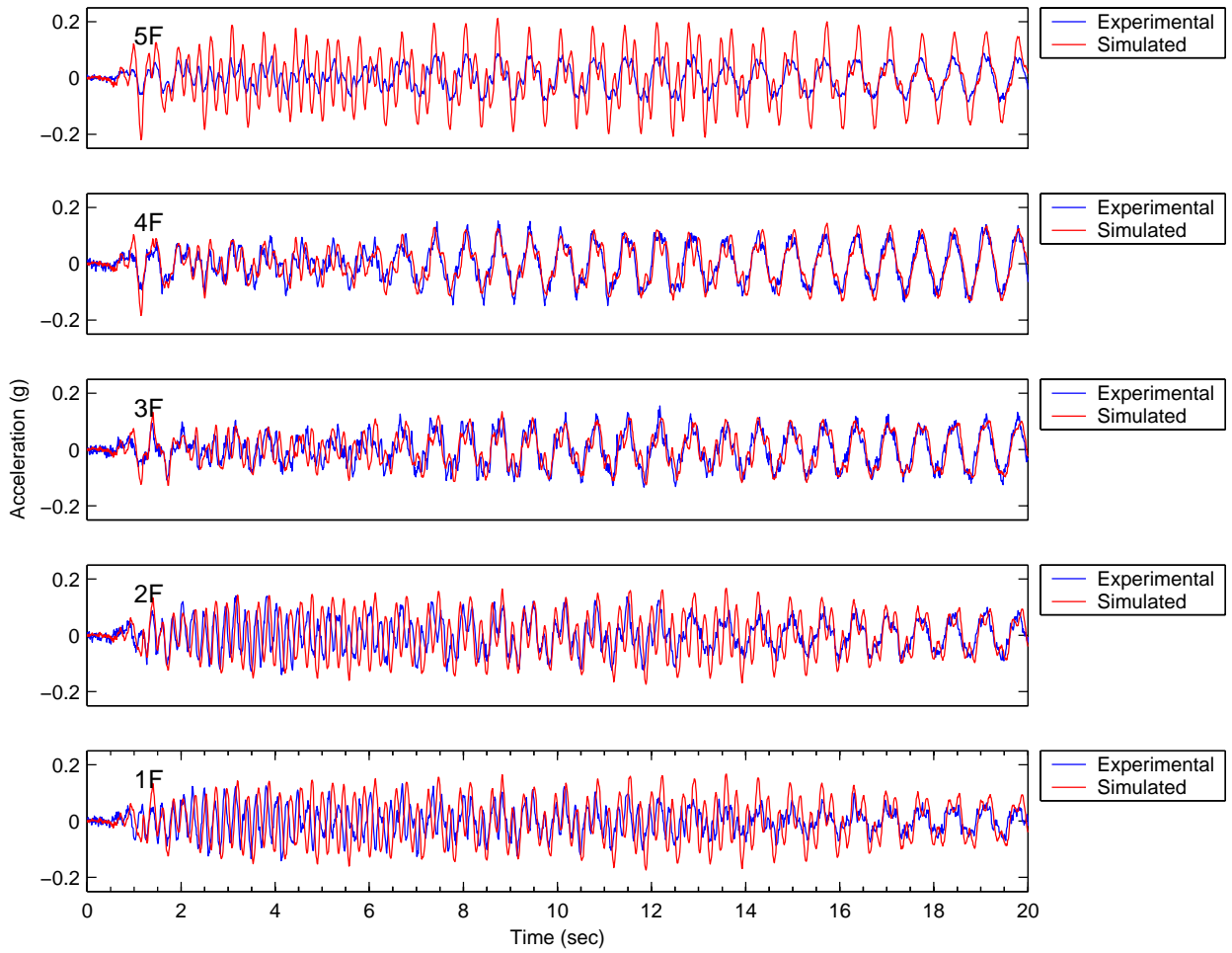


Fig. 5.40 Comparison of acceleration responses of the bare-frame model (Case 1: El Centro, PGA=0.1g)

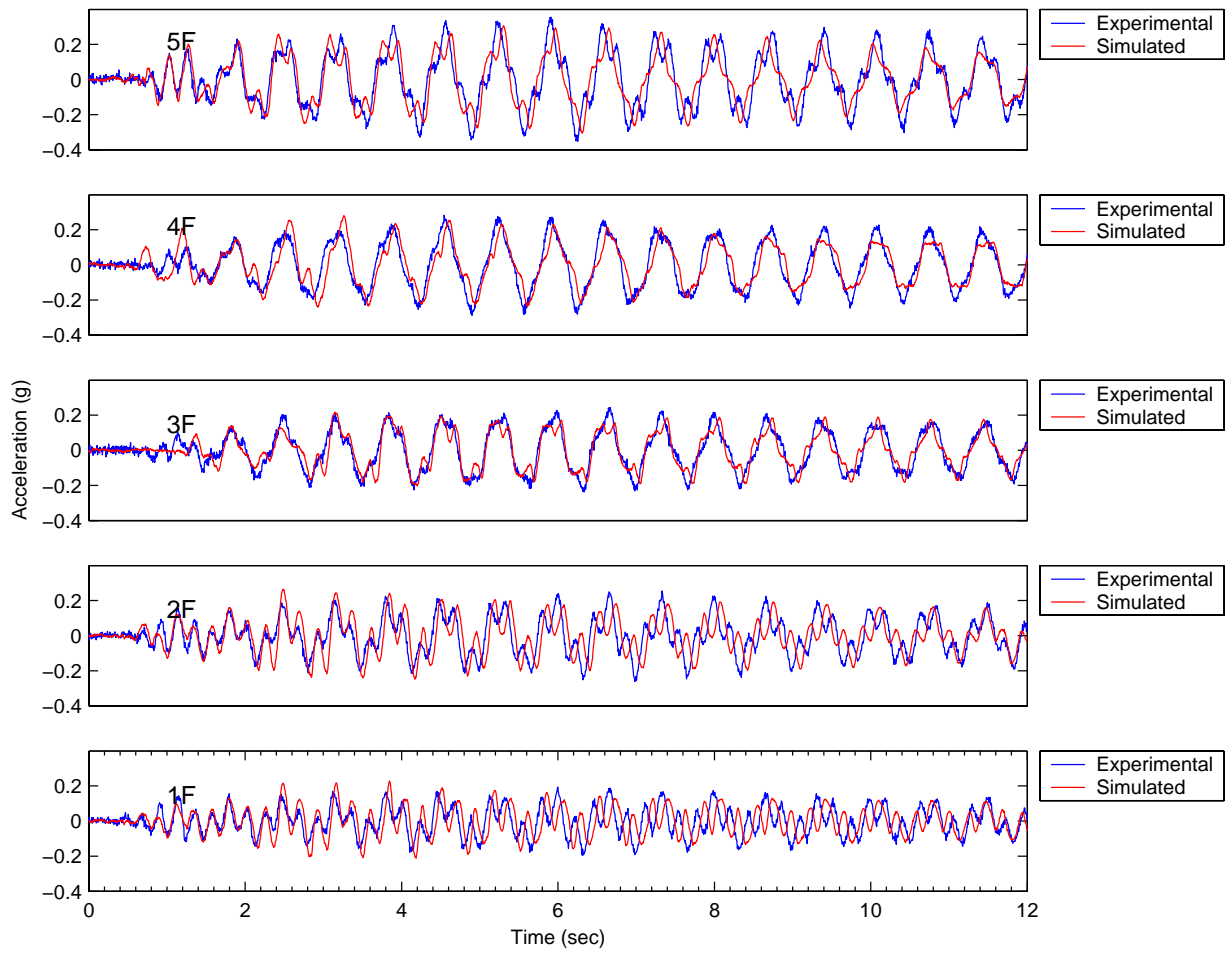


Fig. 5.41 Comparison of acceleration responses of the bare-frame model
(Case 2: Hachinohe, PGA=0.1g)

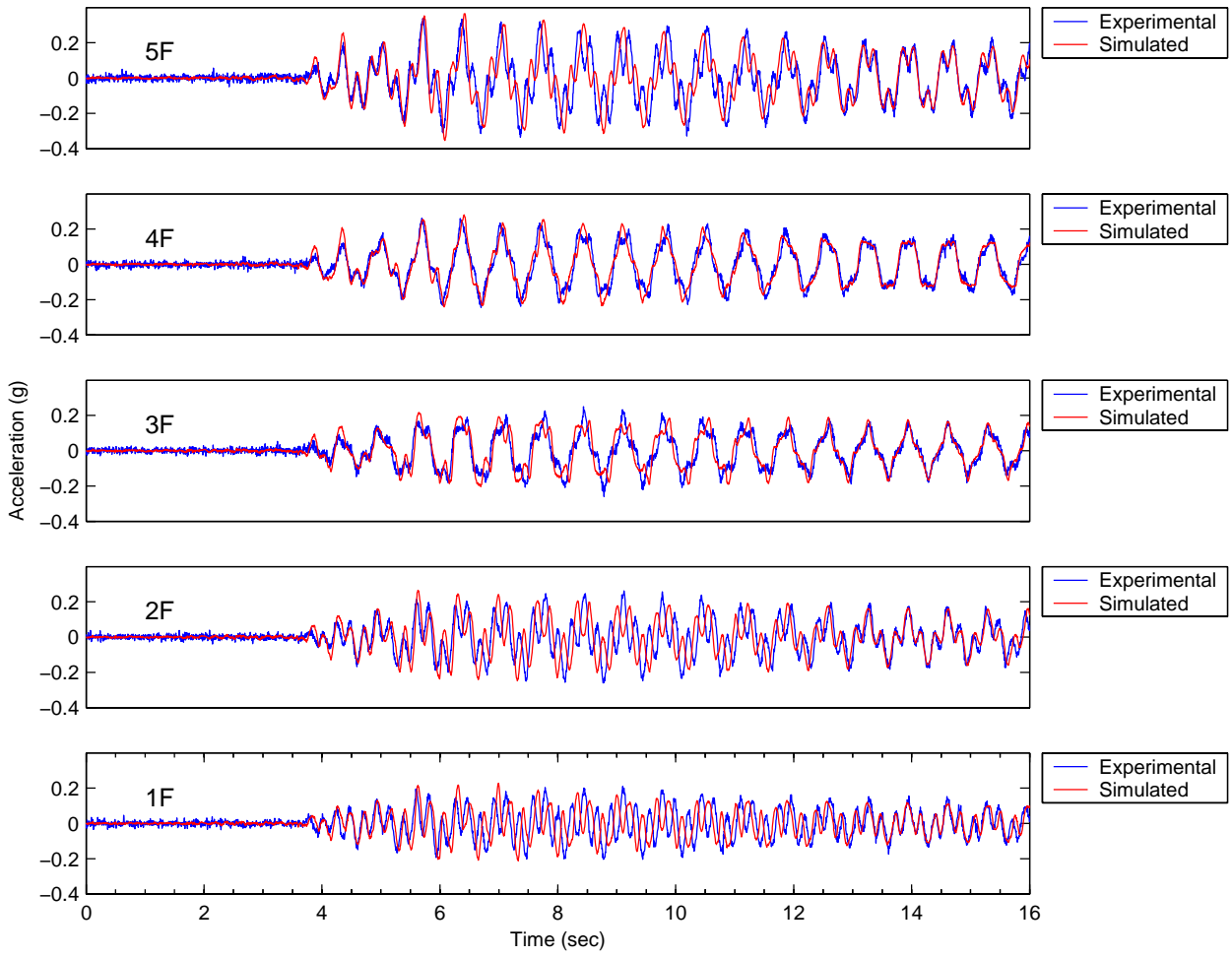


Fig. 5.42 Comparison of acceleration responses of the bare-frame model
(Case 3: Kobe, PGA=0.1g)

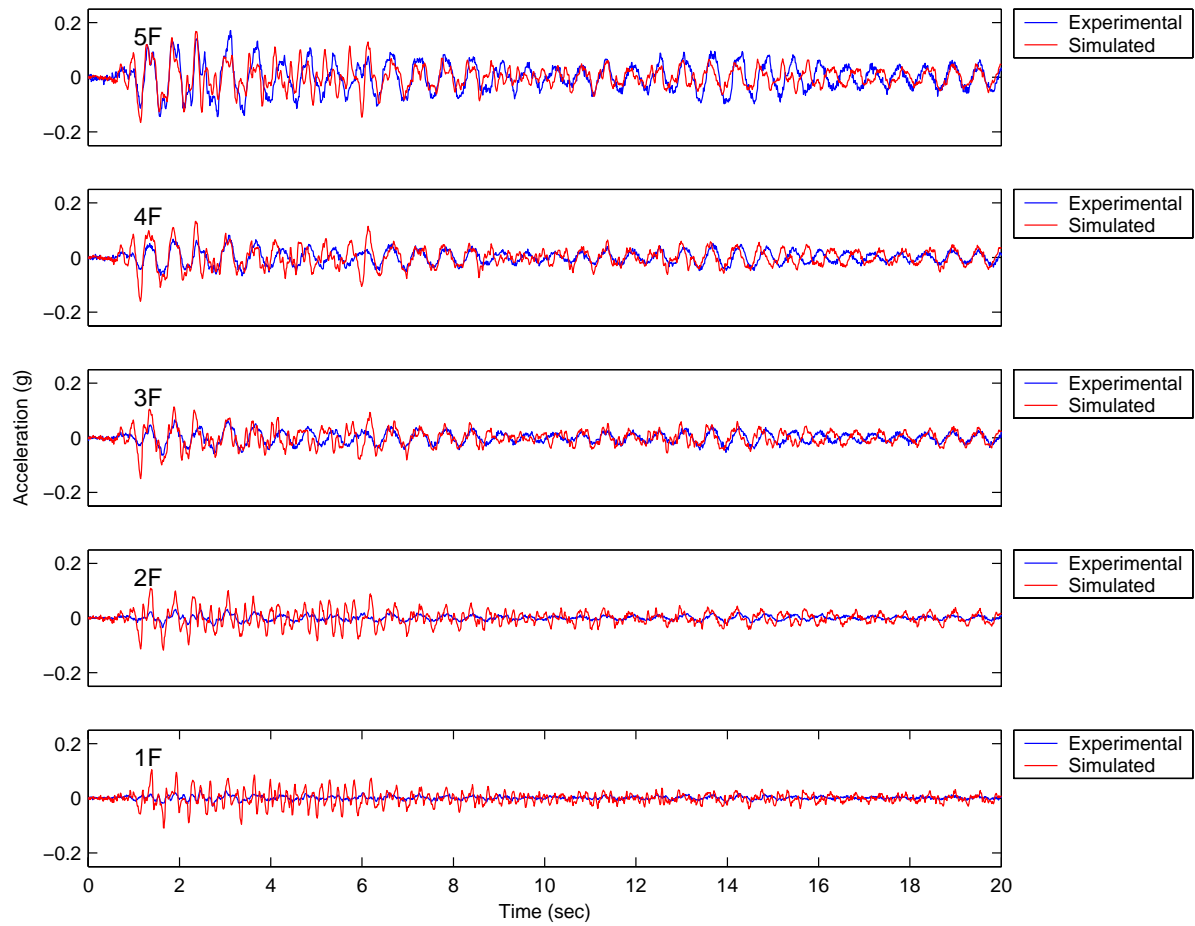


Fig. 5.43 Comparison of acceleration responses of the damper-implemented frame model
(Case 4: El Centro, PGA=0.1g)

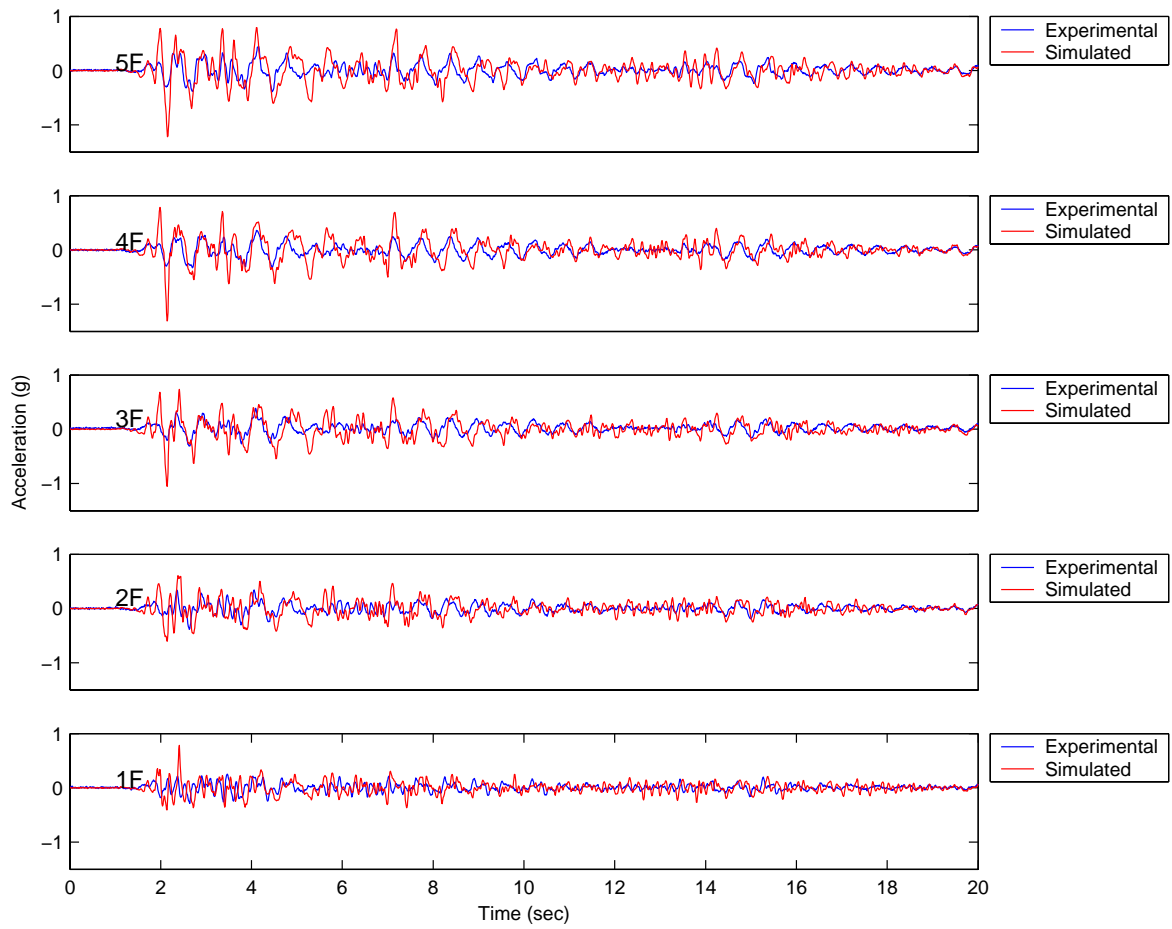


Fig. 5.44 Comparison of acceleration responses of the damper-implemented frame model
(Case 5: El Centro, PGA=0.4g)

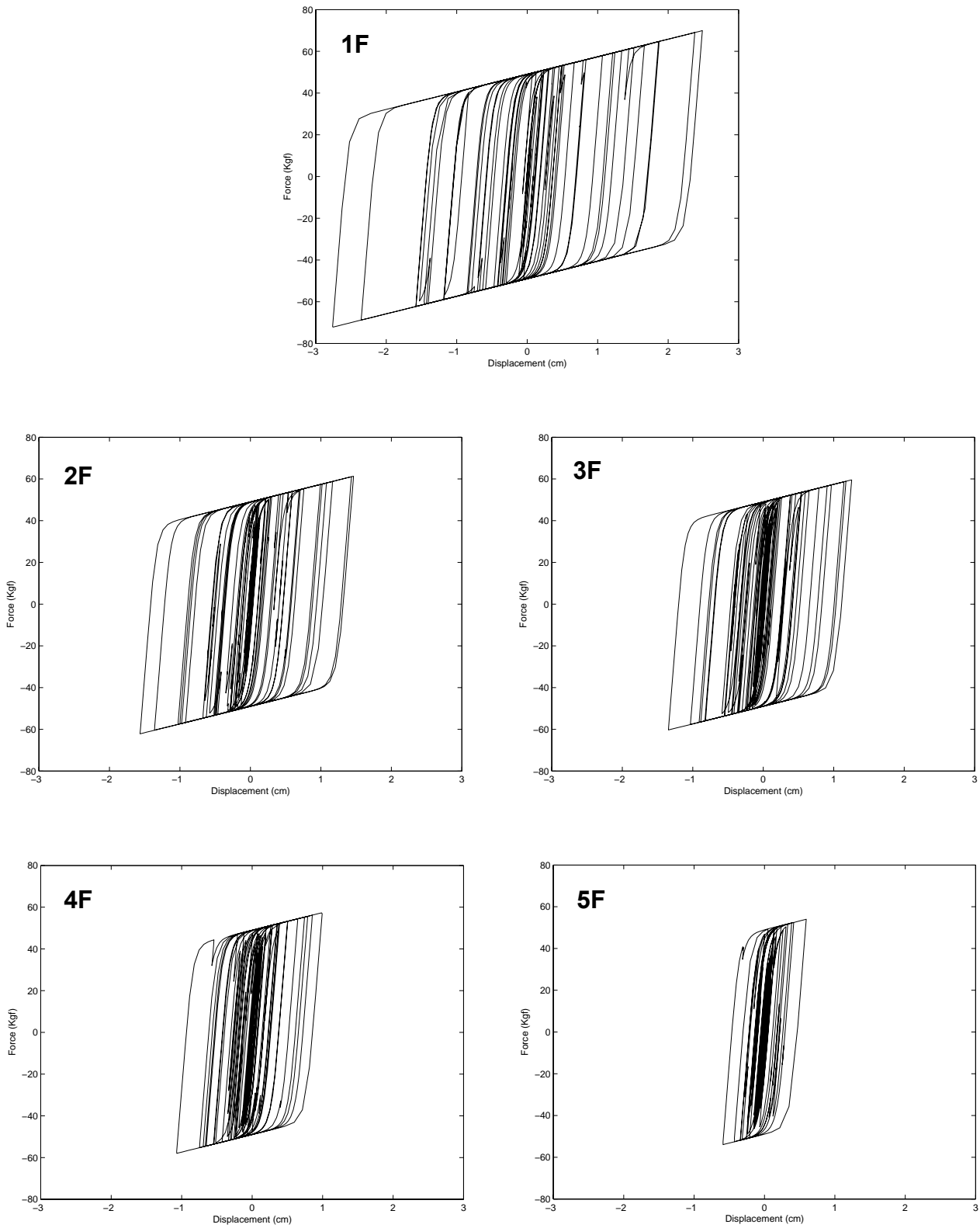


Fig. 5.45 The hysteresses of the damper
(Case 5: El Centro, PGA=0.4g)

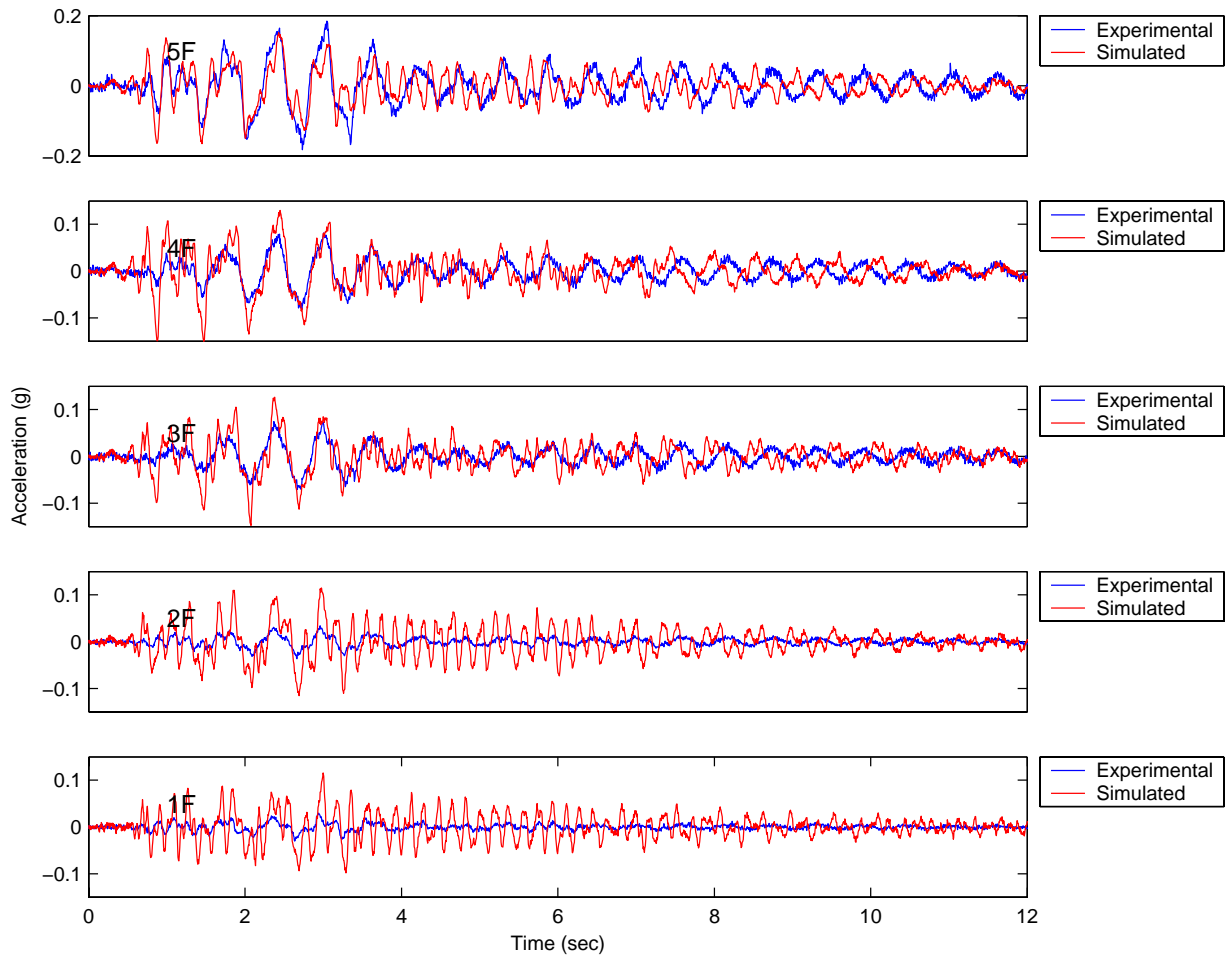


Fig. 5.46 Comparison of acceleration responses of the damper-implemented frame model
 (Case 6: Hachinohe, PGA=0.1g)

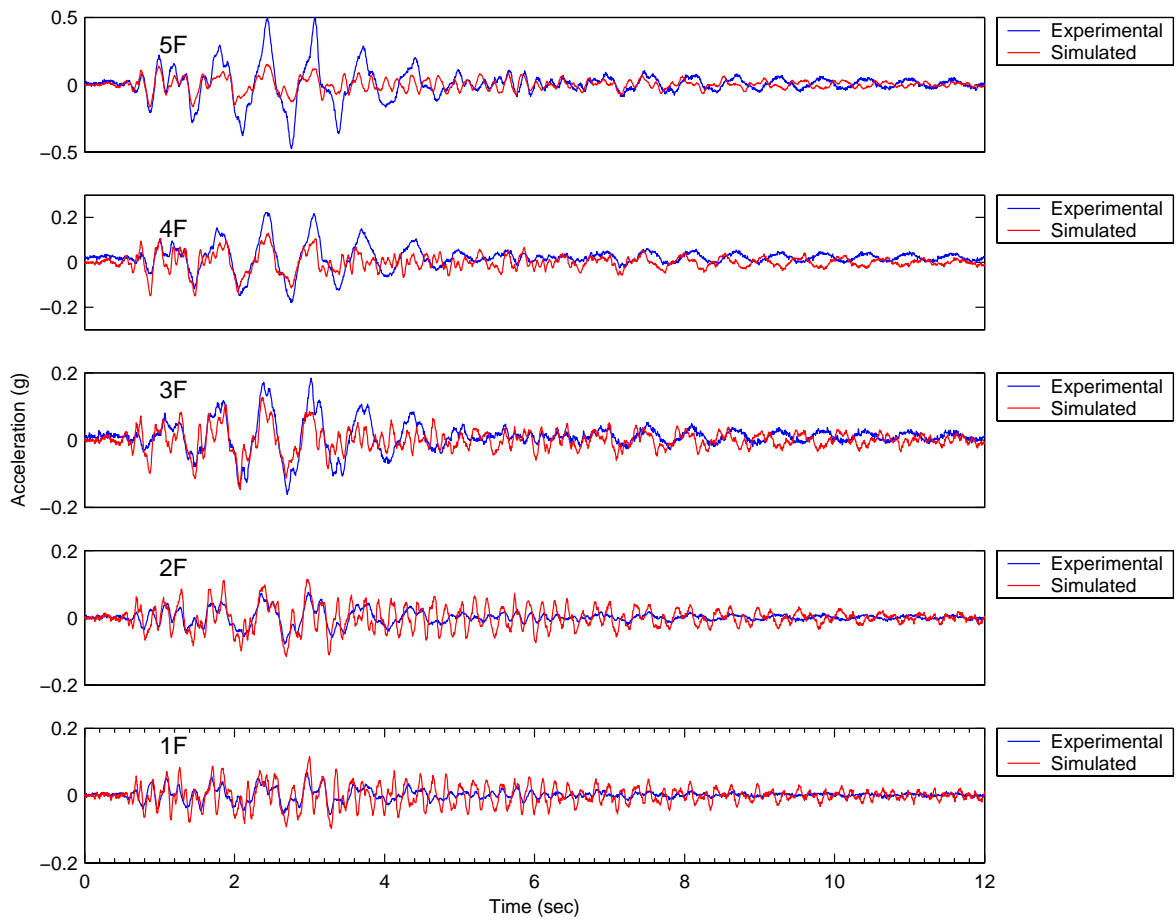


Fig. 5.47 Comparison of acceleration responses of the damper-implemented frame model
(Case 7: Hachinohe, PGA=0.25g)

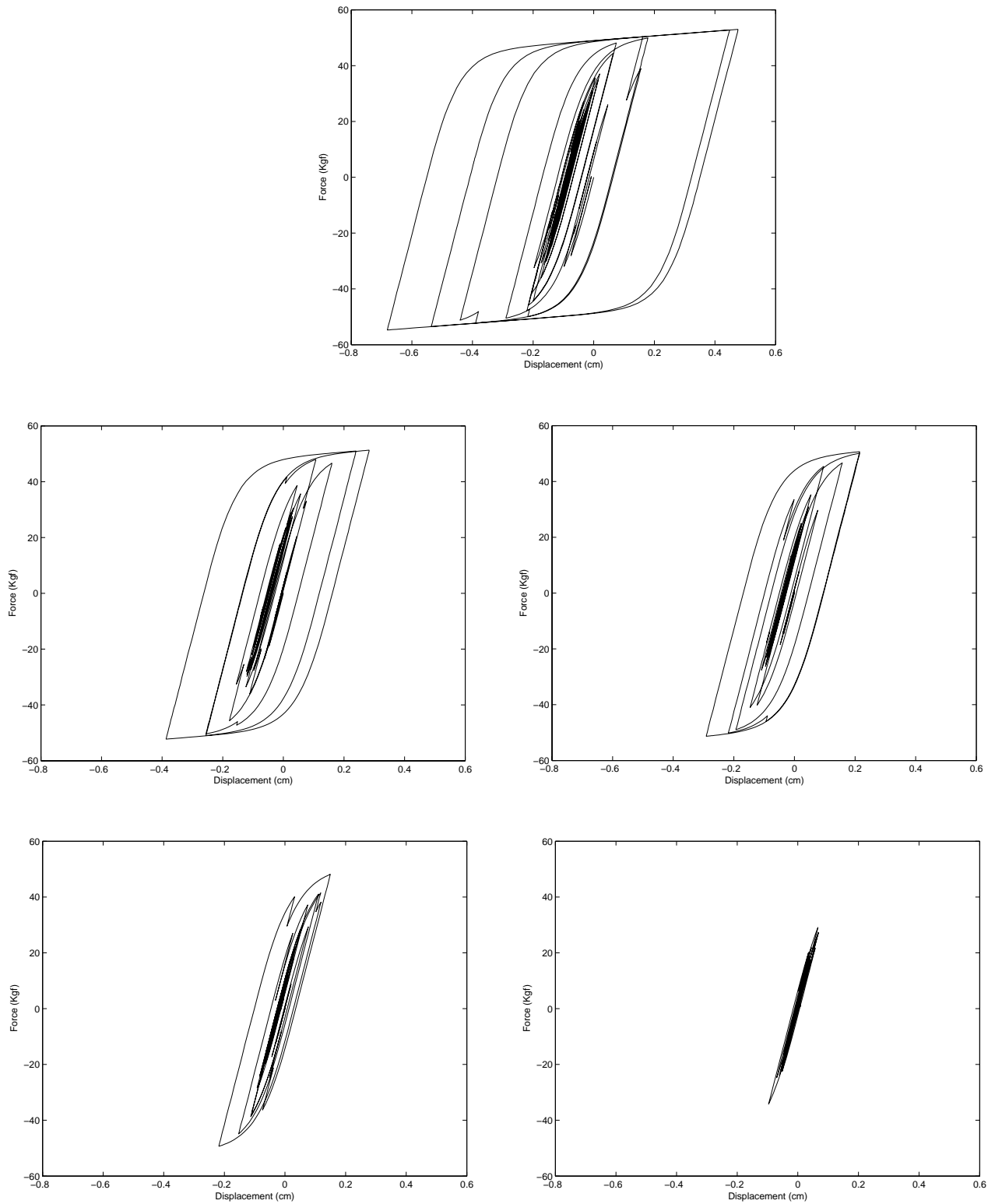


Fig. 5.48 The hystereses of the damper
(Case 7: Hachinohe, PGA=0.25g)

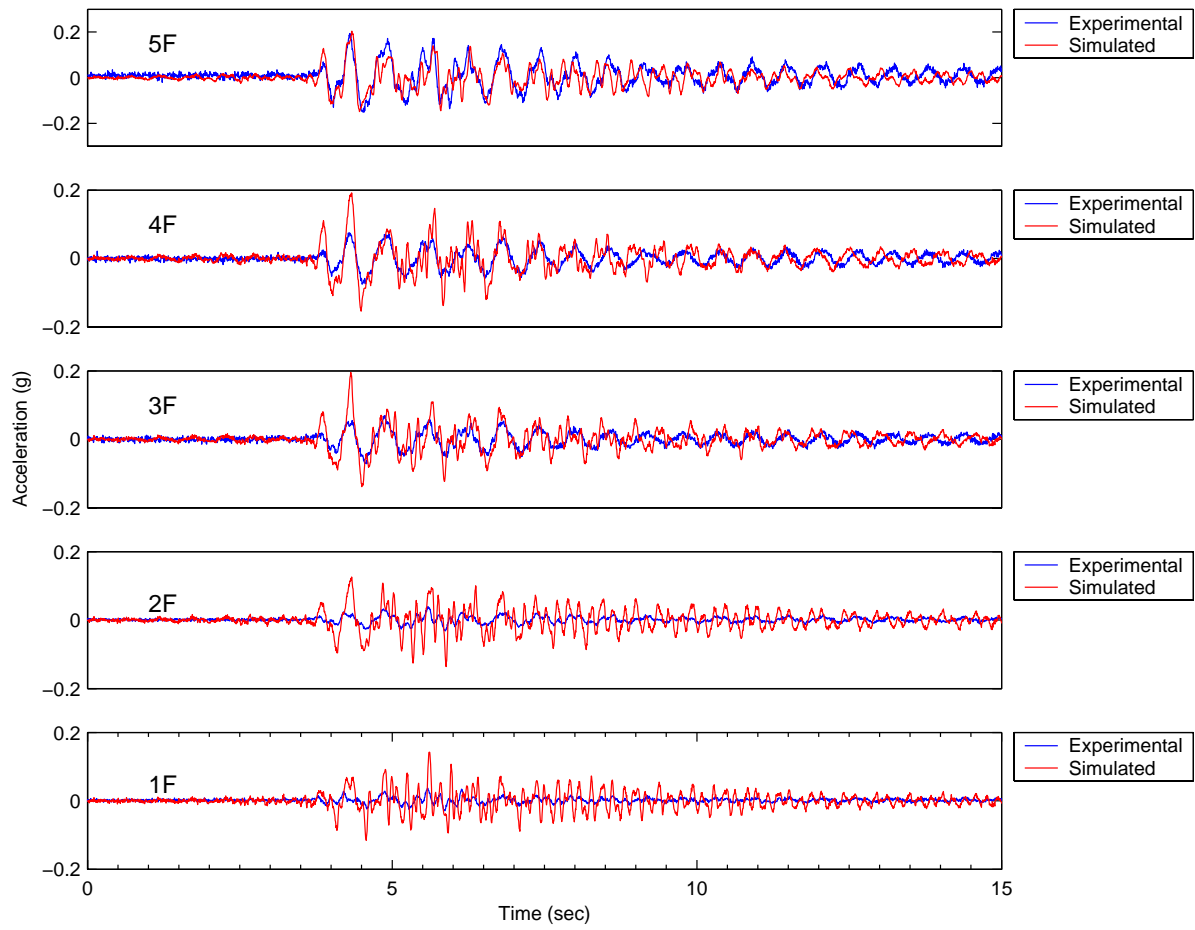


Fig. 5.49 Comparison of acceleration responses of the damper-implemented frame model
(Case 8: Kobe, PGA=0.1g)

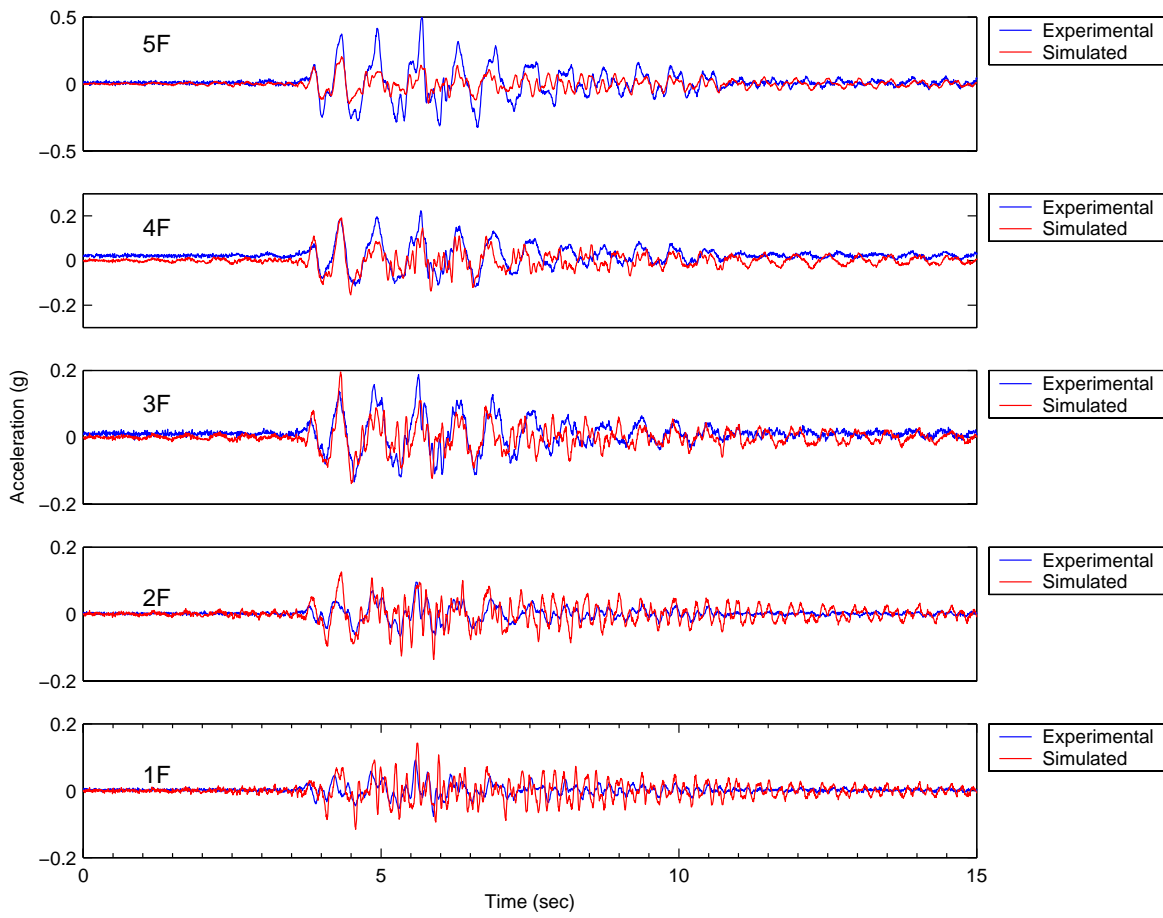


Fig. 5.50 Comparison of acceleration responses of the damper-implemented frame model
(Case 9: Kobe, PGA=0.25g)

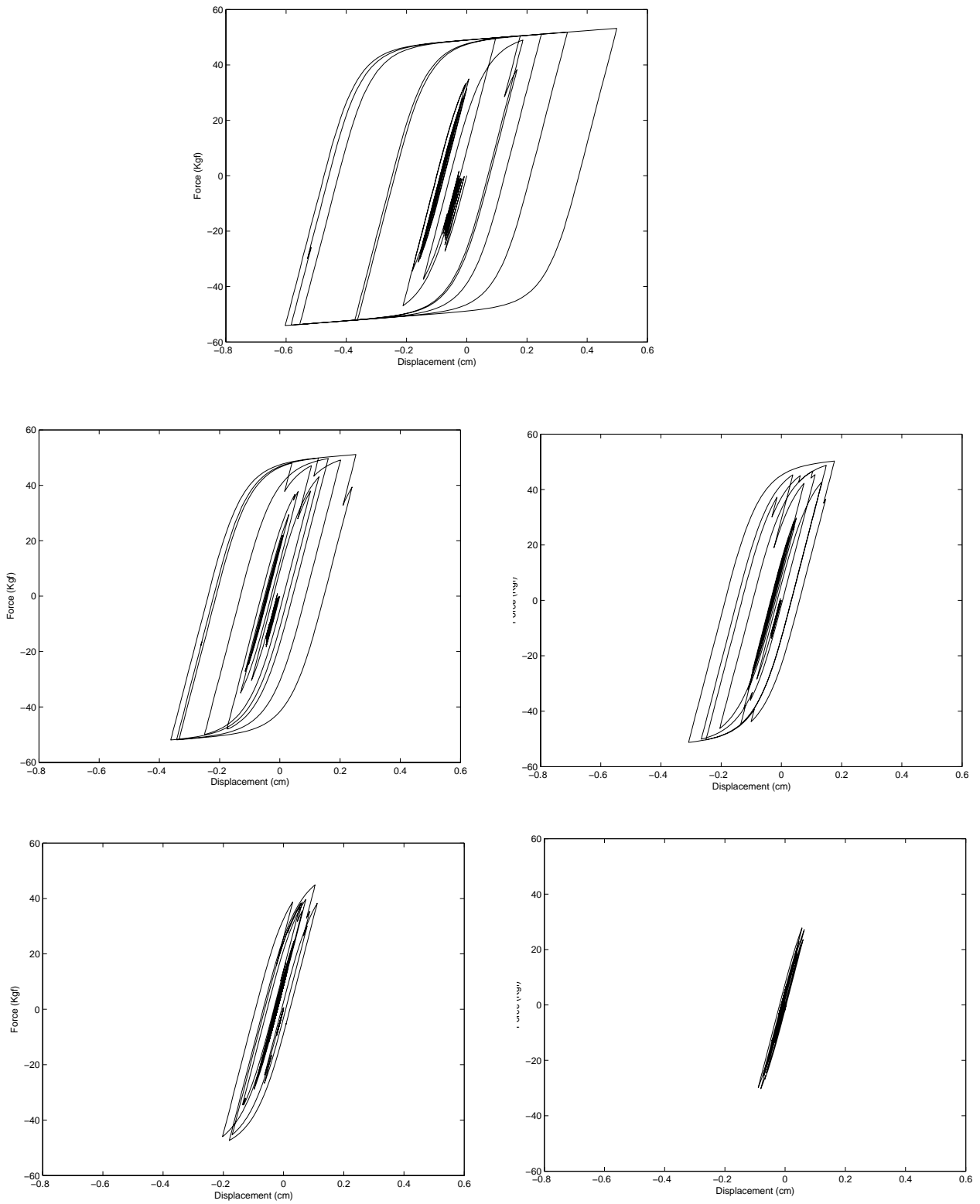


Fig. 5.51 The hystereses of the damper
(Case 9: Kobe, PGA=0.25g)

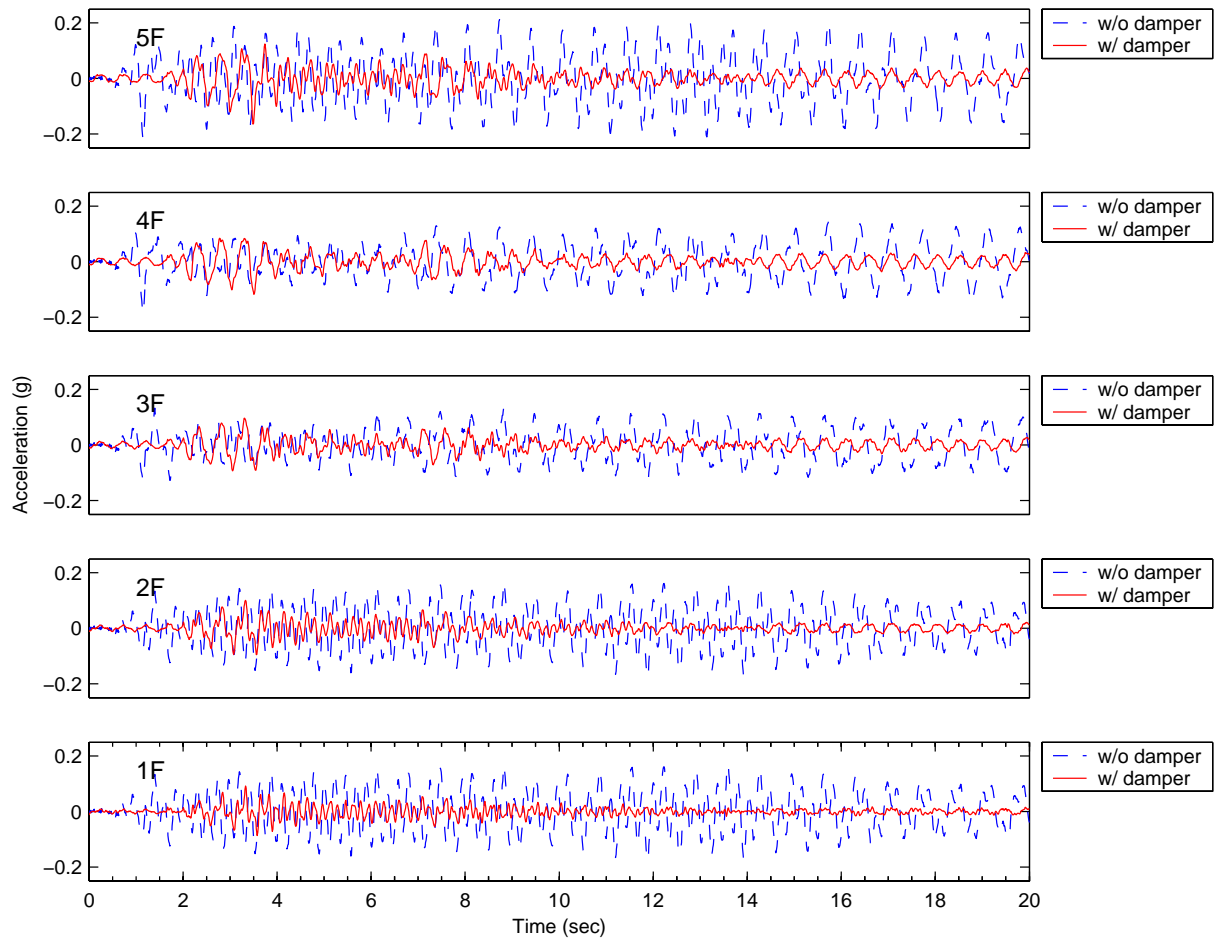


Fig. 5.52 Assessments of seismic performance of the damper
(Case 4: El Centro, PGA=0.1g)

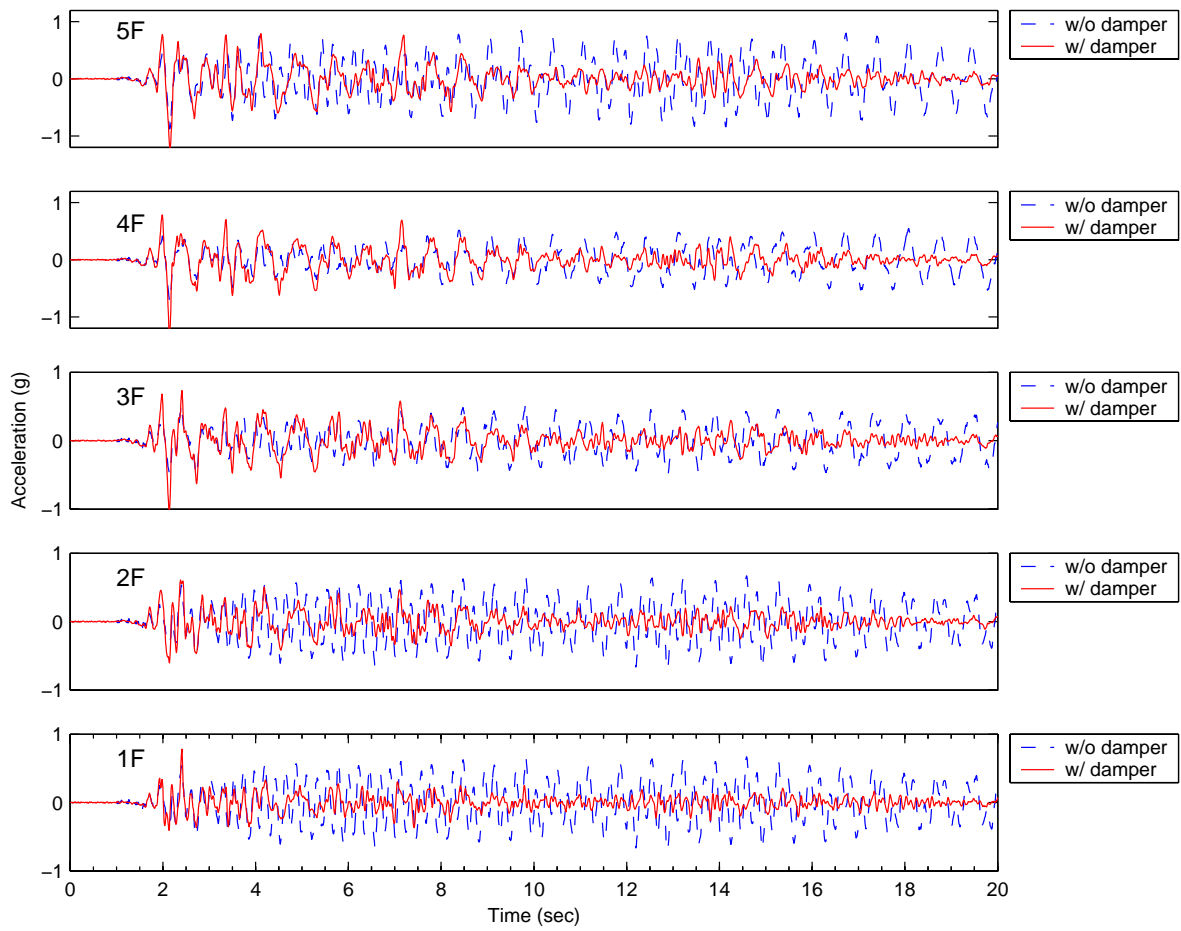


Fig. 5.53 Assessments of seismic performance of the damper
(Case 5: El Centro, PGA=0.4g)

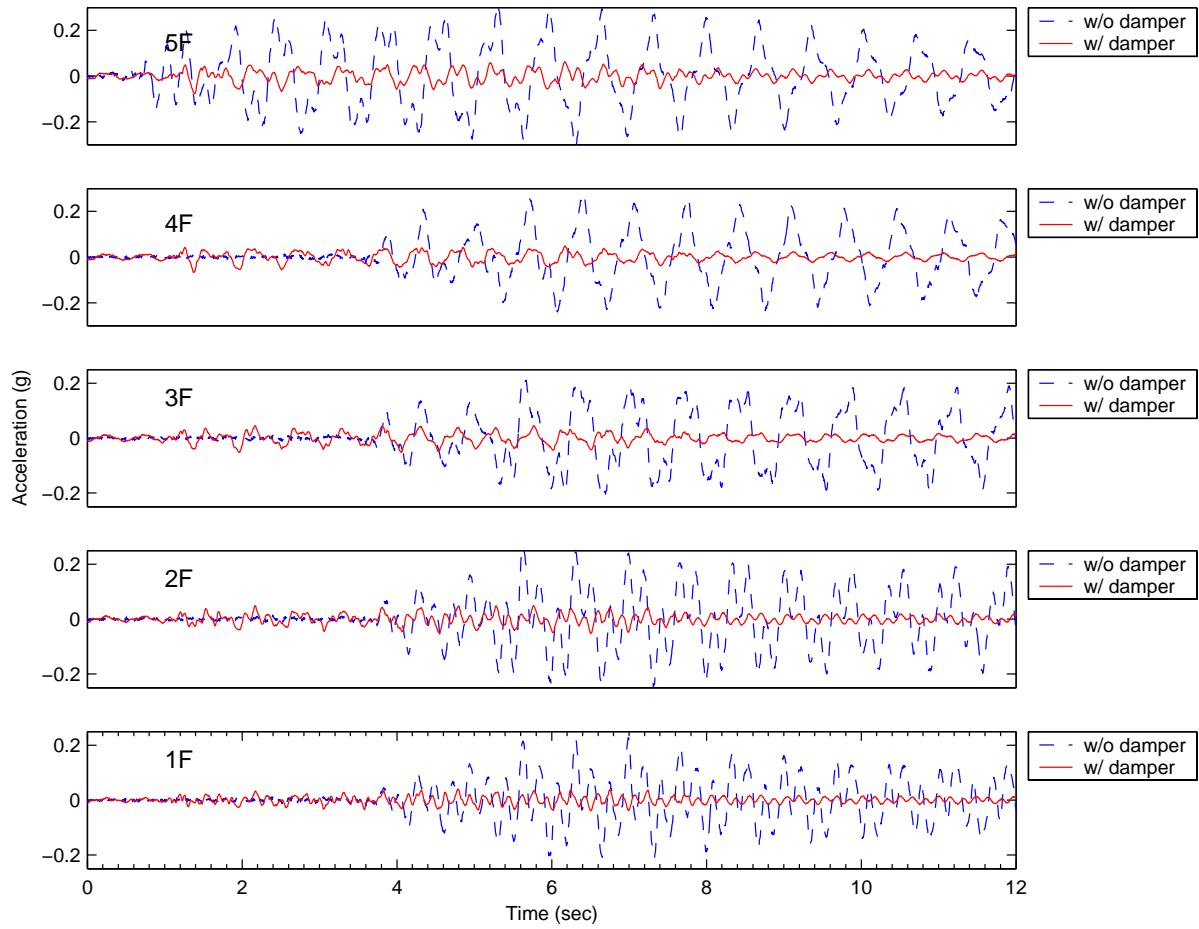


Fig. 5.54 Assessments of seismic performance of the damper
(Case 6: Hachinohe, PGA=0.1g)

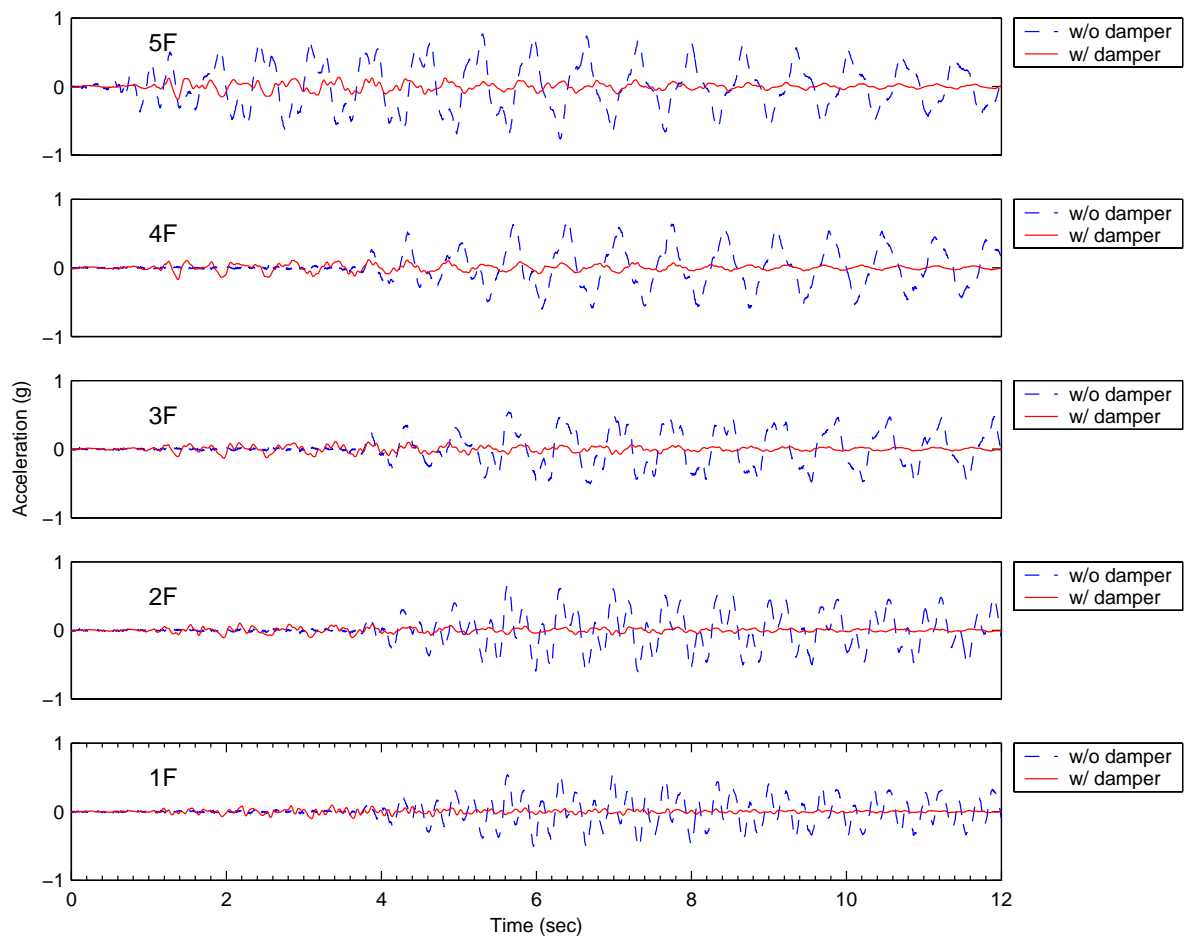


Fig. 5.55 Assessments of seismic performance of the damper
(Case 7: Hachinohe, PGA=0.25g)

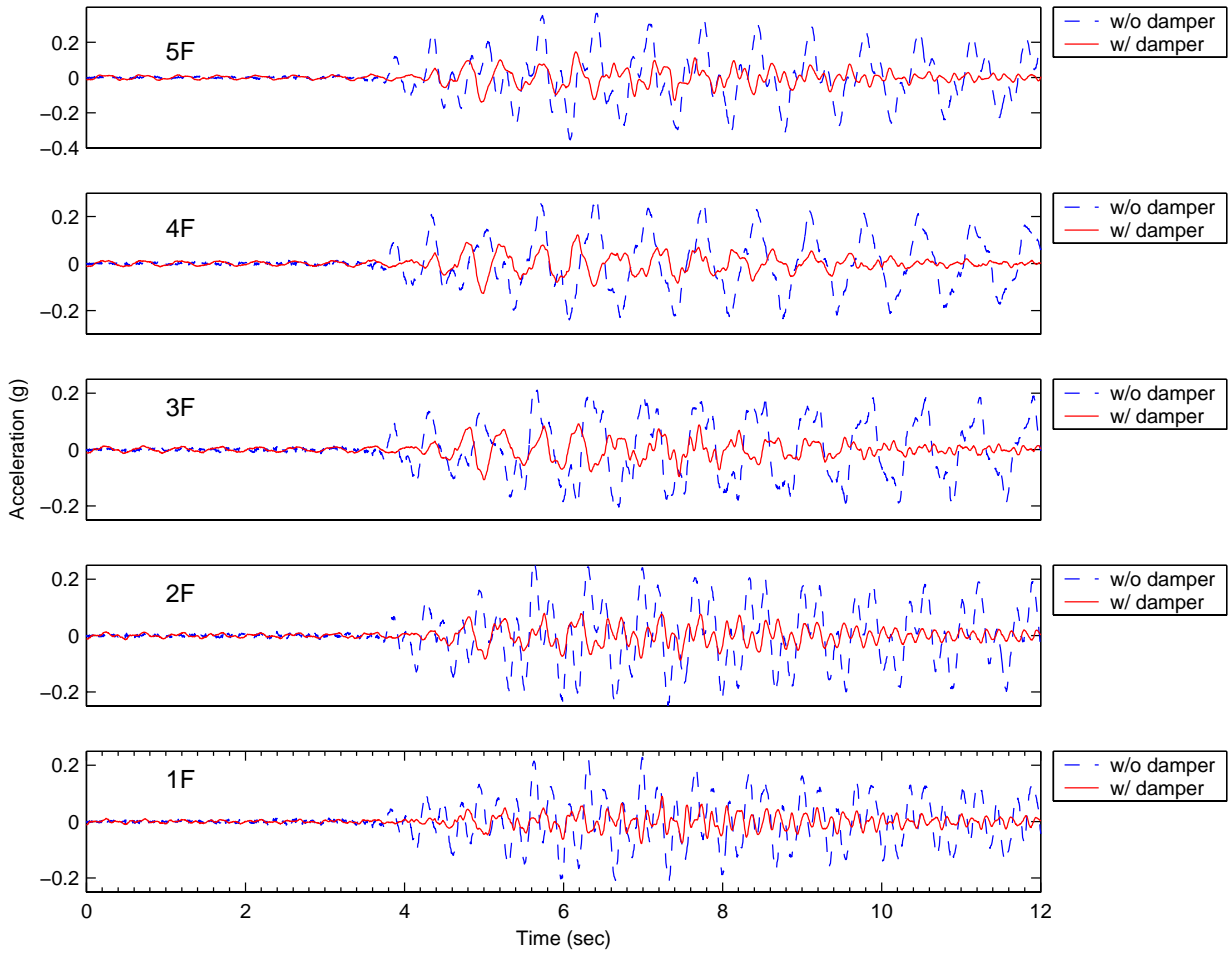


Fig. 5.56 Assessments of seismic performance of the damper
(Case 8: Kobe, PGA=0.1g)

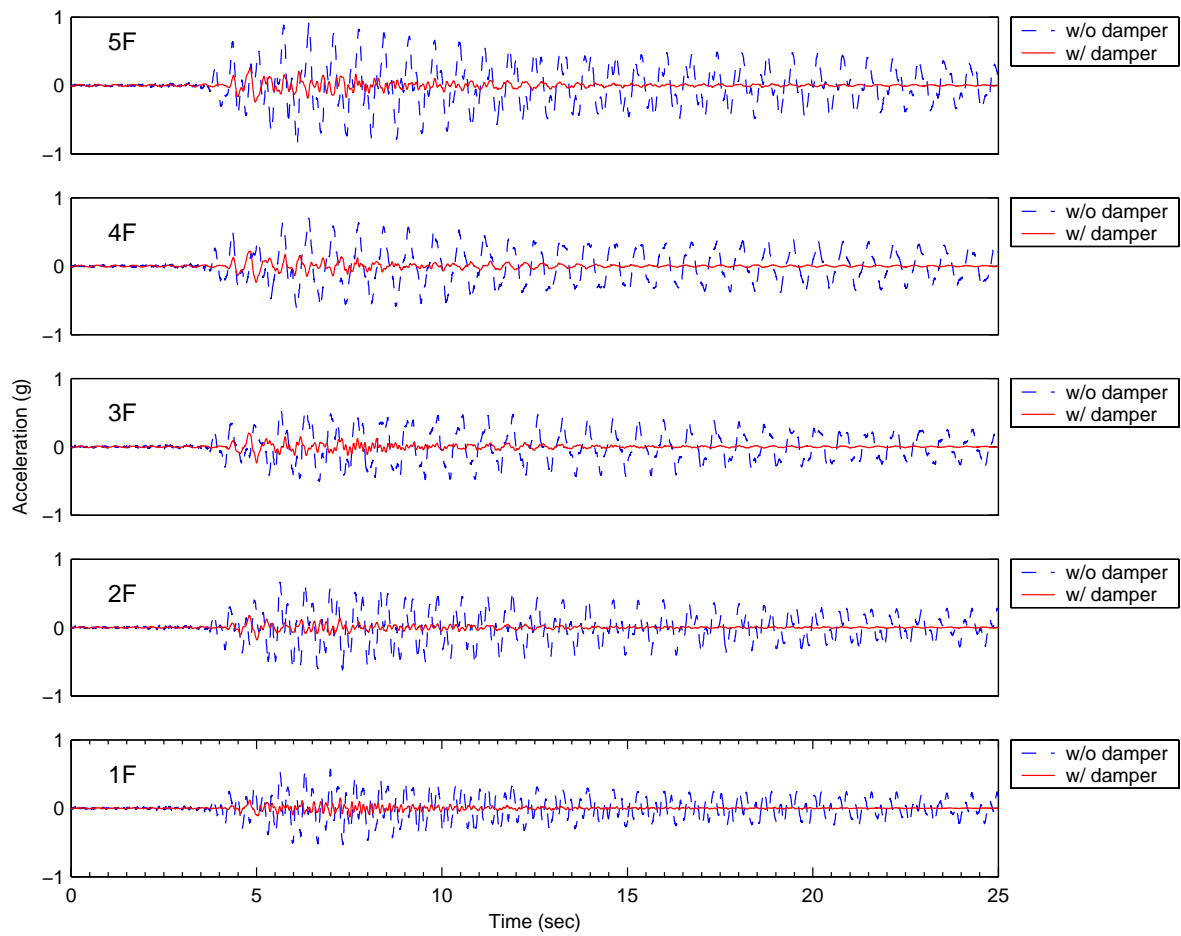


Fig. 5.57 Assessments of seismic performance of the damper
(Case 9: Kobe, PGA=0.25g)

6

Concluding Remarks



In this thesis, a novel methodology for estimating the moment and shear force from strain with the Ramberg-Osgood Hysteresis Model is proposed. To overcome numerical difficulties, an alternative form of the Ramberg-Osgood equations was derived to facilitate programming with the proposed table searching method. Component tests for both full-scale and scaled-down metallic yielding dampers have been conducted. Seismic performance tests of the damper have also been conducted via a series of shaking table tests. Based on the testing results, the conclusions can be drawn in the following:

1. One may predict the inelastic behavior of the metallic yielding damper with satisfactory accuracy by using the proposed measuring methodology for moment and shear.
2. The damper is effective in seismic response control of building structures. Both the displacement and acceleration response of the structure can be simultaneously suppressed to a large extent.
3. The damper performs consistently well regardless of the earthquake and disturbing intensity. The system performs more effectively for stronger earthquakes, in general, due to involvement of more inelastic behavior of the yielded damper.
4. No lateral instability of the damper has been observed throughout the testing. Reliability of the system is confirmed.
5. The same damper units have been used in all the tests conducted repetitively without replacement and maintenance. Durability of the system is confirmed.
6. The responses of structures can be simulated by analytical SAP2000 model with satisfactory accuracy if the model is established appropriately.

Suggestion:

1. The testing platform of component tests for the scale-down damper can be further modified to overcome the result of non-symmetric hysteresis.
2. The effect of axial force which is neglected in this study can be taken into consideration in the further study.

References

1. Brian J. Skinner and Stephen C. Porter, (1993), *The Blue Planet – An Introduction to Earth System Science*, John Wiley & Sons, Inc., 1995.
2. Haluk Sucuoğlu and Altuğ Erberik, ‘*Energy-Based Hysteresis and Damage Models for Deteriorating Systems*’, *Earthquake Engng Struct. Dyn.*, 33:69-88.
3. T. T. Soong and B. F. Spencer Jr, ‘*Supplemental Energy Dissipation: State-of-the-Art and State-of-the-Practice*’, *J. Engng. Struct.*, 24 (2002), 243-259.
4. ‘*Journal of Engineering Mechanics, Special Issue: Structural Control: Past, Present, and Future*’, *J. Engng. Mech.*, ASCE, 1997.
5. Ian D. Aiken, Douglas K. Nims, Andrew S. Whittaker, and James M. Kelly, (1993), ‘*Testing of Passive Energy Dissipation Systems*’, *Earthquake Spectra*, Vol. 9, No. 3.
6. Soong, T.T. and Dargush, G.F. *Passive Energy Dissipation Systems in Structural Engineering*, John Wiley and Sons Inc., New York, 1997.
7. Frahm, H., ‘*Device for Damping Vibration of Bodies*’, U.S. Patent No. 958-989, 1911.
8. Soong, T.T. *Active Structural Control: Theory and Practice*, John Wiley and Sons Inc., New York, 1990.
9. Fediw, A.A., Isyumov, N. and Vickery, B.J. (1993), ‘*Performance of a one-dimensional Tuned sloshing water damper*’ *Wind Engineering*, London, 247-256.
10. Fujino, Y., Sun, L.M., Paceno, B. and Chaiseri, P. (1992), ‘*Tuned Liquid Damper(TLD) for Suppressing Horizontal Motion of Structures*’ *ASCE Journal of Engineering Mechanics*, 118(10), 2017-2030.

11. Yalla, S.K and Kareem, A. (2000a) “*Optimum Absorber Parameters for Tuned Liquid Column Dampers,*” ASCE Journal of Structural Engineering, 125(8), 906-915.
12. Sakai, F. et al. (1989), “*Tuned Liquid Column Damper - New Type Device for Suppression of Building Vibrations,*” Proc. Int. Conf. on High Rise Buildings, Nanjing, China, March 25-27.
13. Sakai, F.,and Takaeda. S. (1991), “*Tuned Liquid Column Damper (TLCD) for cable stayed bridges,*” Innovation in Cable-stayed Bridges, Fukonova, Japan.
14. Balendra, T., Wang, C.M. and Cheong, H.F. (1995) “*Effectiveness of Tuned Liquid Column Dampers for Vibration Control of Towers*” , Engineering Structures, 17(9), 668-675.
15. Gao, H., Kwok, K.C.S. and Samali, B. (1999),“*Charcteristics of multiple Tuned Liquid Column Dampers in suppressing Structural Vibration,*” Engineering Structures, 21, 316-331.
16. Sadek, F., Mohraz, B. and Lew, H.S. (1998)“*Single- and Multiple-Tuned Liquid Column Dampers for Seismic Applications,*” Earthquake Engng. and Struc. Dyn., 27, 439-463.
17. Hitchcock, P.A., Kwok, K.C.S., Watkins, R.D. and Samali, B. (1997), “*Characteristics of Liquid column vibration absorbers (LCVA) -I and II*” , Engineering Structures, 19(2).
18. Farzad Naeim and James M. Kelly, (1999), *Design of Seismic Isolated Structure From Theory to Practice*, John Wiley & Sons, Inc., New York.
19. Buckle, I.G, and Mayes, R.L., “*Seismic isolation: history, application and performance-a world review,*” Earthquake Spectra, Vol. 6, pp. 161-201 (1990).
20. Martelli, A., Parducci, A., and Forni, M.,“*State-of-the-art on development and application of seismic isolation and innovative seismic design techniques in Italy,*”ATC-17-1 Technical Papers on Seismic Isolation, pp. 401-402 (1993).
21. Kelly, J.M., “*Aseismic base isolation: review and bibliography,*” Soil Dynamics and Earthquake Engineering, Vol. 5, pp. 202-216 (1986).
22. Zayas, V.A., Low, S.S., and Main, S.A.,“*The FPS earthquake resisting system, experimental report,*” Report No. UCB/EERC-87/01, Earthquake Engineering Research Center, University of California, Berkeley, California (1987).

23. Kawamura, S., Kitazawa, K., Hisano, M., and Nagashima, I. (1988). '*Study of a sliding-type base isolation system - system composition and element properties.*' Proc. 9th WCEE, Tokyo-Kyoto, Vol. V, 735-740.
24. Mokha, A.S., Constantinou, M.C., and Reinhorn, A.M., "*Experimental study and analytical prediction of earthquake response of a sliding isolation system with a spherical surface,*" Report No. NCEER-90-0020, National Center for Earthquake Engineering Research, State University of New York at Buffalo, N.Y. (1990).
25. Mokha, A.S., Constantinou, M.C., Reinhorn, A.M., and Zayas, V.A., "*Experimental study of friction pendulum isolation system,*" Journal of Structural Engineering, ASCE, Vol. 117, No. 4, pp. 1201-1217 (1991).
26. Constantinou, M.C., Tsepelas, P., Kim, Y.S., and Okamoto, S., "*NCEER-Taisei cooperation research program on sliding seismic isolation system for bridges and analytical study of a friction pendulum system (FPS),*" Report No NCEER-93-0020, National Center for Earthquake Engineering Research, State University of New York at Buffalo, NY (1993).
27. Wang, Yen-Po, Chung, Lap-Loi and Liao, Wei-Hsin (1998), "*Seismic Response Analysis of Bridges Isolated with Friction Pendulum Bearings,*" Earthquake Engineering and Structural Dynamics, 27, 1069-1093.
28. Wang, Y.P., Chung, L.L, Teng, M.C, Lee, C.L. (1998), "*Experimental Study of Seismic Structural Isolation using Sliding Bearings,*" 2WCSC, Kyoto, Japan, pp.83-92.
29. Wang, Yen-Po, and Wei-Hsin Liao (2000), '*Dynamic Analysis of Sliding Structures with Unsynchronized Support Motions*', Earthquake Engineering and Structural Dynamics, 29, pp. 297-313.
30. Wang, Yen-Po, Liao, Wei-Hsin and Lee Chien-Liang (2001), '*A state-space approach for dynamic analysis of sliding structures,*' Engineering Structures 23, pp. 790-801.
31. Wang, Y.P., Teng, M.C. and Chung, K.W.(2001) , '*Seismic Isolation of Rigid Cylindrical Tanks Using Friction Pendulum Bearings,*' Earthquake Engineering and Structural Dynamics, Vol 30, Issue 7, July, pp. 1083-1099.
32. <http://www.earthquakeprotection.com/>
33. James M. Gere and Stephen P. Timoshenko, *Mechanics of Materials*, 4th Ed., 1997.

34. Prof. Dr. Ing and Uwe E. Dorka,
http://www.uni-kassel.de/fb14/stahlbau/eartheng/downloads/3_response_analysis.pdf
35. Steven C. Chapra and Raymond P. Canale, *Numerical Method for Engineers with Programming and Software Applications*, 3rd Ed., 1998.
36. Kim JR Rasmussen, (2001), '*Full-range Stress-strain Curves for Stainless Steel Alloys*', Department of Civil Engineering, The University of Sydney, Research Report No 811.
37. Lee Chien-Liang, (2003), '*A Study on Structural Vibration Control and Experimental Methodology*', A dissertation submitted to department of civil engineering, college of engineering, national Chiao Tung university for the degree of doctor of engineering.
38. Computer and Structures, Inc., (2002), '*SAP2000 Analysis Reference Manual*'.
39. Tsai, K. C., Chen, H. W., Hong, C. P. and Su, Y. F., (1993), "*Design of Steel Triangular Plate Energy Absorbers for Seismic-Resistant Construction*", *Earthquake Spectra*, 9(3), 505-528.
40. Cofie, N. G. and Krawinkler, H. (1985), '*Uniaxial Cyclic Stress-Strain Behavior of Structural Steel*', *J. Engng. Mech., ASCE*, 111(9), 1105-1120.
41. L. M. Moreschi and M. P. Singh, '*Design of Yielding Metallic and Friction Dampers for Optimal Seismic Performance*', *Earthquake Engng Struct. Dyn.* 2003, 32: 1291-1311.
42. Whittaker, A.S., Bertero, V.V., Thompson, C.L. and Alonso, L.J. (1991), '*Seismic Testing of Steel Plate Energy Dissipation Devices*', *Earthquake Spectra*, 7(4), 563-604.
43. Arturo Tena-Counga, (1997), '*Mathematical modeling of the ADAS energy dissipation device*', *Engineering Structures*, Vol.19, No. 10, pp. 811-821.

Appendix A: Source Codes of MATLAB Programs



Main1.m

```

% Main1.m
% by Stainer
% February 22, 2004
%
% The Main Program for Development of Measuring Methodology for
% Moment and Shear via Strain Measurement.
%
%
% Required functions:
% 1. NonlinearBending03.m
% 2. FindTheStress02.m
% 3. Strain02.m (Ramberg-Osgood Streee-Strain Relation)
% 4. CompareHysteresis.m

clear; clc;

global E Sigma_0 Alpha n % Ramberg-Osgood Parameters
global MaxIterationTimes % Iteration Parameters
global Sigma Epsilon % Calculated Values
global TableRO_Sigma TableRO_Epsilon % Table
Sigma = 0; Epsilon = 0; % Initial Values

% Parameters Input by Users =====
% Ramberg-Osgood Parameters
Sigma_0 = 430; % MPa
E = 210; % GPa
Alpha = E/Sigma_0*0.002*1000;
n = 5.33;
% Unit Conversion for Ramberg-Osgood Parameters (DO NOT CHANGE)
E_Output = E; % GPa, for output only
E = E * 10^3; % MPa
% Iteration Parameters
Sigma(1) = 290; % Initial Values, Default: 290
Sigma(2) = 300; % Initial Values, Default: 300
MaxIterationTimes = 200; % Max Iteration Times, Default: 200
NumberOfStep = 3; % Number of step, Default: 3
% Parameters of the X-Shaped Metallic Yielding Damper
% Dimension of the cross-section of the damper where the strain gauge bounded
b = 2.4 /100; % m, width of the cross-section, Default: 2.4/100
h = 1.5 /1000; % m, thickness of the damper, Default: 1.5/1000
H = 3.0 /100; % m, twice the distance of the strain gauge
% from the neck of the X-shaped plate by considering the condition of symmetry
% Control parameters
PauseFlag = 1; % 1: pause, 2: non-pause
% Output parameters
N = 4; % Number of plates in a unit of USD, Default: 4
FID = 2; % FID=1: screen output, FID=2: file output
if(FID==2) PauseFlag = 2; end
% Output File Name
% EPS file
EpsFlag = 1; % EpsFlag=1: Output the EPS file of the figures.
% Resolution of Output Image File
ResolutionString = '-r128'; % 128DPI ==> 1024x768
% for Measured Strain Data Figure (in plotStrain.m)
S_FileName = '0930423-05~20mm-01-Strain3.jpg';
S_FileName2 = '0930423-05~20mm-01-Strain3.eps';
S_TitleString = 'Measured Strain Data from the Experience
(0930423-05~20mm-01-Strain3.asc)';
% for Stress-Strain Hysteresis Figure (in NonlinearBending02.m)
SH_TitleString = 'Ramberg-Osgood Hysteresis Model
(0930423-05~20mm-01-Strain3.asc)';
SH_FileName = '0930423-05~20mm-01-Strain3-SH.jpg';
SH_FileName2 = '0930423-05~20mm-01-Strain3-SH.eps';
% for Shear Force Figure (in plotV.m)
V_FileName = '0930423-05~20mm-01-Strain3-ShearForce.jpg';
V_FileName2 = '0930423-05~20mm-01-Strain3-ShearForce.eps';
V_TitleString = 'Shear Force (0930423-05~20mm-01-Strain3.asc)';
V_TitleString = strcat(V_TitleString, '[N=', num2str(N), ']');
% for Hysteresis Loop Figure (in plotH.m)
H_FileName = '0930423-05~20mm-01-Strain3-Hysteresis.jpg';
H_FileName2 = '0930423-05~20mm-01-Strain3-Hysteresis.eps';
H_TitleString = 'Hysteresis Loop for the Damper [Theoretical]
(0930423-05~20mm-01-Strain3.asc)';
H_TitleString = strcat(H_TitleString, '[N=', num2str(N), ']');
% for Text File of Detailed Calculating Process
TextFileName = '0930423-05~20mm-01-Strain3-Output.txt';

```



```

% for text file of Calculated Hysteresis
HysFileName = '0930423-05~20mm-01-Strain3-PredictedHysteresis.txt';
% Input Filenames
NumberOfData = 1;
% Input Filenames of Strain Gauge Data
FileName1(1) = {'0930423-05~20mm-03-Strain3f.asc'};
% Input Filenames of LVDT
FileName2(1) = {'0930423-05~20mm-03-AC1f.asc'};
% =====

NonlinearBending03;
CompareHysteresis;

fprintf('OK!\n');

```

NonlinearBending03

```

% NonlinearBending03.m
% by Stainer
% February 22, 2004
%
%
% Required functions:
% 1. FindTheStress02.m
% 2. Strain02.m
% 3. GenerateTableRO.m
% 4. SerachTableRO.m
%

% Output parameters
if(FID==1)
    Fid = 1; % screen output
else
    Fid = fopen(TextFileName,'w'); % file output
end

% Print the parameters on the screen
fprintf(Fid,'Nonlinear Bending Analysis\n');
fprintf(Fid,' by Stainer\n');
fprintf(Fid,' February 2004\n');
fprintf(Fid,'\n');
fprintf(Fid,'Date: %s\n',date);
fprintf(Fid,'===== \n');
fprintf(Fid,' INPUT PARAMETERS: \n');
fprintf(Fid,' 1. Ramberg-Osgood Parameters: \n');
fprintf(Fid,' n = %5.2f \n',n);
fprintf(Fid,' Alpha = %5.2f \n',Alpha);
fprintf(Fid,' E = %5.2f (GPa) \n',E_Output);
fprintf(Fid,' Sigma_0 = %5.2f (MPa) \n',Sigma_0);
fprintf(Fid,' 2. Iteration Parameters: \n');
fprintf(Fid,' Initial Values of Stress = %5.2f and %5.2f
(GPa) \n',Sigma(1),Sigma(2));
fprintf(Fid,' Max Iteration Times = %d \n',MaxIterationTimes);
fprintf(Fid,'=====');
fprintf(Fid,'\n');
fprintf(Fid,'\n===== BEGIN ANALYSIS ===== \n');
fprintf(Fid,'\n');

% Nonlinear Bending Analysis
for i=1 : NumberOfData % for1

% Read the strain gauge data
FileNameString1 = strcat(FileName1{i});
cd InputData
templ = load(FileNameString1);
cd ..
Time = templ(:,1); % sec, Time
StrainData = templ(:,2)*(10^-6); % Unit conversion of strain from micro-strain
TurningPoint = templ(:,3); % 1: turning point
LengthOfData = length(StrainData);
MinStrain = min(abs(StrainData));
MaxStrain = max(abs(StrainData));

% STEP 1: Plot the hysteresis loop of the USD
fprintf('Number of data: %4d \n',LengthOfData);
fprintf(Fid,' i = %2d \n', i);
fprintf(Fid,' The data being processing: "%s" \n',FileName1{i});
fprintf(Fid,' Number of data : %5d \n',LengthOfData);
fprintf(Fid,' Number of plates : %2d \n',N);

```

```

fprintf(Fid,' MinStrain          : %6.5f\n',MinStrain);
fprintf(Fid,' MaxStrain          : %6.5f\n',MaxStrain);
fprintf(Fid,' STEP 1 : Generate the Ramberg-Osgood Hysteresis Model of the
USD\n');

% Read the LVDT data
FileNameString2 = strcat(FileName2{i});
cd InputData
temp2 = load(FileNameString2);
cd ..
D = temp2(:,2) - mean(temp2(:,2)); % Displacement
D = -D; % cm

% Calculate the Corresponding Stress & Generate the Ramberg-Osgood Hysteresis Model
k = 1; % Index for StressData(k) and StrainData(k)
IsEndFlag = false; % If the end of StrainData is reached, IsEndFlag will be set
to TRUE.

% Determine the number of Turning Point & TurningPointIndex
NumberOfTurningPoint = 0;
TurningPointIndex = find(TurningPoint);
for qqq=1 : LengthOfData
    if(TurningPoint(qqq)==1)
        NumberOfTurningPoint = NumberOfTurningPoint + 1;
    end
end

% The first segment of the hysteresis loop
FLAG2 = 1; % Curve Index
Epsilon_A = 0; Epsilon_B = 0; % for FLAG2=1
Sigma_A = 0; Sigma_B = 0; % for FLAG2=1
while (TurningPoint(k)~=1)
    StressData(k) = FindTheStress02(StrainData(k),FLAG2,0,0);
    fprintf(Fid,' k = %3d Stress = %6.2f Strain =
%8.6f\n',k,StressData(k),StrainData(k));
    if(TurningPoint(k)==9) % Reach the end of the StrainData
        IsEndFlag = true;
        break;
    end
    k = k + 1;
end
if(PauseFlag==1) pause; end

% Determine the CalculationTimes
if((mod(NumberOfTurningPoint,2)==1)) % Odd NumberOfTurningPoint
    CalculationTimes = (NumberOfTurningPoint+1)/2;
else % Even NumberOfTurningPoint
    CalculationTimes = NumberOfTurningPoint/2;
end

% The main part of the loop
IsFirstTime = true;
DeltaSigma = 0.01; % for GenerateTableRO.m

for j=1 : CalculationTimes % =====
    % This for loop can finish the hysteresis loop.
    fprintf(Fid,' ===== The loop j=%3d =====\n',j);
    if(IsFirstTime)
        % The first segment of the hysteresis is using Secant Method which
        % is implemented in FindTheStress02.m.
        StressData(k) =
FindTheStress02(StrainData(k),FLAG2,Epsilon_B,Sigma_B);
        IsFirstTime = false;
    else
        % The other parts of the hysteresis is using Table Searching method.
        clear TableRO_Epsilon TableRO_Sigma;
        GenerateTableRO(DeltaSigma,FLAG2,Epsilon_B,Sigma_B);
        StressData(k) = SearchTableRO(StrainData(k),FLAG2,Epsilon_B,Sigma_B);
    end
    Sigma_A = StressData(k-1); % This is the turning point A
    Epsilon_A = StrainData(k-1); % This is the turning point A
    %if(Sigma_A<0) Sigma_A = 1; fprintf(' T\n'); end % Tricky
    fprintf(Fid,' k = %3d * Epsilon_A = %8.4f Sigma_A =
%7.2f\n',k,Epsilon_A,Sigma_A);
    fprintf(Fid,' =====> Turn to Eq. 2.\n');
    if(mod(k,50)==0) fprintf(' k = %3d\n',k); end
    k = k + 1;
% Eq.2
FLAG2 = 2;
clear TableRO_Epsilon TableRO_Sigma;
GenerateTableRO(DeltaSigma,FLAG2,Epsilon_A,Sigma_A);
while (TurningPoint(k)~=1)
    if(IsEndFlag) break; end
    StressData(k) = SearchTableRO(StrainData(k),FLAG2,Epsilon_A,Sigma_A);

```

```

        fprintf(Fid,' k = %3d Strain = %8.6f Stress = %6.2f
(MPa)\n',k,StrainData(k),StressData(k));
        if(TurningPoint(k)==9) % Reach the end of the StrainData
            IsEndFlag = true;
            break;
        end
        if(mod(k,50)==0) fprintf(' k = %3d\n',k); end
        k = k + 1;
    end % end of while
    if(PauseFlag==1) pause; end
    if(~IsEndFlag) % not yet end
        StressData(k) = SearchTableRO(StrainData(k),FLAG2,Epsilon_A,Sigma_A);
        Sigma_B = StressData(k-1); % This is the turning point B <====
        Epsilon_B = StrainData(k-1); % This is the turning point B <====
        %if(Sigma_B>0) Sigma_B = -1; fprintf(' T\n'); end % Tricky
        fprintf(Fid,' k = %3d * Epsilon_B=%8.4f
Sigma_B=%7.2f\n',k,Epsilon_B,Sigma_B);
        fprintf(Fid,' =====> Turn to Eq. 3.\n');
        if(mod(k,50)==0) fprintf(' k = %3d\n',k); end
        k = k + 1;
    else
    end % end of if
    % Eq.3
    FLAG2 = 3;
    clear TableRO_Epsilon TableRO_Sigma;
    GenerateTableRO(DeltaSigma,FLAG2,Epsilon_B,Sigma_B);
    while (TurningPoint(k)~=1)
        if(IsEndFlag) break; end
        StressData(k) = SearchTableRO(StrainData(k),FLAG2,Epsilon_B,Sigma_B);
        fprintf(Fid,' k = %3d Strain = %8.6f Stress = %6.2f
(MPa)\n',k,StrainData(k),StressData(k));
        if(TurningPoint(k)==9) % Reach the end of the StrainData
            IsEndFlag = true;
            break;
        end
        if(mod(k,50)==0) fprintf(' k = %3d\n',k); end
        k = k + 1;
    end % end of while
    if(PauseFlag==1) pause; end
end % end of for j =====

fprintf(Fid,' The Ramberg-Osgood Hysteresis Model is generated.\n');

% Find the first moment, moment and shear force
fprintf(Fid,' STEP 2 : Find the moment and shear force of the USD\n');
for k=1 : LengthOfData
    M(k) = (b*h^2*StressData(k)) / 6 * 10^6; % N-m
    V(k) = (2*M(k))/H / 9.8; % Kgf
    V(k) = V(k)*N; % Kgf, N: number of plates in a unit of USD
end
fprintf(Fid,' Calculation of shear force is completed.\n');

% Save the Hysteresis Data to a text file: [Displacement Force]
V = V';
Hysteresis = [D V]; % mm, Kgf
cd InputData
Fid2 = fopen(HysFileName,'w');
for k=1 : LengthOfData
    fprintf(Fid2,'%12.4e %6.2f\n', Hysteresis(k,1), Hysteresis(k,2));
end
fclose(Fid2);
cd ..

% Plot the figures
plotH;
plotV;
plotSH;
plotStrain;

end % end of for1

fprintf(Fid,'\n===== ANALYSIS COMPLETE =====\n');
fprintf(Fid,'\n');

% Output parameters
if(FID==1)

else
    fclose(Fid);
end

% ===== THE END =====

```

Strain02.m

```
function Strain = Strain02(Sigma,FLAG2,Epsilon_A,Sigma_A)
global E Sigma_0 Alpha n % Ramberg-Osgood Parameters

% "Strain02.m" is a function of "FindTheStress02.m".
% The Ramberg-Osgood Stress-Strain relationship is adopted in this program.

if (FLAG2==1)
    %FLAG2
    Strain = (Sigma/E) + (Sigma_0*Alpha)/E*(Sigma/Sigma_0).^n;
elseif (FLAG2==2)
    %FLAG2
    Strain = Epsilon_A - ...
        ((Sigma_A-Sigma)/E) - ...
        (2*Sigma_0*Alpha)/E*((Sigma_A-Sigma)/(2*Sigma_0)).^n;
else
    fprintf('\nArguments Error in Strain02.m !\n\n');
end
```

GenerateTableRO.m

```
function GenerateTableRO(DeltaSigma,FLAG2,Epsilon_A,Sigma_A)
% GenerateTableRO.m
% by Stainer
% February 22, 2004
%
%
% Generate the table (Ramberg-Osgood Stress-Strain relation).
% Use the series of testX.m to check the table.
%
% Example:
% GenerateTableRO(0.01,2,0.015,333)
%
global E Sigma_0 Alpha n % Ramberg-Osgood Parameters
global TableRO_Sigma TableRO_Epsilon % Table

% File name
if(FLAG2==2)
    e = num2str(Epsilon_A);
    S = num2str(Sigma_A);
    F = num2str(FLAG2);
    FileName = strcat('E',e,'_S',S,'.ro',F);
elseif(FLAG2==3)
    e = num2str(-Epsilon_A);
    S = num2str(-Sigma_A);
    F = num2str(FLAG2);
    FileName = strcat('E',e,'_S',S,'.ro',F);
else
    fprintf(' *** Error FLAG2! (FLAG2=2 or 3)\n');
end

% Factor
F = 4; % Default: 1.5

% Generate the table
if(FLAG2==2)
    %fprintf(' Generate the Table of Ramberg-Osgood Stress-Strain Relation:\n');
    %fprintf(' FLAG2 = %1d\n',FLAG2);
    %fprintf(' Generating... Please wait...\n');
    TableRO_Sigma = Sigma_A : -DeltaSigma : -Sigma_A*F;
    TableRO_Epsilon = Epsilon_A - ...
        (Sigma_A-TableRO_Sigma)/E - ...
        (2*Alpha*Sigma_0)/E*((Sigma_A-TableRO_Sigma)/(2*Sigma_0)).^n;
    TableRO_Epsilon = TableRO_Epsilon';
    TableRO_Sigma = TableRO_Sigma';
    % Save to a file
    %Fid = fopen(FileName,'w');
    %for i=1 : length(TableRO_Sigma)
    % fprintf(Fid,'%12.9f %12.3f \n', TableRO_Epsilon(i), TableRO_Sigma(i));
    %end
    %fclose(Fid);
    %fprintf(' The table was generated and saved in file %s !\n',FileName);
    %fprintf(' Precision = %5.2e \n',abs(TableRO_Epsilon(1)-TableRO_Epsilon(2)));
elseif(FLAG2==3)
```



```

Sigma_A = -Sigma_A;
Epsilon_A = -Epsilon_A;
fprintf(' Generate the Table of Ramberg-Osgood Stress-Strain Relation:\n');
fprintf(' FLAG2 = %d\n',FLAG2);
fprintf(' Generating... Please wait...\n');
TableRO_Sigma = Sigma_A : -DeltaSigma : -Sigma_A*F;
TableRO_Epsilon = Epsilon_A -...
(Sigma_A-TableRO_Sigma)/E - ...
(2*Alpha*Sigma_0)/E*((Sigma_A-TableRO_Sigma)/(2*Sigma_0)).^n;
TableRO_Epsilon = -TableRO_Epsilon;
TableRO_Sigma = -TableRO_Sigma;
% Save to a file
%Fid = fopen(FileName,'w');
%for i=1 : length(TableRO_Sigma)
% fprintf(Fid,'%12.9f %12.3f \n', TableRO_Epsilon(i), TableRO_Sigma(i));
%end
%fclose(Fid);
fprintf(' The table was generated and saved in file %s !\n',FileName);
fprintf(' Precision = %5.2e \n',abs(TableRO_Epsilon(1)-TableRO_Epsilon(2)));
end

```

SearchTableRO.m

```

function CorrespondingStress = SearchTableRO(GivenEpsilon,FLAG2,Epsilon_A,Sigma_A)
% SearchTableRO.m
% by Stainer
% February 22, 2004
%
%
% Search the table generated by GenerateTableRO.m.
% Use the series of testX.m to check the table.
%
% Example:
%
%
global TableRO_Sigma TableRO_Epsilon % Table

% Search the table
if(FLAG2==2||FLAG2==3)
% Search the table for the GivenEpsilon
for i=1 : length(TableRO_Epsilon)
if ( abs((TableRO_Epsilon(i)-GivenEpsilon)<(10^(-7)) )
CorrespondingStress = TableRO_Sigma(i);
%-7
return;
end % end of if
end % end of for i
for i=1 : length(TableRO_Epsilon)
if ( abs((TableRO_Epsilon(i)-GivenEpsilon)<(10^(-6)) )
CorrespondingStress = TableRO_Sigma(i);
%-6
return;
end % end of if
end % end of for i
for i=1 : length(TableRO_Epsilon)
if ( abs((TableRO_Epsilon(i)-GivenEpsilon)<(10^(-5)) )
CorrespondingStress = TableRO_Sigma(i);
%-5
return;
end % end of if
end % end of for i
for i=1 : length(TableRO_Epsilon)
if ( abs((TableRO_Epsilon(i)-GivenEpsilon)<(10^(-4)) )
CorrespondingStress = TableRO_Sigma(i);
%-4
return;
end % end of if
end % end of for i
for i=1 : length(TableRO_Epsilon)
if ( abs((TableRO_Epsilon(i)-GivenEpsilon)<(10^(-3)) )
CorrespondingStress = TableRO_Sigma(i);
%-3
return;
end % end of if
end % end of for i
for i=1 : length(TableRO_Epsilon)

```



```

        if( abs((TableRO_Epsilon(i)-GivenEpsilon)<(10^(-2)) )
            CorrespondingStress = TableRO_Sigma(i);
            fprintf('  -2\n');
            return;
        end % end of if
    end % end of for i
    for i=1 : length(TableRO_Epsilon)
        if( abs((TableRO_Epsilon(i)-GivenEpsilon)<(10^(-1)) )
            CorrespondingStress = TableRO_Sigma(i);
            fprintf('  -1\n');
            return;
        end % end of if
    end % end of for i

    fprintf('\n\n *** Error when using Table Searching Method to find stress!!\n');
    CorrespondingStress = 0;
    return;

else

    fprintf(' *** Error FLAG2! (FLAG2=2 or 3)\n');

end % end of if

```

GenerateTurningPoint.m

```

% GenerateTurningPoint.m
%
% (The next point of local max/min value) ==> Turning Point
%
% NOTE: The data files you are going to processing must be located in \InputData\
%
% Input File: 2 column strain data
%           First column: Time
%           Second column: micro-strain
% Output File: 3 column strain data (TurningPoint Column will be added!)
%           Third column: Turning Point (1: truning point, 9: end point)
%
% Programming Concept:
% 1. Find the point that strain equals to zero. This will divide the total
%    strain data into several segments.
% 2. Find the local max value / min value in each segment and set value of the
%    third column to 1. This is the Turning Point.
% 3. Set the third column of last data to 9. This is the end point.

clear; clc;

% Number of data
NumberOfData = 1;

% Input Filenames of Strain Gauge Data
FileName1(1) = {'0930423-05~20mm-03-Strain3f.asc'};
FileName1(2) = {'0920930-Kobe(0.25g)-Gage12.asc'};

% Generate the Turning Point Column
for i=1 : NumberOfData

    clear Fid Flag L LocalExtremeValue Result Temp Temp2
    clear TurningPoint TurningPointIndex ZeroStrainIndex
    clear Time Strain n j p qqq

    fprintf('i = %2d: %s\n',i,FileName1{i});

    % Load the strain data
    FileName = strcat(FileName1{i});
    cd InputData
        Temp = load(FileName);
    cd ..

    % The three columns
    Time = Temp(:,1);
    Strain = Temp(:,2);
    for j=1 : length(Time)
        TurningPoint(j) = 0;
    end
    TurningPoint = TurningPoint';

    % Find the points that strain equal to zero
    Temp2 = 1; % Index for ZeroStrainIndex

```

```

for qqq=1 : length(Strain)
    if (qqq==length(Strain))
        break;
    end
    % Find the points that strain equal to zero
    if (((Strain(qqq)>0)&&(Strain(qqq+1)<0)) || ...
        ((Strain(qqq)<0)&&(Strain(qqq+1)>0)))
        ZeroStrainIndex(Temp2) = qqq;
        Temp2 = Temp2 + 1;
    end
end % end of for qqq

% Right-shift of ZeroStrainIndex Array
for qqq=length(ZeroStrainIndex) : -1 : 1
    ZeroStrainIndex(qqq+1) = ZeroStrainIndex(qqq);
end
ZeroStrainIndex(1) = 0;

% Generate the Turning Point Index
L = 1; % Initial Length
for j=1 : length(ZeroStrainIndex)-1

    n = ZeroStrainIndex(j+1) - ZeroStrainIndex(j); % Number of a segment
    LocalExtremeValue = abs(Strain(L));

    for p=1 : n
        if (abs(Strain(L+p))>LocalExtremeValue)
            LocalExtremeValue = abs(Strain(L+p));
            Flag = L + p + 1; % Flag: Index of Turning Point
        end
    end % end of for p

    L = L + n;

    TurningPointIndex(j) = Flag;
end % end of for j

% Generate the Turning Point Column
for j=1 : length(TurningPointIndex)
    TurningPoint(TurningPointIndex(j),1) = 1;
end

% Generate the end point
TurningPoint(length(Strain),1) = 9;

% Save to file
cd InputData
Result = [Time Strain TurningPoint];
Fid = fopen(FileName,'w');
for j=1 : length(Strain)
    fprintf(Fid,'%6.2f %12.4e %ld\n', ...
        Result(j,1), Result(j,2), Result(j,3));
end
fclose(Fid);
cd ..

end

```

CompareHysteresis.m

```

% CompareHysteresis.m
% by Stainer
% 2004-0428
%
% Compare the experimental hysteresis with the predicted one.
%

clear; clc;

% Parameters
% Direct Measurement Hysteresis (from the component test in NctuCE Project - 05)
% Format: [Displacement Force Time]
FileNameString1 = '0930423-05~20mm-03-ExperimentalHysteresis.TXT';
% Predicted from Strain Hysteresis (from the nonlinear bending analysis in NctuCE
Project - 08)
% Format: [Displacement Force]
FileNameString2 = '0930423-05~20mm-01-Strain3-PredictedHysteresis.TXT';
% Properties of Figure

```

```

TitleString = '0930423-05~20mm-01-Strain3';
TitleString = strcat('Comparison of Hysteresis (',TitleString,')');
% Output
JpgFileNameString = strcat(TitleString, '.jpg');

% Load the data
cd InputData
Temp1 = load(FileNameString1);
Temp2 = load(FileNameString2);
cd ..

% Post-processing
D1 = Temp1(:,1); % mm
F1 = Temp1(:,2); % Kgf
D2 = Temp2(:,1); % mm
F2 = Temp2(:,2); % Kgf

% Plot the figure
plot(D1(24:5714),F1(24:5714),'GREEN--', ...
     D2(54:5714),F2(54:5714),'RED');

% Properties of the figure
%title(TitleString);
xlabel('Displacement (mm)');
ylabel('Force (Kgf)');
legend('Direct Measurement','Predicted from Strain',4);
set(findobj(gca,'Type','line','Color','RED'),'Color','RED','LineWidth',1.2);
set(findobj(gca,'Type','line','Color','GREEN'),'Color','GREEN','LineWidth',1.2);
grid on;
set(gca,'YMinorTick','on');
%text(7,-60,'\alpha = 1.7    n=10');
%text(7,-75,'\sigma_0 = 450 MPa');
%text(7,-92,'E = 210 GPa');

% Output
print('-f1', '-djpeg90', '-r128', JpgFileNameString);
EpsFileNameString = strcat(TitleString, '.eps');
if(EpsFlag==1) print('-f1', '-r600', '-depsc', EpsFileNameString); end

```



FilterDisplacement.m

```

% FilterDisplacement.m
% by Stainer
% 2004-0428
%

clear; clc;

% Parameters
InputFileNameString = '0930423-05~20mm-03-AC1.asc';
OutputFileNameString = '0930423-05~20mm-03-AC1f.asc';

% Load the data
cd InputData
Temp1 = load(InputFileNameString);
cd ..

% Post-processing
Displacement = Temp1(:,2); % Displacement
Time = Temp1(:,1); % Time

% Filter
[num,den] = butter(20,0.6);
Displacement1 = filter(num,den,Displacement);

% Comparison
plot(Time,Displacement, Time,Displacement1);
legend('Original','Filter');

% Save to file
cd InputData
Result = [Time Displacement1];
Fid = fopen(OutputFileNameString,'w');
for j=1 : length(Displacement)
    fprintf(Fid,'%6.2f %12.4e\n', ...
           Result(j,1), Result(j,2));
end

```



```

fclose(Fid);
cd ..

% Complete
fprintf('==> %s is done.\n',OutputFileNameString);

```

plotH.m

```

Fig02 = figure('visible', 'on');
plot(D(14:5714),V(14:5714),'BLACK');
%title(H_TitleString);
xlabel('Displacement from LVDT (cm)');
ylabel('Force (Kgf)');
axis([-15 15 -120 100]);
grid on;
%set(findobj(gca,'Type','line','Color',[0 0 1]),'Color','BLUE','LineWidth',1.2);
print('-f1', '-djpeg90', ResolutionString, H_FileName);
if(EpsFlag==1) print('-f1', '-r600', '-depsc', H_FileName2); end
close(Fig02);

```

plotSH.m

```

Fig04 = figure('visible', 'on');
plot(StrainData,StressData,'BLACK');

% Figure Properties
%title(SH_TitleString,'FontSize',12);
xlabel('\epsilon','FontSize',12);
ylabel('\sigma (MPa)', 'FontSize',12);
grid on;
set(get(gca,'YLabel'),'Rotation',0.0);
%set(findobj(gca,'Type','line','Color',[0 0 1]),'Color','BLUE','LineWidth',1.2);
print('-f1', '-djpeg90', ResolutionString, SH_FileName);
if(EpsFlag==1) print('-f1', '-r600', '-depsc', SH_FileName2); end
close(Fig04);

```

plotStrain.m

```

Fig03 = figure('visible', 'on');
plot(Time,StrainData*10^6,'BLACK');
%title(S_TitleString);
xlabel('Time (sec)');
ylabel('Micro-Strain');
axis([0 700 -4000 4000]);
grid on;
%set(findobj(gca,'Type','line','Color',[0 0 1]),'Color','BLUE','LineWidth',1.2);
print('-f1', '-djpeg90', ResolutionString, S_FileName);
if(EpsFlag==1) print('-f1', '-r600', '-depsc', S_FileName2); end
close(Fig03);

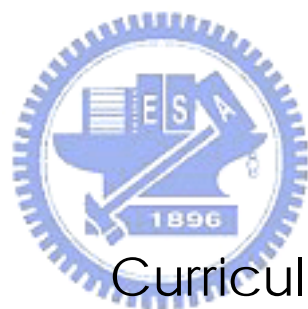
```

plotV.m

```

Fig04 = figure('visible', 'on');
plot(V,'BLACK');
title(V_TitleString);
xlabel('Number');
ylabel('Force (Kgf)');
grid on;
%set(findobj(gca,'Type','line','Color',[0 0 1]),'Color','black','LineWidth',1);
print('-f1', '-djpeg90', ResolutionString, V_FileName);
if(EpsFlag==1) print('-f1', '-r600', '-depsc', V_FileName2); end
close(Fig04)

```



Curriculum Vitae

- 1985~1991 Chung-Cheng Elementary School
- 1991~1994 Tun-Hua Junior High School
- 1994~1997 Chien-Kuo Senior High School
- 1998~2002 Tamkang University
 - Major: Civil Engineering
 - Minor: Computer Science
- 2002~2004 National Chiao Tung University
 - Major: Civil Engineering (Structural Engineering)